

**CONTROLLING SURFACE PROPERTIES POLYMER MATERIALS  
THROUGH PHOTODIRECTED THIOL-ENE WRINKLE SYSTEMS**

by

Stephen J. Ma

A dissertation submitted to the Faculty of the University of Delaware in partial fulfillment of the requirements for the degree of Doctor of Philosophy in Chemical Engineering

Spring 2018

© 2018 Stephen J. Ma  
All Rights Reserved

**CONTROLLING SURFACE PROPERTIES POLYMER MATERIALS  
THROUGH PHOTODIRECTED THIOL-ENE WRINKLE SYSTEMS**

by

Stephen J. Ma

Approved: \_\_\_\_\_  
Eric M. Furst, Ph.D.  
Chair of the Department of Chemical and Biomolecular Engineering

Approved: \_\_\_\_\_  
Babatunde Ogunnaike, Ph.D.  
Dean of the College of Engineering

Approved: \_\_\_\_\_  
Ann L. Ardis, Ph.D.  
Senior Vice Provost for Graduate and Professional Education

I certify that I have read this dissertation and that in my opinion it meets the academic and professional standard required by the University as a dissertation for the degree of Doctor of Philosophy.

Signed:

---

Christopher J. Kloxin, Ph.D.  
Professor in charge of dissertation

I certify that I have read this dissertation and that in my opinion it meets the academic and professional standard required by the University as a dissertation for the degree of Doctor of Philosophy.

Signed:

---

Norman J. Wagner, Ph.D.  
Professor in charge of dissertation

I certify that I have read this dissertation and that in my opinion it meets the academic and professional standard required by the University as a dissertation for the degree of Doctor of Philosophy.

Signed:

---

April M. Kloxin, Ph.D.  
Member of dissertation committee

I certify that I have read this dissertation and that in my opinion it meets the academic and professional standard required by the University as a dissertation for the degree of Doctor of Philosophy.

Signed:

---

Michael E. Mackay, Ph.D.  
Member of dissertation committee

I certify that I have read this dissertation and that in my opinion it meets the academic and professional standard required by the University as a dissertation for the degree of Doctor of Philosophy.

Signed:

---

Xinqiao Jia, Ph.D.

Member of dissertation committee

## ACKNOWLEDGMENTS

To those who didn't make my time at Delaware suck. These last six and a half years have been a tremendous learning experience, not just in terms of my career development, but also in understanding myself better. It has taken the support of many people to help me reach this stage of my career and in my life.

It has certainly not been an easy path to train me into a competent scientist but I am extremely grateful to my advisors, Chris and Norm, for their unbounded patience and enthusiasm in all things science. To Norm for encouraging and giving me opportunities to step outside beyond the laboratory. And to Chris – I doubt any other professor would have let me troll them the way I trolled you...and for not calling me a 'muppet'. I'd like to thank my committee members, particularly Dr. April Kloxin for insightful discussions on my research throughout the last few years. To my fellow Wagner group members, who have helped me since my first year, and I would especially like to thank Paul Mwasame and Ru Chen, who despite being younger than me have consistently looked out for me during their time here. And pretty much everyone in the Kloxin group – for not only commiserating with me over the grad school experience, but also following me in trolling Chris - Melissa Gordon, Andrew Tibbits, Bassil El-Zaatari, Abhishek Shete, Kaleigh Reno Nicastro, Bryan Sutherland, Nicole Halaszynski, Mukund Kabra, Jonathan French, Srimoyee Dasgupta, as well the all the undergrads that have passed through our lab – Samantha Mannino, Jon Galarraga, Justin Paloni, Stephanie Anderson, Laura Mumper, Grant Knappe, Derek Bischoff, and most of all to Benjamin Carberry, who stuck it out working with me for the better part of his

undergraduate career, despite the ongoing research setbacks. I have been very surprised at how cohesive our group has been even with new members joining over time, without being overly-attached...for the most part.

As the first graduate student in Chris's lab, the learning curve was very steep and I've had to rely on the kindness of strangers to execute research ideas over the years. While there are too many people I would like to thank who have helped me, either through research discussions or training on equipment, I want to give a shout out to the Epps group, especially Cameron, Ming and Jill, thank you for helpful discussions and training on flowcoating. Also to Eden ford, who has been instrumental in cell culture experiments for the surface functionalization project. Kathie Young, Mary Walsh, Cinda Younce, Chil Alba, Gary and George, Alan Price, Al Lance, Jeff Ricketts, Weihua Dong, and Neil Garrett all deserve a ton of acknowledgement as well as they are the people who really keep the department running so smoothly.

On a side note, the members of EmPOWER also deserve a lot of praise. EmPOWER was borne out of discussions with my fellow grad students about the issues that many students faced over the course of their graduate careers and how we as students tackle issues like depression and imposter syndrome associated with our academic careers. As a grad student, it's not easy to set aside research time to establish an entirely brand new program to help other grad students, but I really appreciate the mentors who stepped up and help get this program rolling – Amber, Eden, Paige, Kat, Elisa, Victoria, Kim, Michaela, Stijn, as well as the faculty mentors, UD Counselling, Kathie Young, and Mary Martin. While I wish I had more time to carry the program forward, I am excited to see what the EmPOWER mentors will achieve after I am gone.

One thing I did not expect coming to UD was the friendships that I would eventually make. For the better part of two years, while I was physically in Delaware, my mind and heart were still in NYC and so I was reluctant to integrate myself into the department. After going through the five stages of grief and accepting that DE was going to be my home for many more years, I eventually started getting more involved with department activities. Even after the friends I made from my year and from upper years have left, I am still surprised by all the supportive people I continue to meet in the department. In addition to some of the people I mentioned above, I'd also like to thank Annie, Scott, Jennifer, Bryan, Matt, James, Camil, Jackie, Tyler and Lilian.

This list isn't complete without also acknowledging everyone back home, many of whom I've known for over ten years now. With all of our individual schedules, it's not always easy to stay in touch. I would like to thank my friends, from my middle school friend, Sarah, to high school - Diana, Jason, Matt, Angela, Michelle, Anthony, Anita and to college - Jessica, Henry, Brigitte, Phil, Z, Q, Lilian, Richard, and Alex. Special thanks to my undergraduate mentors, Prof. Ilona Kretzschmar and Prof. Raymond Tu, the role models who got me started on this career path over 10 years ago.

I would like to thank, my girlfriend Caitlin Wood, who has been by far the most supportive and understanding person that I've ever met. As terrible as I thought my last two years here would have been trying to finish up, she has made it infinitely better. I am very grateful that she's been by my side thus far.

And lastly, my parents. It has taken me most of my life to fully appreciate the sacrifices they have made to help me get to where I am today. While I have never been particularly good at expressing my gratitude to them, I want to highlight that my

achievements culminating in this doctorate degree is as much their success as it is mine.  
Without them, nothing I have done up to now would have been possible.

## TABLE OF CONTENTS

LIST OF FIGURES .....	xii
ABSTRACT .....	xxi

### Chapter

1	INTRODUCTION .....	1
1.1	Material Wrinkling/Buckling Theory .....	4
1.2	Wrinkle Applications.....	13
1.3	Photopolymerizations .....	16
1.4	‘Click’ Chemistry and Polymer Networks .....	19
1.4.1	Thiol-ene kinetics .....	20
1.4.2	Polymer Networks .....	23
1.5	Thiol-Ene Networks .....	25
1.6	Thesis Overview .....	28
2	PHOTOWRINKLING ON A THIOL-ELASTOMER: TWO-TIERED POLYMERIZATION [124] .....	30
2.1	Introduction .....	30
2.2	Materials and Methods .....	32
2.2.1	Materials .....	32
2.2.2	Elastomer formulation .....	32
2.2.3	AFM Modulus Measurements .....	33
2.2.4	Wrinkle Formation .....	33
2.2.5	Wrinkle gradients and photopatterning .....	34
2.3	Results and Discussion .....	35
2.4	Conclusion.....	42
3	CHEMICAL SURFACE FUNCTIONALIZATION OF WRINKLED THIOL-ENE ELASTOMERS.....	43
3.1	Introduction .....	43

3.2	Materials and Methods .....	45
3.2.1	Materials .....	45
3.2.2	Generation of wrinkled elastomers.....	46
3.2.3	Peptide Synthesis.....	47
3.2.4	LAP Synthesis .....	47
3.2.5	Functionalization .....	48
3.2.6	Contact Angle Goniometry.....	49
3.2.7	X-ray photoelectron spectroscopy (XPS).....	49
3.2.8	Fourier Transform Infrared Spectroscopy (FTIR).....	49
3.2.9	Nuclear Magnetic Resonance (NMR) spectroscopy .....	50
3.2.10	Human mesenchymal stem cell culture and seeding.....	50
3.2.11	Confocal Microscopy .....	51
3.3	Results and Discussion .....	53
3.4	Conclusion.....	69
4	PHOTO-WRINKLE FORMATION VIA FLOWCOATING – SUB- MICRON WAVELENGTHS WITH INDEPENDENT CONTROL OVER MODULUS AND CHEMISTRY.....	71
4.1	Introduction .....	71
4.2	Materials and Methods .....	73
4.2.1	Materials .....	73
4.2.2	Thiol-rich Elastomer formulation:.....	73
4.2.3	Flowcoating Ene-rich films: .....	74
4.2.4	Measuring film thickness: .....	75
4.2.5	Transferring films to the elastomers.....	75
4.2.6	Dynamic Mechanical Analysis (DMA).....	75
4.2.7	Optical Microscopy .....	76
4.2.8	Scanning electron microscopy.....	76
4.2.9	Thermogravimetric Analysis (TGA) .....	76
4.2.10	Atomic Force Microscopy (AFM) Modulus .....	76
4.3	Results .....	78
4.4	Conclusion.....	89
5	CONCLUSION AND FUTURE DIRECTIONS .....	92
5.1	Conclusions .....	92
5.2	Future Directions – Stimuli responsive wrinkles .....	95
5.3	Future Directions – Wrinkled Particles .....	101

REFERENCES ..... 105

Appendix

A PERMISSION LETTERS ..... 153

## LIST OF FIGURES

- Figure 1.1 Wrinkle Formation Schematic.** Wrinkles form when a thick foundation exerts lateral compressive stresses on a thinly adhered skin layer. Wrinkle wavelength is a function of skin (or film) modulus ( $E_s$ ), foundation (or substrate) modulus ( $E_f$ ) and thickness of the film,  $h_s$ . ..... 5
- Figure 1.2 Criteria for Local vs Global Buckling.** A) When a thick substrate exerts lateral compressive stresses on a thin film, local or global buckling may occur. Local buckling results in periodic sinusoidal structures, otherwise known as wrinkling. In global buckling, the bilayer experiences a deformation that affects the entire material. B) The global to local buckling transition is governed by the ratio of the material length to the film thickness as well as the substrate to film thickness ratio. Images adapted with permission from Wang S. *et al. Appl. Phys. Lett.*, **2008**, 93, 023126. Copyright 2008 AIP Publishing LLC. [49]..... 8
- Figure 1.3 Phase diagram for various wrinkling structures.** Type of topography is dictated by the film modulus to substrate modulus ratio ( $\mu_f/\mu_s$ ), the mismatched strain ( $\epsilon_m$ ) and normalized adhesion energy ( $\Gamma/\mu_s H_f$ ). Image adapted with permission from Wang, Q. and Zhao, X. *Scientific Reports*, **2015**, 5, 8887. Copyright 2015 Nature Publishing Group. [51] ..... 10
- Figure 1.4 Thiol- Michael and thiol-ene reaction schemes.** A) In a thiol-Michael reaction, a catalytic base abstracts a hydrogen from a thiol monomer, generating a thiolate anion, which will subsequently form a covalent bond to an electron deficient ene. This generates a carbanion on the ene species which can further abstract another proton from a thiol monomer, thus repeating the entire cycle. B) The thiol-ene reaction follows a similar mechanism except that it requires an initiator (i.e., photoinitiator) to catalyze the reaction. .... 22

<b>Figure 1.5</b>	<b>Typical thiol and ene structures.</b> Number of functional groups and molecular architecture (i.e., ring structures) dictate thermomechanical properties of resultant crosslinked network. The blue enes are electron deficient enes, requiring the use of a nucleophile or base catalyst. The red enes are electron rich, requiring a radical initiator to catalyze the reaction. Many of these compounds are commercially available.....	27
<b>Figure 2.1</b>	<b>Linear stage set up for uniaxial and biaxial strain.</b> Polymers were cut, centered, and held in place with tape. Samples were then strained and released in a sequential manner. ....	34
<b>Figure 2.2</b>	<b>Method of Generating Wrinkles on a thiol-ene surface.</b> Monomers <b>a)</b> pentaerythritol tetramercaptopropionate (PETMP) and tetraethylene glycol diacrylate (TEGDA) were reacted with triethylamine, photoinitiator (I184), and photoabsorber (T328) to produce a <b>(b)</b> thiol-ene network with a uniform crosslink density and excess pendant acrylates (first-stage polymerization). <b>(c)</b> Applying strain and 365 nm light induces radical polymerization of the acrylates (second stage polymerization). The photoabsorber confines the light to a thin skin layer at the surface. <b>(d)</b> Upon releasing the strain on the film, wrinkles are formed with a crosslink density (modulus) gradient .....	36
<b>Figure 2.3</b>	<b>Stylus profilometry of wrinkle wavelength versus dosage.</b> a) Films with a coverslip (red circles) and without a coverslip oxygen barrier (black squares) were irradiated for 5 to 40 seconds using 365nm light at 80 W/m <sup>2</sup> . Wrinkle wavelength increased as a function of increasing irradiation duration. Samples masked with a coverslip exhibited larger wrinkles than the unmasked samples due to the absence of oxygen inhibition. Inset: Stylus profilometry schematic. b) Profilometry from wrinkle gradients (solid black line) shows good agreement with discrete wavelength data (red circles) (0 to 20 seconds, 365 nm at 80 W/m <sup>2</sup> with coverslip). Accompanying amplitude data (inset) are consistent with scaling equation (see supporting information for profilometry setup). ....	38

<b>Figure 2.4</b>	<b>Wrinkle formation via photopatterning on a biaxially stretched specimen.</b> a) Photolithography guides the alignment of the wrinkles perpendicular to the low stress regions of the thiol-ene elastomer. Samples were irradiated for 20 seconds under 365 nm light at 80 W/m <sup>2</sup> . Scale bar represents 10 mm (inset: corresponding photomasks) b) Photopolymerized sample showing alternating wrinkle wavelengths. This pattern is created by stepwise dosing, first with a coverslip only (80 W/m <sup>2</sup> , 5 seconds) followed by two photomasks (80 W/m <sup>2</sup> , 5 seconds and 80 W/m <sup>2</sup> , 10 seconds). c) Employing two different photoinitiators allows for wrinkle formation and shape memory. Wrinkles were formed using a procedure similar to (a). The coil shape was held in place using tape and exposed to 405 nm light (60 W/m <sup>2</sup> , 16 minutes).....	40
<b>Figure 3.1</b>	<b>Nuclear alignment quantification.</b> (A) The direction of wrinkles was assigned as 0° and nuclei direction was determined as the angle relative to the wrinkle direction. (B) Nuclei were stained with DAPI for visualization. Scale bar 100 μm. (C-D) Nuclei images were processed and each nucleus fitted with an ellipse, from which the angle of orientation was determined. Scale bar = 50 μm. ....	52
<b>Figure 3.2</b>	<b>Two-tiered polymerization for wrinkle formation.</b> Tetrathiol, PETMP, and excess diacrylate, TEGDA, were mixed with photoinitiators (Irg 651 and Irg 819), photoabsorber (T479), and TPP to generate an acrylate-rich elastomeric substrate. Straining and irradiating the elastomer with 365nm UV light triggers radical polymerization of the pendant acrylates. The photoabsorber, which absorbs 365 nm light, prevents light penetration into the bulk, thus confining the second polymerization to the surface. Upon destraining the material, wrinkles are generated due to the elastic moduli mismatch between the film and substrate.....	54
<b>Figure 3.3</b>	<b>Conversion data of thiol and ene during elastomer formation.</b> In situ FTIR measurements of the 1:2 PETMP:TEGDA system confirms quantitative conversion of thiol and roughly 50% conversion of the acrylates, which is consistent with the thiol:ene stoichiometry used in formulation. ....	55
<b>Figure 3.4</b>	<b>Dark polymerization observed in the free radical polymerization.</b> Despite irradiating the thin film elastomer substrate for only 5 seconds (green highlighted region), acrylate conversion continues to rise for another 30 seconds before hitting a plateau conversion. This dark polymerization is likely due to diffusion limited radical termination. ....	56

- Figure 3.5 Wrinkle wavelength vs Time and Intensity.** As light controls the film formation necessary to generate wrinkles, both light intensity and irradiation time dictate the size of wrinkle features. Increasing both the intensity and time will lead to increasing wrinkle wavelengths..... 57
- Figure 3.6 Chemical modification of the acrylate-rich elastomer surface.** Wrinkled surfaces are irradiated with 405 nm light to induce bulk radical polymerization of the remaining acrylates. This post-processed material is then submerged into a solution of tetrathiol, PETMP, which converts the acrylate-rich surface into a thiol-rich surface via the thiol-Michael reaction. In generating the thiol-rich surface, a second modification can be carried out. In the presence of a nucleophile or base catalyst, the pendant thiols will undergo a second thiol-Michael reaction with electron-poor enes (i.e., hydroxyethyl acrylate). Alternatively, thiols can react with electron-rich enes (i.e., allyl) through a photoinitiated radical thiol-ene mechanism. Because this latter reaction is light-triggered, spatial control over chemical functionalization is possible. A RGDS containing peptide was synthesized with an alloc-protected lysine amino acid residue, which contains the electron rich ene that can be coupled to the thiol-rich elastomer. .... 58
- Figure 3.7 XPS spectra of fluorine peak area versus PFDT solution concentration.** XPS data confirms that even at 0.31 M (15 mg/mL) of the PFDT in solution, the amount of fluorine approaches saturation. Further increases in solution concentration does not increase the surface concentration of the PFDT. Using a tetrathiol, PETMP (MW = 488 g/mol), to do the actual surface modifications yields roughly four times the amount of thiol at the same mass concentration as the PFDT (MW = 480 g/mol), which ensures excess thiol functionality at the surface of the polymer. .... 59
- Figure 3.8 ESI MS of AF647-RGDS peptide.** Calculated mass:  $[m+1, H+] = 1059$  Da,  $[m+2H+] = 1060$  Da. Measured  $[m+1, H+] = 1058.5$  Da,  $[m+2H+] = 529.76 \times 2 = 1059.52$  Da..... 61
- Figure 3.9 NMR Spectra of PETMP/HEA with base catalyst DBU in Acetonitrile-d** before (top) and after (bottom) reaction. Reaction achieves roughly 80% conversion as determined by the peaks located between 5.5-6.5 ppm associated with the C=C acrylate moieties of the HEA (red hydrogens). The peak at 6.8 ppm is the trimethylbenzene reference peak..... 62

- Figure 3.10 NMR Spectra of PETMP/K(alloc) with photoinitiator LAP in 70/10 Acetonitrile-d/D2O before (top) and after (bottom) reaction.** Reaction achieves roughly 30% conversion as determined by the peaks located between 5.5-6.5 ppm associated with the C=C acrylate moieties of the HEA (red hydrogens). The peak at 6.8 ppm is the trimethylbenzene reference peak. .... 63
- Figure 3.11 Static Contact angle measurements on functionalize elastomer surfaces.** Native surfaces exhibited a contact angle of  $32 \pm 1.8^\circ$ . When functionalized with hydrophobic PETMP, the contact angle rises to  $75.5 \pm 4.3^\circ$ . With further modification of the thiols with either hydrophilic hydroxyethyl acrylate (HEA) or AF647-RGDS, the contact angle of the surfaces decrease again to  $37.5 \pm 1.2^\circ$  and  $65.6 \pm 4.3^\circ$ , respectively. .... 64
- Figure 3.12 hMSCs seeded on flat functionalized surfaces.** a) Representative confocal microscopy images of hMSCs seeded on various functionalize surfaces (Native, PETMP (thiol-rich), PETMP/HEA (hydrophilic), PETMP/RGDS, and RGDS only). Scale bar represents 100  $\mu\text{m}$ . Cell nuclei are stained blue, while the cytoskeleton is shown in red. hMSCs seeded on PETMP/RGDS-functionalized surfaces exhibited significant improvements in cell spreading (b) and cell density (c) as compared to other functionalization conditions. For PETMP-functionalized samples, hMSCs attached and spread to a lesser degree, possibly due to nonspecific interactions with the free thiol moieties. Homopolymerization of the allyl moiety in the AF647-RGDS sequence (RGDS only) to the free acrylates may also promote hMSC attachment. .... 66
- Figure 3.13 hMSCs seeded on PETMP/RGDS-functionalized wrinkled substrates with increasing wrinkle wavelength.** a) Representative confocal microscopy images of hMSCs seeded on wrinkled substrates reveal alignment of cells with the troughs of wrinkles structures versus a flat PETMP/RGDS-functionalized flat substrate. Scale bar represents 100  $\mu\text{m}$ . Cell nuclei are stained in blue while the cytoskeleton is stained red. b) As the cells tend to settle and spread along the troughs of the wrinkle structures, increasing the wrinkle wavelengths increase the accessible surface area in the troughs for the cells to spread. c) Cell density decreases with increasing 365 nm irradiation time. .... 67

- Figure 3.14 Nuclear Alignment vs wrinkle wavelength on PETMP/RGDS surfaces.** Cell alignment measurements, taken as  $\pm 15^\circ$  parallel to the wrinkle wavelength, demonstrated two-fold increase in nuclear alignment of hMSCs on PETMP/RGDS-functionalized wrinkle substrates as compared to a flat substrate. Red stars denote significance as compared to flat PETMP/RGDS functionalized sample..... 69
- Figure 4.1 Modulus of thin films.** Modulus histograms for AFM peak force tapping measurements of PETMP/TATATO (1:1.1) thin films. A) Poly(styrene) standard with a mean of 3.37 GPa and a standard deviation of 0.87. b) PETMP:TATATO thin film with a mean of 3.59 GPa and a standard deviation of 0.34. C) Second replicate of PETMP:TATATO film with an average of 4.75 and a standard deviation of 0.46. D) Third replicate of the PETMP:TATATO thin film with an average of 4.17 and a standard deviation of 0.39. These data indicate that these film thicknesses of the PETMP:TATATO films retain their glassy bulk modulus. .... 77
- Figure 4.2 Thiol-ene Film and Elastomer Formulation for Polymer Wrinkling.** Two independent thiol-ene formulations are employed to generate the thick elastomeric substrate and the thin, high modulus film necessary for wrinkling. A) Tetrathiol and triene (1:1.1 thiol:vinyl functional group stoichiometry) are mixed with photoinitiator (Irgacure 651) and dissolved in toluene. This solution is used to flowcoat nanometer thick films on a glass slide, which are subsequently crosslinked to form a high modulus polymer with excess vinyl functional groups and post-heated to remove residual solvent. B) Separately, tetrathiol, dithiol, and diene (1.5:2:3 thiol:thiol:vinyl functional group stoichiometry, respectively) are mixed with photoinitiator and photocured between two glass slides to generate a thicker low modulus elastomer with excess thiol functional groups..... 79
- Figure 4.3 Film Transfer of Flowcoated Film onto a Thiol-ene Elastomer for Wrinkle Formation.** a) Thin films are flowcoated and polymerized on a silicon wafer (or glass slide) and before they are placed in contact with a strained thiol-ene elastomer (b). Irradiation initiates reaction of the excess vinyls at the film interface with the excess thiols at the elastomer interface, to form a covalently attached laminate. The coating substrate is subsequently removed by submerging the entire..... 81

<b>Figure 4.4</b>	<b>Film thickness versus coating velocity and monomer concentration</b> A) Film thickness plotted as a function of velocity shows a linear increasing trend. As velocity increases, more monomer is left behind on the flowcoated substrate, thereby increasing the film thickness. B) The film thickness increases with increasing monomer concentration. ....	83
<b>Figure 4.5</b>	$\text{Log}_{10}(\text{Film Thickness})$ plotted as a function of $\text{Log}_{10}(\text{Velocity})$ yields an 0.62 scaling, consistent with the Landau-Levich theory. ....	84
<b>Figure 4.6</b>	As predicted by Equation 2, wrinkle wavelength scales with $h$ . ....	85
<b>Figure 4.7</b>	<b>Observed thickness scaling deviations of the wrinkle wavelength as film thickness approaches 40 nm;</b> the wavelength scaling on thickness becomes $\lambda \sim h^{1.43}$ instead of the expected $h^1$ . ....	86
<b>Figure 4.8</b>	<b>Wrinkle wavelength vs film thickness for films of different moduli.</b> Wrinkle wavelength can be tuned through modulus of the thin films via monomer structure and/or thiol:ene stoichiometry. Thiol:ene formulations using 1:1.1 (modulus = 1.9 GPa) yield larger wrinkle wavelengths as compared to 0.7:1.1 formulations (modulus = 1.5 GPa). A similar concept can be applied to the elastomer substrate as well. ....	87
<b>Figure 4.9</b>	<b>Spatial Control over Wrinkle Formation using Flow-coated Photopolymerization.</b> A) After flowcoating monomer thin films, a photomask is overlaid on top of the preirradiated film, separated by a thin spacer (1 mm). Exposure to UV irradiation spatioselectively crosslinks the materials, after which the unexposed, unreacted monomer is rinsed away with toluene. The photopatterned film is transferred to the strain elastomer (as described in Scheme 1). Releasing the strain produces wrinkles approaching submicron wavelengths, resulting in iridescent films. B) Patterned films reveal very distinct boundaries (yellow box – scale bar 500 $\mu\text{m}$ ). Unidirectional strain generates aligned wrinkles perpendicular to the strain direction, regardless of the pattern orientation (green and red boxes – scale bar is 5 $\mu\text{m}$ ). ....	88

**Figure 4.10 Spatially Confined Formation of Multi-Wavelength Wrinkle Patterns** A) Two layers of monomer were flowcoated with 10 wt% monomers in toluene at 7 mm/s and photopatterned using the two patterns shown in the inset. Unreacted monomers were rinsed away between each coating step. B) Upon film transfer, three distinct regions are observed – larger wrinkles associated with two layers, small wrinkles corresponding to one layer of crosslinked polymer, and areas with no wrinkles where the unreacted monomers were rinsed away. C) Corresponding large ( $h \sim 190$  nm,  $\lambda \sim 2.75$   $\mu$ m) and small wrinkle ( $h \sim 130$  nm,  $\lambda \sim 1.75$   $\mu$ m) regions (left and right images, respectively), with the transition region shown in the center image. .... 90

**Figure 5.1 Various photoresponsive moieties and their incorporation into flowcoated thin films.** a) Ene monomers containing azobenzene molecules can be synthesized and reacted with thiols on a flowcoating substrate. Prealignment of the liquid crystal molecules must be induced prior to photopolymerization to ensure liquid crystallinity. Upon transfer to an elastomer substrate (no strain required) and irradiation with a 365 nm light source, the film can undergo macroscopic shrinkage due to trans-cis isomerization of the azobenzene moiety, thus causing shrinkage. Exposure to heat or blue light will return the surface to the original flat state. b) Partially crosslinked thiol-ene films containing coumarin in the network backbone can be transferred onto a strained elastomer. Upon irradiation with  $>300$  nm light, 2+2 dimerization is induced in the coumarin, forming a four-membered ring and increasing the modulus of the film. Upon strain release, wrinkles are formed. Irradiation with 254 nm light will restore the surface to a flat state. c) High modulus thiol-ene films containing trithiocarbonate moieties and photoinitiator can be created and transferred onto a strained elastomer, which upon destrain will form wrinkles. Irradiation with 365 nm light (or a light source matching photoinitiator absorbance) will create bond reshuffling, relaxing the stress in the thin film that was introduced during the wrinkle process, thus regenerating a flat surface. If the bilayer is restrained, and the surface irradiated with light, the thin film will relax in the elongated state, and upon destrain will wrinkle again. The generic functional group, R, denotes attachment to a thiol-ene network. .... 99

**Figure 5.2 Photo-Copper Catalyzed Azide Alkyne Reaction.** A photoinitiator radical reduces copper(II) to copper(I) which will trigger reaction between the azide ( $-N_3$ ) and alkyne ( $-C \equiv C$ ) resulting in the formation of the triazole ring. .... 100

**Figure 5.3. Formation of wrinkled particles using CuAAC ‘click’ chemistry.** Organic multifunctional azide and alkyne monomers and organic solvent are suspended in an aqueous solution containing copper (I) and stabilized at the oil-water droplet interface by surfactant. Because specific species of copper (I) do not readily dissolve in the organic phase, polymerization is limited to the droplet interface, forming a shell. Diffusion of the copper into the droplet will dictate shell thickness. Upon filtering the particles and deswelling the organic solvent, wrinkles will spontaneously form due to the elastic modulus mismatch between the harder shell and the liquid core..... 103

## ABSTRACT

Wrinkling/buckling on elastomers represents a cost-effective approach to creating surface topography, leading to a broad range of coating and templated assembly applications. Despite the versatility of wrinkling, several challenges hinder the development of wrinkled performance materials including a limited ability to confine and orient the wrinkles and the lack of commercial scalability due to the processing techniques that are currently utilized in wrinkle formation.

Using thiol-ene ‘click’ chemistries, characterized by rapid kinetics and high selectivity under ambient conditions, we have developed rapidly-curing photo-wrinkle systems. To generate wrinkles, tetra-thiol and excess di-acrylate, embedded photoinitiator and photoabsorber, is reacted to form a thick acrylate-rich elastomer. Upon straining and irradiating the material with UV light, the photoinitiator triggers free radical polymerization of the pendant acrylates in the network, while the photoabsorber confines the light to a thin layer at the surface of the elastomer, thus creating the conditions necessary for wrinkling. Light affords spatiotemporal control over wrinkle formation, which enables facile wrinkle alignment and confinement, the formation of complex patterns with multiple distinct wrinkle wavelengths, and the formation of gradient wrinkles, all under ambient conditions.

Leveraging oxygen inhibition of the free radical polymerization, we can also post-functionalize the wrinkled surfaces through sequential thiol-ene reactions of functional monomers. By first reacting the surface acrylates to excess tetra-thiol in solution, which converts the acrylate-rich surface into a thiol-rich surface, we develop

a functionalization scheme that enables photopatterning of chemical moieties using a second photoinitiated thiol-ene reaction. As a demonstration, we employ these wrinkled substrates as cell culture platforms for the alignment of human mesenchymal stem cells (hMSCs) towards tissue engineering applications. Specifically, substrates functionalized with an RGDS-containing peptide showed drastic increases in hMSC density and spreading. Importantly, when cultured on wrinkled substrates, these hMSCs exhibit cell alignment along the troughs of the wrinkle structures, demonstrating the importance of both topography and chemistry in controlling surface properties.

Alternatively, wrinkles can be formed via flowcoating and polymerizing thiol-ene monomer thin films, which can be transferred onto a softer thiol-ene elastomeric substrate. The flowcoating process enables formation of sub-micron wrinkle wavelengths by controlling film thickness and modulus mismatch between the film and the substrate layers. Through photopatterned UV light, wrinkle features can be spatially confined and aligned, and using a layer-by-layer process, wrinkle features can be discretely tuned across the surface. Importantly, due to the modular nature of thiol-ene ‘click’ chemistry, monomers can be exchanged to not only independently control the modulus of the film and the substrate, but may also facilitate future development of functional and stimuli-responsive polymer thin film systems.

The versatility of the thiol-ene polymerization allows the design of more intricate polymer networks towards wrinkling applications. Through careful selection of the monomers used and precise stoichiometric control, the ‘click’ nature of the thiol-ene reaction ensures high tunability of the of the elastomer, ultimately enabling tailored control over modulus, chemistry and topography for targeted material applications.

## Chapter 1

### INTRODUCTION

Polymer science and engineering, first investigated in the early-1800s, has expanded into a rich field of research, which has led to the development of widely-recognized materials including nylon, Kevlar, Teflon/PTFE, poly(styrene), bisphenol A, among many others. Even DNA, itself a polymer, has been self-assembled into unique configurations such as the iconic smiley-face, in what is now known as DNA origami. [1] While the library of polymerization techniques and chemistries has expanded, the main motivation for polymer science and research has remained consistent – understanding structure-property relationships, which enable tunability of properties toward materials development.

For fields such as biotechnology, coatings, thin films and nanotechnology, understanding the surface properties of polymers is vital to new materials development. Viscoelasticity is a critical property that is controlled to engineer polymer surfaces. In pressure sensitive-adhesives (PSAs), for example, it has been shown that the storage ( $G'$ ) and loss ( $G''$ ) shear moduli determine the end-use applications of the PSA, [2] as the elastic and dissipation components of the shear modulus will affect how the PSA will adhere to and delaminate from a surface. Another example of moduli-influenced behavior is in the biomaterials field, where many authors have demonstrated moduli-dependent cell proliferation and differentiation. [3-9]

Surface chemistry presents another avenue for surface property tunability. From physical adsorption to covalent reactions of functional moieties, different methods have

been employed to modify the chemistry at the surface of a material. Glass, for example, has been functionalized through both covalent (i.e., silane agents) [10,11] and noncovalent means (i.e., layer-by-layer (LbL)). [12] Commercial products, such as Rain-X, which renders car windshields hydrophobic through adsorption of a proprietary chemical mixture, have also been developed. 3,4-dihydroxyphenylalanine (DOPA), a chemical found in the adhesive protein of mussel glue, has found uses in coating applications, including adhesives and electroless metal deposition [13-16]. Polytetrafluoroethylene (PTFE) (i.e., Teflon) has been used in a number of coating applications (i.e., non-stick pans, biomedical devices, etc.) [17] due to its high chemical inertness which is a direct consequence of strong carbon-fluorine intramolecular bonding. With the rapid growth in biomaterials and biotechnology research, significant efforts have been invested in mediating or preventing cell attachment (antifouling) to material surfaces. [18-20]

Despite the extensive body of literature on the effects of modulus and surface chemistry on material performance, there is a limit on these two material parameters in designing polymer surfaces. While polymer materials with moduli ranging from pascals to gigapascals have been developed, to induce different responses from either the material or the environment that a material is in, requires changing the moduli several orders-of-magnitude. In the case of PSAs, a roughly two order-of-magnitude difference in the storage and viscous moduli are required to tailor the application of the PSA (i.e., from cold temperature PSAs to high-shear PSAs). [2] Likewise, neural stems cells can differentiate into neurons on substrates with moduli ranging from 100-500 Pa or glial cells on substrates with moduli ranging from 1000 – 10,000 Pa. [21] More recent studies have also shown that substrate modulus will affect the efficiency of cell attachment.

[18] Surface functionalization is limited by the available surface area that can be functionalized.

To overcome these limitations, researchers are increasingly focused on nature – specifically on a diverse set of naturally occurring materials that contain texture or topography. Topography is a critical component in materials design, responsible for a multitude of naturally-occurring phenomena like the superhydrophobicity and self-cleaning properties of the lotus leaf. [22-24] the drag reduction of shark skin, [24] the bed-bug-trapping capability of a special bean leaf that has microhooks on its surface, [25] and the quintessential example of topography in action – the gecko foot. [26-32] The gecko foot contains nearly five hundred thousand hair-like setae, which branch off into billions of nanoscopic spatulae. Combined, these hairs create billions of adhesive contacts due to molecular van der Waals interactions between the gecko foot and the surface to which it is attached. The result is a reversible, super adhesive that leaves no residue and can be used repeatedly across just about any surface.

Because of the unique properties afforded by topography, there has been concentrated efforts in adapting these micro- and nano- structures to synthetic materials such as polymers. Synthetic gecko tape, for example, is being developed by NASA as a potential replacement for Velcro in space, while the micropapule structures on the surface of lotus leaves have led to the development of superhydrophobic polymer materials. [23] Interestingly, Velcro itself is a bio-inspired material based on burr seeds, which contain millimeter-sized hooks that allow the seeds to cling to animal fur for dissemination.

To create these ‘bioinspired’ designs, various techniques have been employed to replicate the surface structures on polymeric materials, including chemical etching,

[33-36] e-beam lithography/laser ablation, [37,38] imprint lithography, [35,39] and more recently 3D-printing. [40,41] However, many of these protocols are time and labor intensive, which prohibit translation into industrially relevant applications. An alternative approach to generating topography is material wrinkling or buckling on polymer surfaces. Though wrinkles are traditionally viewed as defects, they were deliberately introduced onto polymer surfaces in 1998, and have since provided a rapid, low-cost method for generating topography, ranging from millimeter to nanometer length scales, over large surface areas. Because of the facile fabrication techniques to produce wrinkled structures, the last 20 years has seen a rapid growth in the volume of wrinkle literature towards phenomenological understanding and application development.

The following sections will introduce wrinkling theory, wrinkling applications and provide an overview of photopolymerizations, polymer networks and ‘click’ chemistry concepts.

### **1.1 Material Wrinkling/Buckling Theory**

Wrinkling or buckling are out-of-plane mechanical instabilities that occur in composite materials, leading to the formation of a periodic surface topography that can span length scales ranging from kilometers to nanometers. Traditionally, buckling has been viewed as a material defect (i.e., buckling railroad tracks under heat [42] or the buckling of composite airplane wings during WWII [43]), with studies dating back to 1744, when Euler analyzed columns under compressive loads. [44] More recent investigations of wrinkling phenomenon in the last 60-70 years has led to the development of important wrinkling theories and equations which lend themselves to

the understanding and characterization of wrinkled features. [42,44,45] The simplest view of wrinkling is a two-layer composite plate [42,44,45] (Figure 1.1).

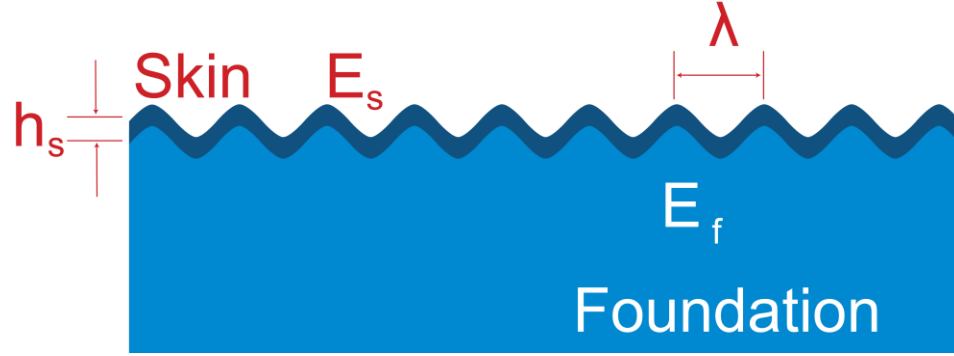


**Figure 1.1 Wrinkle Formation Schematic.** Wrinkles form when a thick foundation exerts lateral compressive stresses on a thinly adhered skin layer. Wrinkle wavelength is a function of skin (or film) modulus ( $E_s$ ), foundation (or substrate) modulus ( $E_f$ ) and thickness of the film,  $h_s$ .

The first layer is an infinitely thick elastic foundation with a modulus of  $E_f$ . This foundation layer is deformed, most typically through thermal expansion, solvent swelling, or mechanical strain, upon which a thin, high modulus ( $E_f$ ) skin layer is strongly adhered. When the deformation on the foundation is released, it will exert an in-plane compressive stress on the skin layer. Above a critical force, sinusoidal wrinkle structures spontaneously form in the skin, the result from the minimizing the bending energy of the skin layer (which favors large wavelengths) under compression and the stretching energy of the foundation (which favors small wavelengths). [43] The equation for wrinkle wavelength is:

$$\lambda = 2\pi h \left[ \frac{(1-\nu_f^2)E_s}{3(1-\nu_s^2)E_f} \right]^{\frac{1}{3}} \quad (1.1)$$

where  $\lambda$  is the wrinkle wavelength,  $h$  is the height of the skin layer, subscript  $f$  and  $s$  are the foundation and skin, respectively,  $\nu$  is the Poisson ratio and  $E$  is the elastic modulus. As shown in Equation (1), the wrinkle wavelength is a function of the material properties of the skin and foundation layers and scales linearly with the thickness of the skin layer. The wrinkle amplitude equation is given as [46]:

$$A = h \left( \frac{\varepsilon}{\varepsilon_c} - 1 \right)^{\frac{1}{2}} \quad (1.2)$$

where  $\varepsilon$  is the applied strain and  $\varepsilon_c$  is the critical strain, defined only by the modulus mismatch of the skin and foundation layers:

$$\varepsilon_c = \frac{1}{4} \left( \frac{3E_f(1-\nu_s^2)}{E_s(1-\nu_f^2)} \right)^{\frac{2}{3}} \quad (1.3)$$

There are several considerations that must be considered when applying the above equations. First, these equations assume a linear mechanical response in the material under strain. For viscoelastic materials (e.g., polymers), the applied strain must lie within the linear viscoelastic region (LVR) for that specific material. Under large deformations, Jiang and coworkers demonstrated a strain-dependent wrinkle wavelength and amplitude [47]:

$$\lambda = \frac{\lambda_0}{(1+\varepsilon)(1+\xi)^{\frac{1}{3}}} \quad (1.4)$$

$$A = \frac{A_0}{\sqrt{(1+\varepsilon)(1+\xi)^{\frac{1}{3}}}} \quad (1.5)$$

where  $\lambda_0$  and  $A_0$  are the wrinkle wavelength and amplitude equations 1.1 and 1.2 respective, and  $\xi = 5\varepsilon(1+\varepsilon)/32$ .

The second limit occurs when either the skin layer is too thick or the foundation layer is too thin, resulting in a macroscopic bending of the entire bilayer composite as shown in Figure 1.2. This phenomenon is known as global buckling (as opposed to wrinkling, which is called ‘local buckling’). Wang et al. investigated material conditions that led to the local to global buckling transition, developing a global critical strain equation,  $\varepsilon_c^{global}$ , [48] and found that the type of buckling was determined by the ratio of the film and substrate thicknesses and the ratio of the length of the material to the film thickness (Figure 1.2b).

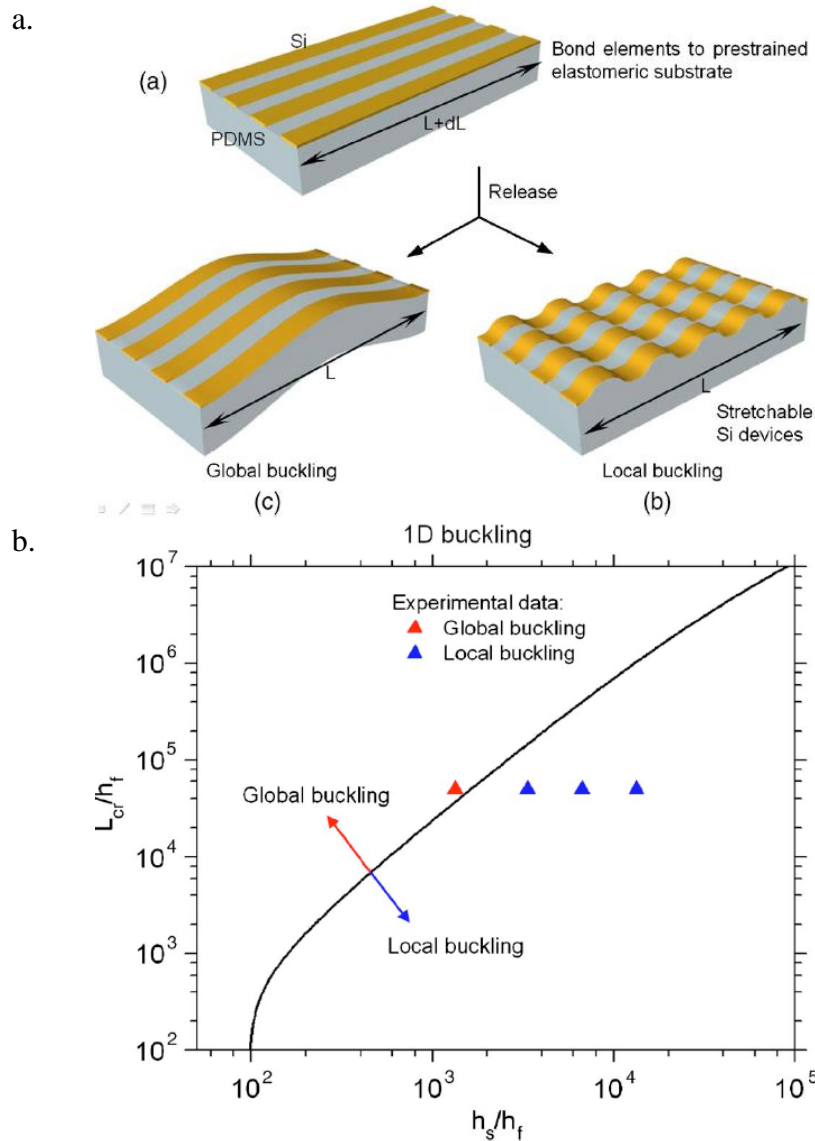


**Figure 1.2 Criteria for Local vs Global Buckling.** A) When a thick substrate exerts lateral compressive stresses on a thin film, local or global buckling may occur. Local buckling results in periodic sinusoidal structures, otherwise known as wrinkling. In global buckling, the bilayer experiences a deformation that affects the entire material. B) The global to local buckling transition is governed by the ratio of the material length to the film thickness as well as the substrate to film thickness ratio. Images adapted with permission from Wang S. *et al. Appl. Phys. Lett.*, **2008**, 93, 023126. Copyright 2008 AIP Publishing LLC. [49]

A multitude of non-sinusoidal wrinkled structures have been experimentally and theoretically identified, including ridges, folds, creases, double wrinkles (period-double), and delamination. In 2015, Wang et al. through computational and experimental design, created the first wrinkle phase diagram, carefully mapping out the prerequisite conditions for each of these phases [50]. As shown in Figure 1.3, the three parameters that dictate wrinkle morphology are modulus mismatch, mismatched strain (defined as  $[\text{Length}_{\text{skin}} - \text{Length}_{\text{foundation}}] / \text{Length}_{\text{skin}}$ ), and adhesion strength of the skin to the foundation. At low strains and low moduli mismatch (i.e., below the critical strain), bilayer materials will remain in a flat state as expected. Increasing the modulus mismatch at low strains will induce sinusoidal wrinkling structures, while the opposite will introduce creasing and folds. At high strains and high modulus mismatch, ridges and period doubling will occur. The adhesion parameter affects where these transitions occur, with low adhesion energy favoring delamination of the skin layer.

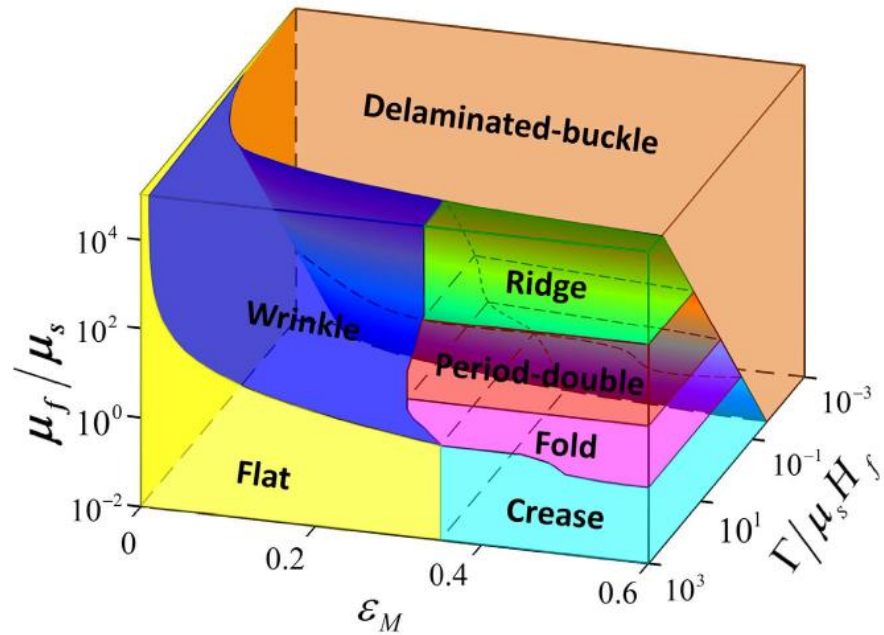


**Figure 1.3 Phase diagram for various wrinkling structures.** Type of topography is dictated by the film modulus to substrate modulus ratio ( $\mu_f/\mu_s$ ), the mismatched strain ( $\epsilon_m$ ) and normalized adhesion energy ( $\Gamma/\mu_s H_f$ ). Image adapted with permission from Wang, Q. and Zhao, X. *Scientific Reports*, **2015**, 5, 8887. Copyright 2015 Nature Publishing Group. [51]

Experimentally, many wrinkling systems have been developed with various combinations of elastic polymer foundations (elastomers) and high modulus skin layers. With these material systems, three methods of elastomer deformation have been commonly utilized to form wrinkles: thermal expansion, solvent or monomer swelling, or mechanical strain.

In the very first demonstration of controlled wrinkling by Bowden and coworkers in 1998, a thin skin layer of gold or titanium was deposited via electron beam evaporation onto a poly(dimethylsiloxane) (PDMS) elastomer foundation. [52] In this example, mechanical deformation was introduced via local heating of the PDMS surface

during the gold deposition process; heating of the polymer surface results in thermal expansion at the surface. Upon cooling, the PDMS surface returned to its original length and given the modulus mismatch between the gold layer and the PDMS elastomer, wrinkles were formed. Following this work, Bowden et al. developed an alternative method of wrinkle formation. [53] Exposing a heated PDMS elastomer surface to oxygen plasma, the siloxane at the PDMS surface was chemically transformed into a hard, nanometer-thick silicate (glass) skin. Upon cooling the system, wrinkles were again, spontaneously generated. This process was unique as it enabled the formation of a covalently-bound skin layer, preventing delamination of the skin from the foundation, especially when the material was exposed to large deformations. A number of other groups have also employed PDMS elastomers, either opting to form the skin layer through other oxidation methods (i.e., UV-ozone (UVO) or strong acids [54-58]) or by transferring thin, flowcoated/spincoated polymer films onto a strained PDMS elastomer. [59,60] The latter option enables more tunability of the surface properties (i.e., thermo- or photoresponsive wrinkle systems). [61,62]

Swelling-induced wrinkling has also been studied. The Crosby group, for example, used stencils to mask specific areas of the PDMS surface, selectively oxidizing only the exposed portions of an unstrained PDMS elastomer surface. [63] Though in the absence of strain, this bilayer system remained planar, solvent could be swelled into the material to induce wrinkling. Alternatively, Chan and Crosby used photocurable n-butyl acrylate as the swelling agent. In this instance, the n-butyl acrylate could be photocured after swelling into the PDMS, thereby stabilizing the wrinkle structures that were formed. Guvendiren and coworkers developed a photocured hydrogel system, using poly(hydroxyethyl methacrylate) (PHEMA), photoinitiator, and a crosslinked

ethylene glycol dimethacrylate (EGDMA). [64] Due to oxygen inhibition of the photopolymerization, a modulus gradient was introduced into the surface of the hydrogel. Upon water exposure, lamellar, peanut, and hexagonal patterns were observed, depending on the amount of crosslinker that was added, since the crosslinker amount affects mechanical properties at the surface of the hydrogel. As the authors noted, the swelling-induced structures formed as a result of competing forces of osmotic pressure at the surface and lateral confinement of the material. It is worth noting, because swelling ratios can be large, especially in hydrogel systems, the mechanical deformation that is introduced into the polymer is far greater than the critical strain necessary for wrinkling. This results in high aspect ratio creasing structures, rather than the low aspect ratio sinusoidal wrinkles.

One of the main drawbacks of thermal or swelling-induced wrinkling is poor wrinkle alignment. In the first works by Bowden et al. for example, wrinkle alignment could only be induced by placing physical stencils on top of the PDMS elastomer or by introducing step changes in the PDMS elastomer surface prior to the skin formation. These two processes introduced boundaries, which forced the wrinkles to align perpendicular to these boundaries. In swelling-induced wrinkling, because the osmotic pressure at the surface of the polymer is isotropic, the resultant wrinkle structures may form in any orientation, only aligning at material boundaries.

Rather than using thermal expansion or solvent swelling to form wrinkles, Efimenko and coworkers showed that aligned wrinkles could be formed by uniaxial mechanical straining a PDMS. [56] Upon skin formation and destrain, wrinkles aligned perpendicular to the direction of strain. Interestingly, the authors showed that the wrinkling phenomenon exhibited a hierarchical fractal design under high prestrain.

Similar to the multi-length scale hairs found on the gecko foot, five generations of wrinkle wavelengths, ranging from tens of nanometers to hundreds of microns, were discovered through slow and careful destaining of the PDMS/silicate system. Each generation of wrinkles were ‘nested’ in the next larger generation of wrinkles, thereby forming a fractal structure. Yang and coworkers extended this concept to two dimensions, creating well-aligned herringbone structures through sequential biaxial strain. [65]

## **1.2 Wrinkle Applications**

Wrinkling has found its way into a plethora of material applications. Because of the optical transparency of many polymers, wrinkles and wrinkling techniques have been applied to the development of optical coatings, diffraction gratings, and lense-like materials. Chandra et al. developed concave and convex microarray lenses, employing a hexagonally packed hole array copper grid to pattern UVO-treated, strained PDMS. [57] Upon removal of the mask and destain, the exposed holes on the surface of the PDMS buckled, generating the microarray. Because of the elastic properties of the PDMS, the microarray focal length could be tuned simply by stretching the film. Kim and workers used wrinkled photovoltaic devices to increase light harvesting in their organic photovoltaic device, demonstrating a 47% improvement in photocurrent compared to a flat control device. [66] Finally, Ende et al. established a voltage-controlled wrinkling system. Using a dielectric elastomer, sandwiched between two conducting electrodes, wrinkles could be removed by simply turning the power source on or off. The wrinkle wavelengths themselves were tuned by the amount of voltage that was applied. As the authors note, such a system offers promising applications in

switchable mirrors, smart glass, and variety of other tunable electricity-based systems. [67]

Exploiting the topography from wrinkles, a number of different coatings applications have also been developed. Wrinkled PDMS substrates, for example, were shown to exhibit increased resistance to marine fouling (i.e., barnacles) for over 16 months when submerged into seawater and also aided in removal of smaller marine organisms by gentle wiping using a Kimwipe. [68] Wrinkles can also be used to fabricate materials capable of tunable adhesion. Lin et al. demonstrated increased adhesion as a wrinkled PDMS elastomer was slowly stretched due to increased contact surface area between the PDMS elastomer and a glass probe that was used to measure the pull-off force required to detach from the elastomer. [69] Davis et al. noted modulus and wavelength-dependent adhesion of the probe to PDMS elastomers with varied mechanical properties. [70] Several researchers have also combined wrinkles with other forms of topography to enhance material functionality, fabricating hierarchical structures. Jeong and coworkers, for example, introduced periodic pillars on top of microwrinkled PDMS ( $\lambda = 75 \mu\text{m}$ ), creating an adhesive that maintained its original adhesion strength over 100 cycles of attachment and detachment, similar to a gecko's foot. [71]

The influence of topography on cell response has attracted considerable interest in the fields of biomaterials and tissue engineering. Specifically, topography has been shown to induce physical alignment of the cell body and has also been shown to promote cell differentiation among several stem cell lines. [20,36-38,40,72-85] In the human body, for example, major tissues, such as cardiac, neural, and bone tissue, require cellular alignment for appropriate biological function. Wrinkles have been utilized as a

material platform for inducing cell alignment and differentiation. [64,77,78,80,86] Through directed cell differentiation, human mesenchymal stem cells, for example, exhibited osteogenic differentiation when cultured on lamellar wrinkle morphologies, while hexagonal wrinkle morphologies promoted adipogenic differentiation. [64] Myogenic differentiation was also established using an alternative poly( $\epsilon$ -caprolactone) wrinkle system with smaller wavelengths. [81] Wrinkles, being dynamically tunable, have also been employed to control hMSC alignment. Using fibronectin-coated, wrinkled PDMS, Guvendiren and Burdick demonstrated reversible cell alignment through stretching and destretching of the polymer. [87] In a prestretched state, the material exhibits no wrinkling and thus cannot align the hMSCs. However, upon destrain, wrinkles formed, thus directing cell alignment. This process could be repeated to either induce hMSC alignment or to remove it.

Stafford and coworkers even adapted the wrinkling phenomenon in developing a new measurement technique, *strain-induced elastic buckling instability for mechanical measurements* (SIEBIMM) to probe the elastic moduli of thin films. [59,88] In this approach, a thin high modulus polystyrene film was either spincoated or flowcoated onto a silicon wafer. Through interferometry, the thickness of the film was measured, and transferred onto a strained PDMS elastomer of known modulus. Upon releasing the strain on the PDMS, wrinkles, with wavelength  $\lambda$ , were formed. Employing the wrinkle wavelength equation with the measured wrinkle wavelength, skin thickness, and elastomer modulus, the modulus of the skin layer is obtained. The authors demonstrated that they were able to accurately capture the modulus of the polystyrene films as thin as 40 nm.

### 1.3 Photopolymerizations

Photochemistry describes a class of reactions that are activated upon application of light (ultraviolet (UV), visible or infrared (IR)) and is a versatile tool in the polymer chemistry toolbox, with applications in dental materials, [89-94] 3d-printing, [95] microchip fabrication, [96] stimuli-responsive materials, [97-103] among many others.

For a photochemical reaction to occur, the absorption spectra of the initiating species (i.e., photoinitiator) must have some overlap with the emission spectra of the light source. Upon irradiation, the initiating molecule will absorb an incoming photon; in photochemical processes, one photon will lead to a single reaction event. However, for the reaction schemes discussed in this thesis, the initiating species triggers a ‘cascade’ event. If the absorbed photon has sufficient energy, electrons in the target molecule will transition to an excited singlet state. [104] At this point, the excited molecule can experience either (1) fluorescence (excited state to ground state), (2) intersystem crossing (ISC) to a triplet state, which generates a reactive intermediate that can trigger the desired chemical reaction, (3) phosphorescence (triplet state to ground state), or (4) dissipation of the absorbed energy in the form of heat. In the context of photochemical reactions, only (2) can lead to a chemical transformation in the form of isomerizations, bond forming or bond breaking, all of which have been demonstrated in a variety of photopolymerization systems.

Photochemistry offers several unique advantages over traditional reactions. First, due to the high energy of photons, photochemical reactions can be carried out rapidly under ambient conditions. [104] The energy of a single photon can be calculated using  $E_{\text{photon}} = hc/\lambda$ , where  $h$  is Planck’s constant,  $c$  is the speed of light, and  $\lambda$  is the wavelength of light used. At commonly used wavelengths, including 365 nm, 405 nm, and 470 nm, the energy of an incident photon is roughly 130 times, 120 times, and 100

times, respectively, more than the thermal energy,  $kT$ , required to activate a reaction at room temperature. A consequence of using such high energy photoinitiation is that photoactive species tend to be stable at room temperature in the absence of the light source. This leads to the second advantage, spatiotemporal control. By simply turning the light source on or off, the reaction can be activated or deactivated, offering a facile means to initiate or terminate a photochemical process at any time. Moreover, photochemical reactions can also be controlled spatially, often utilized in development of micro- or nano- structured polymer materials. For 2D spatial control, photomasks are employed to selectively expose or shield the photoactive material to the light in a process known as photolithography. Exposed areas will polymerize, while the unexposed areas remain unreacted and can subsequently be rinsed away with solvent. With more complex optical setups, it is also possible to gain 3D spatial control, enabling the formation of 3D polymeric structures with nanoscale resolution. [105-108] Lastly, because many photochemical procedures can operate in the absence of solvent or harsh processing environments, they are also considered a ‘greener’ process.

While photochemistry offers excellent control over reactions, there are two primary limitations. First, reactions are affected by the light intensity and is governed by the Beer-Lambert Law, as shown in Equation 1.6:

$$I = I_0 10^{-\epsilon cd} \quad (1.6)$$

where  $I$  is the intensity exiting the photoactive material,  $I_0$  is the incident intensity,  $\epsilon$  is the molar absorption coefficient,  $c$  is the concentration of the absorbing species and  $d$  is the optical path length (i.e., thickness of the photoactive material). In other words, light intensity decays exponentially as it passes through a material. For

photopolymerizations, because the rate of polymerization  $R_p$ , scales with absorbed light intensity,  $I_a$  [109]:

$$R_p \sim (I_a[PI])^\alpha \quad (1.7)$$

where  $[PI]$  is the photoinitiator concentration and  $\alpha$  is a constant (0.5 for bimolecular termination and 1.0 for unimolecular termination), the rate of reaction in the lower layers of the material will be slower compared to the rate at the surface. Additionally, the absorption profile may change as a function of time. As the photopolymerization occurs, and various species chemically transform, the absorbance of the material can increase (photodarken) or decrease (photobleaching), which may further alter the rate of polymerization. Because of the Beer-Lambert law, the absorption profile of a material may also be tuned via the addition of photoabsorbers, compounds that absorb specific wavelengths of light strongly but do not contribute to the reaction. For commercial photoabsorbers, the energy absorbed by the photoabsorbing molecule is converted into an intramolecular bond-forming process. The above factors must be considered when designing photopolymerized systems, particularly if the samples are ‘optically thick’, as the variation in polymerization rates may lead to variations in material property within the sample.

Photolithography also sets a lower limit on polymerization resolution. Because of light diffraction, it is impossible to spatially pattern features smaller than the wavelength of the light source that is used. However, recent advances have enabled patterning of sub-diffraction features, including multiphoton absorption [105-107] and two-beam optical lithography. [108,110,111] In multiphoton absorption, the photoactive species must absorb  $n$  photons to reach an allowed excited state. Through a pulsing femtosecond infrared laser, focused through a high numerical aperture

microscope objective, it is possible to confine features down the hundreds-of-nanometers length scale. In two-beam optical lithography, two beams are superimposed over the area where reaction is desired. The first beam is used to excite the photoactive molecules. A second donut-shaped beam (center of the beam is dark) is overlapped with the former, inducing depletion of the excited state of the molecules in the outer areas around the first beam, inhibiting any reaction from occurring where the two beams overlap. This process has led to the polymerization of nanowires with as low as 9 nm diameters. [110]

#### **1.4 ‘Click’ Chemistry and Polymer Networks**

In 2001, Sharpless, Kolb and Finn defined a new concept for the chemical synthesis called ‘click’ reactions, allowing the linking of heteroatoms (C-X-C). [112,113] To be considered a ‘click’ reaction, it had to be ‘modular, wide in scope, give very high yields, generate only inoffensive by products that can be removed by nonchromatographic methods, and be stereospecific’. Other criteria included insensitivity to oxygen and water, reacting under mild conditions, and orthogonality to other chemical reaction schemes. These criteria pointed to one thing – simplicity. The purpose of the ‘click’ concept was to develop a library of simple reactions, regardless of when the reaction was first discovered.

One of the more widely utilized ‘click’ chemistries is the thiol-ene reaction. Despite being utilized as early as the 1930s, thiol-ene chemistry wasn’t recognized as a ‘click’ reaction until 2010 by Hoyle and Bowman. [114,115]

The thiol-ene reaction is a reaction between a thiol with a vinyl (C=C) functional group, generating a single covalent S-C bond. The reaction can proceed via one of two mechanisms as shown in Figure 1.4, which is dictated by the ene species. If the ene is

electron deficient, this reaction will proceed through Michael-type addition (Figure 1.4a). In the presence of a base catalyst, a hydrogen will be abstracted from the thiol, generating a thiolate anion. This thiolate anion will subsequently attack an ene, forming a S-C bond and a carbanion. Finally, this carbanion can abstract a hydrogen from a new thiol molecule, creating another thiolate anion. In the presence of a nucleophilic catalyst, a carbanion is generated on the ene as the starting point in the reaction rather than a thiolate. It is also worth mentioning that special photo-caged base catalysts have been developed to afford spatiotemporal control to the thiol-Michael reaction. [116,117] These photo-caged bases are molecules that cleave when irradiated with a specific wavelength of light, generating a highly reactive base catalyst to trigger the thiol-Michael reaction.

If the ene is electron-rich, the thiol-ene reaction will proceed through a radical-mediated pathway in the presence of a radical initiator (Figure 1.4b). The reaction mechanism is similar to that of the base-catalyzed Michael reaction, with the thiyl radical being formed rather than the thiolate anion. It is important to note that despite being a radical mechanism, this reaction is not inhibited by oxygen, unlike traditional free radical homopolymerizations. This is because when a thiyl radical reacts with oxygen ( $O_2$ ) to form S-O-O $\cdot$ , which can further abstract a hydrogen from a thiol to continue the reaction cascade.

### **1.4.1 Thiol-ene kinetics**

The structure of thiol and ene monomers will affect the reactivity and kinetics. [114,115,118-121] With respect to ene monomers, the functional group reactivity increases as the electron density of the ene decreases, as follows:

norbornene > vinyl ether > propenyl > alkene > N-vinylamide > allyl ether > allyltriazine/allylisocyanurate > acrylate > N-substituted maleimide > methacrylate > styrene > conjugated diene

The four exceptions to the reactivity trends here are norbornene, which has the highest reactivity associated with instability due to ring strain, and methacrylates/styrene/conjugated dienes which are less reactive, being a more stable intermediate when a hydrogen is abstracted.

For radical mediated thiol-ene reactions kinetics, the more electron-rich the C=C is, the faster the reaction will proceed. Because the C=C is adjacent to an electron donating moiety, these reactions will proceed in a step-growth mechanism with thiol monomers rather than a chain growth mechanism with itself, which commonly associated with free radical polymerizations.

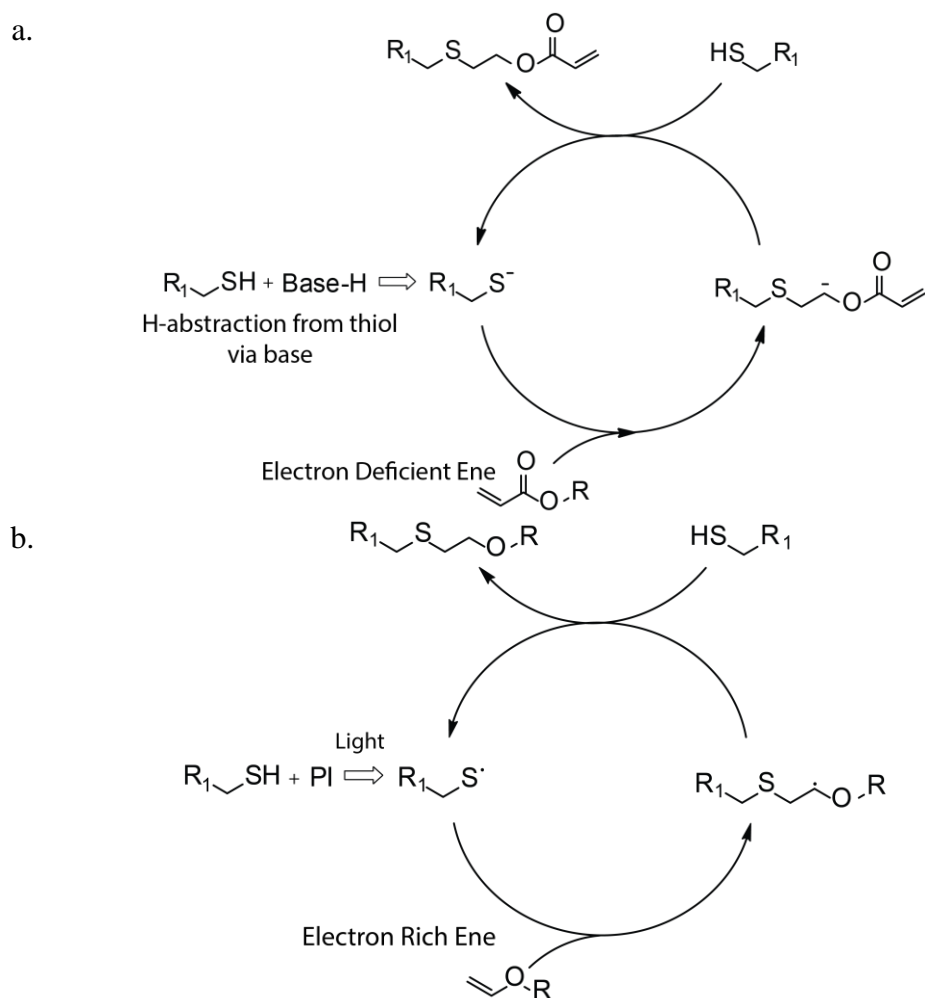


**Figure 1.4 Thiol- Michael and thiol-ene reaction schemes.** A) In a thiol-Michael reaction, a catalytic base abstracts a hydrogen from a thiol monomer, generating a thiolate anion, which will subsequently form a covalent bond to an electron deficient ene. This generates a carbanion on the ene species which can further abstract another proton from a thiol monomer, thus repeating the entire cycle. B) The thiol-ene reaction follows a similar mechanism except that it requires an initiator (i.e., photoinitiator) to catalyze the reaction.

For thiol-Michael reactions, Chan et al. showed varied success when reacting different base catalysts with thiol and electron-deficient ene monomers. Simple alkylamine and catalysts (i.e., triethylamine) showed faster kinetics with increasing nucleophilicity of the catalytic species. [119] The authors also employed a series of tri-substituted phosphine nucleophilic catalysts, which exhibited reaction rate constants orders of magnitude higher than their alkylamine counterparts. Other nucleophiles that can be used include water-soluble bicyclic amidines and imidazoles. Beyond the rapid kinetics of the nucleophile-mediated Michael addition, Chatani and co-workers introduced temporal control, combining catalytic amounts of triphenylphosphine with methanesulfonic acid. [122] The incorporation of methanesulfonic acid created an induction period, where no reaction occurred. After the induction period, the reaction proceeded at the same rate as if no acid was introduced. This temporal control is significant as it allows time for the thiol-ene monomers to be mixed and cast without any significant reaction occurring. One final important consideration in the utilization of nucleophilic catalysts is the potential to trigger unwanted side reactions including the aza-Michael or oxa-Michael reaction in the presence of water. However, given the speed of the reaction, the temporal control, and the relatively small amount of nucleophilic species added (catalytic), the desired thiol-Michael reaction is easily achieved with minimal side reaction.

### **1.4.2 Polymer Networks**

To form the elastomers used in wrinkling applications, liquid monomers are typically reacted to form a single, continuous polymer network. Multifunctional monomers can be used to physically or chemically join two or more polymer chains together, known as ‘crosslinking’. As conversion,  $p$ , for a liquid monomer species goes

from zero (no reaction) to one (complete conversion), low molecular weight polymer chains begin to form. As the polymer molecular weight increases further, the polymer will become insoluble in the liquid monomer, thus forming a gel. The conversion at which an infinite polymer network is formed through linking of smaller polymer units is called the 'gel point'. [123] Further conversion of the liquid monomer will add to the solid gel until the liquid monomer is either fully reacted or cannot reach a reactive site due to diffusion limitations.

The molecular weight evolution of the polymerization can occur through two distinct reaction mechanisms, step-growth and chain-growth. A step-growth mechanisms are characterized by very rapid consumption of the monomers to form a distribution of low molecular weight species, which ultimately further react to form a continuous network. The presence of the low molecular weight species at the initial stage of the polymerization enables the reaction to proceed to very high functional group conversions before gelation occurs. Macroscopically, networks formed via step growth mechanisms tend to be more homogeneous.

A chain-growth mechanism, on the other hand, is characterized by a very rapid increase in polymer molecular weight at low monomer conversions. As opposed to forming smaller dimers/trimer/tetramer units which will add to one another, chain-growth polymerizations promote addition of monomers to a few propagating chains. Because high molecular weight polymers are generated rapidly, chain-growth polymers achieve gelation at lower monomer conversions, which can lead to diffusion-limited conversion of the monomer species and a more heterogeneous network compared to a step-growth polymer.

The mechanical properties (i.e., modulus) of the resultant networks can be tuned by the molecular structure of the monomer species and number of functional groups per monomer. Monomer species containing flexible aliphatic chains (polybutadiene), for example, will yield more stretchable polymers, whereas monomer species with more rigid ring structures (i.e., BPA, polycarbonate) will yield much higher modulus materials. The number of functional groups per monomer affects the crosslink density of a network, which is a measure of how many crosslinks exist per unit volume and can be related to the macroscopic material modulus via equation 1.8.

$$G = \nu kT \quad (1.8)$$

where  $G$  is the shear modulus,  $k$  is the Boltzmann's constant,  $T$  is the temperature, and  $\nu$  is the crosslink density. As demonstrated in Equation 1.8, the modulus increases with increasing crosslink density. Thus, selection of monomers with a high degree of functionality will yield higher crosslinked or higher modulus materials.

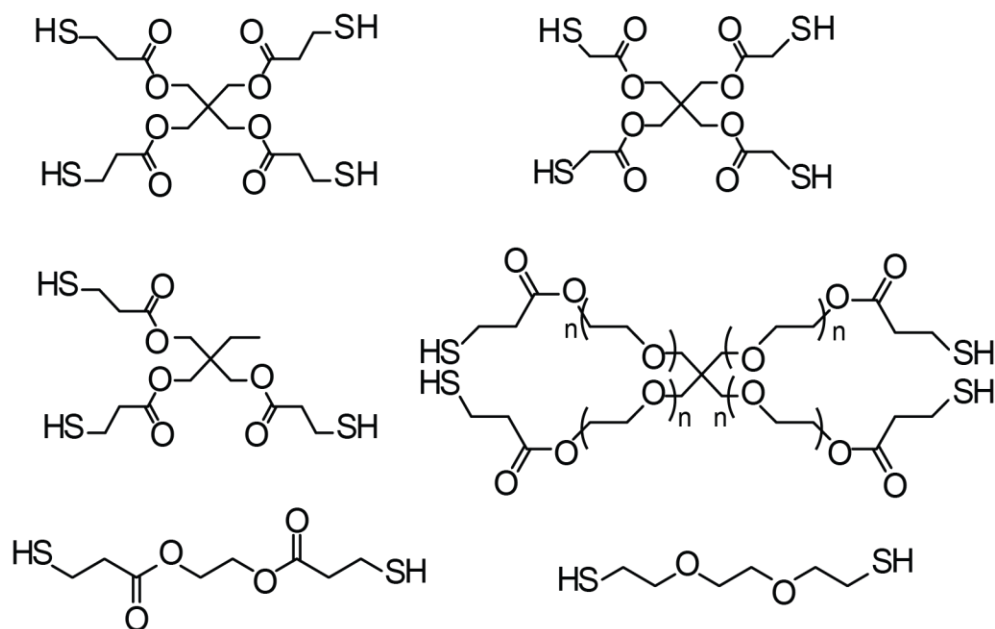
## 1.5 Thiol-Ene Networks

Thiol-ene chemistry has been utilized extensively to form polymer networks. Mechanistically, both the thiol-Michael and the thiol-ene reactions proceed via step-growth polymerization. As such, thiol-ene networks typically achieve full monomer conversion forming a macroscopically homogenous material.

The versatility of thiol-ene chemistry in creating polymer networks lies in the diverse library of thiols and enes that are either readily synthesized or commercially available. As shown in Figure (1.5), there is a wide variety of multifunctional thiols and enes that can be selected to create a thiol-ene network. As mentioned previously, careful selection of the monomer species as well as the number of functional groups per monomer will lead to the formation of networks with tunable mechanical properties

ranging in several orders of magnitude. Because the thiol-ene reaction is self-limiting (i.e., reaction terminates once one species is fully reacted), controlling the stoichiometry of the thiols and enes monomers will enable tunability of the chemistry. Specifically, if a polymer is created with either excess thiols or excess enes, those residual functionality will remain unreacted in the network after their complementary functionality has achieved full conversion. These tools are instrumental in the design and formulation of thiol-ene materials.

## THIOLS



## Enes

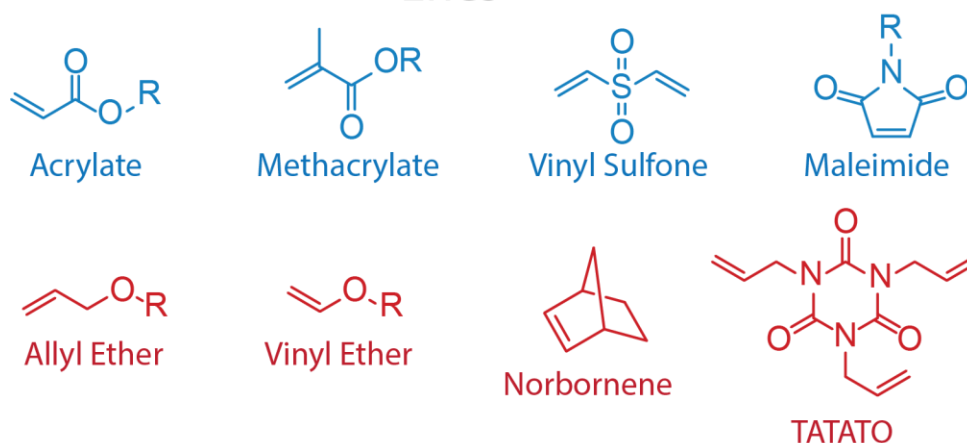


**Figure 1.5 Typical thiol and ene structures.** Number of functional groups and molecular architecture (i.e., ring structures) dictate thermomechanical properties of resultant crosslinked network. The blue enes are electron deficient enes, requiring the use of a nucleophile or base catalyst. The red enes are electron rich, requiring a radical initiator to catalyze the reaction. Many of these compounds are commercially available.

## 1.6 Thesis Overview

The goal of this thesis was to develop a multi-tiered approach to control polymer surface properties through elastic modulus, surface chemistry and surface topography. Specifically, spatially confined and aligned wrinkle structures were developed using thiol-ene chemistry and photolithography, which enable rapid formation of surface texture. These wrinkled surfaces were modified in a step-by-step functionalization process to enable control over surface chemistry. Finally, through thiol-ene formulation, polymers with moduli ranging from MPa to GPa could be easily formed, thus affording control over modulus. As many of the techniques and processes employed in this thesis, including photopolymerization, are a widely-utilized industrial techniques, the work described in this thesis should provide a template for facilitating commercial scale-up of wrinkling technology.

The development of a rapid, facile method to generate wrinkled surfaces using a two-tiered polymerization approach is presented in Chapter 2. The first thiol-ene polymerization generates the chemically-crosslinked, low modulus elastomeric foundation, while the second acrylate free-radical photopolymerization creates the higher modulus skin layer. This process is faster than previously established wrinkle systems and affords control over wrinkle orientation, confinement and material shape, facilitating potential efforts for commercialization. In Chapter 3, surface topography meets surface chemistry. Through ‘click’ chemistry, I demonstrate the ability to efficiently functionalize the surface of these wrinkle structures, leveraging oxygen inhibition effects associated with the photopolymerization process used to form the wrinkles initially. As a demonstration of a potential application, in collaboration with Dr. April Kloxin’s biomaterials group, human mesenchymal stem cells (hMSCs) are cultured on the surface of wrinkled polymer. In the presence of covalently

functionalized RGDS-peptides, the hMSCs will bind to the polymer surface. However, surface passivation is also possible by introducing hydrophilic moieties, hydroxyl ethyl acrylate, which prevent the hMSCs from spreading. More importantly, the hMSCs exhibit cellular alignment when seeded on the wrinkled topography of the polymer. This is of particular interest to the tissue engineering community, where cellular alignment is often required for tissue functionality (i.e. nerves, muscles, and bones). The simplicity of the ‘click’ reactions allow for a wide array of functionality to be introduced to the material surface, presenting an additional control handle for materials development. In Chapter 4, submicron photowrinkle formation is introduced. Employing flowcoating processes, a nanoscale thiol-ene skin layer is generated with ene-rich functionality. This skin layer is subsequently transferred to a thiol-rich thiol-ene elastomer. The excess functional groups are linked through photopolymerization, producing a covalently attached bilayer wrinkle system. Flowcoating enables the sub-micron wrinkles formation via nanometer-thick films, affords control over the skin and foundation moduli through formulation, and allows spatial confinement and alignment of wrinkles through photolithography. These features offer an unprecedented level of control over modulus, chemistry and topography. Importantly, the ability to flowcoat photocurable monomer systems enables new thin film applications (i.e. membranes) and stimuli responsive systems through the incorporation of custom-synthesized ene monomers, which can be integrated into the thiol-ene formulation. Finally, in Chapter 5, summary and perspective on future directions for photodirected wrinkling is provided.

## Chapter 2

### PHOTOWRINKLING ON A THIOL-ELASTOMER: TWO-TIERED POLYMERIZATION [124]

All text and figures reprinted with permission from Ma, S. J., Mannino, S. J., Wagner, N. J. and Kloxin, C. J., *ACS Macro Letters*. **2013**, 2, 474-477. Copyright 2017 American Chemical Society.

#### 2.1 Introduction

The majority of the investigations of wrinkling phenomenon in elastomer materials utilize poly(dimethylsiloxane) PDMS [52-59,63,65,70,87,125-141]. This is because (1) the material is commercially available as a two-component precursor which can be easily mixed in specific ratios to achieved a desired modulus, (2) the material is easily deformable and (3) the surface is readily converted into a high modulus, thin silicate skin layer upon exposure to UV–Ozone (UVO), plasma oxidation, or strong acids (i.e., nitric acid). A variety of techniques have been reported for deforming the PDMS foundation, including thermal expansion, [53,142] swelling, [129,136,143] and mechanical strain. [43,46,54,56,65,68,69,133,144] Bowden and coworkers demonstrated wrinkling through thermal expansion of a PDMS substrate followed by subsequent UVO treatment [53] or gold deposition [52] atop the heated surface. Upon cooling, the PDMS foundation will contract to its original size and the mismatch between the skin and foundation layers generates buckles. Crosby and coworkers presented a novel one-step swelling approach to wrinkle formation by using acrylic monomers to both form and swell the foundation layer using UV-oxygen. [143] Lin et

al. [65] established the ability to create well-ordered herringbone structures through sequential biaxial mechanical strain on PDMS.

Despite this growing body of research, the precise control and orientation of the wrinkle formation necessary to engineer the surface topography for specific applications remains a challenge. Spatial variations of modulus can direct wrinkling through lateral stress-dissipation, which results in the alignment of wrinkles perpendicular to regions of lower modulus. [43,53] However, as UVO treatment is a flood cure process, the spatial control of stress-dissipation has primarily been limited to physical stencils, [43,53] or holes placed into the PDMS foundation [54] prior to UVO treatment. After UVO treatment, the unoxidized regions allow the harder silicate layer to dissipate the high lateral stress and direct wrinkling. Huck et al. [145] demonstrated a novel alternative to generate wrinkles, where PDMS was swollen in a dichloromethane-benzophenone solution and irradiated using photomasked UV light (254nm, 10-30 min), resulting in a higher crosslink density in the exposed regions. The sample was subsequently heated, causing different extents of thermal expansion in the elastomer due to differences in the moduli between the exposed and unexposed regions. These samples were also coated with gold prior to cooling, providing a greater modulus mismatch and enhancing wrinkling. Importantly, the photopatterned regions were shown to establish a boundary condition that directs the wrinkling phenomenon in a manner similar to the utilization of physical constraints. [145]

In this chapter, I introduce a new method to generate highly ordered and confined wrinkles using a photodirected two-tiered polymerization approach. Thiol-ene elastomer is formulated with excess acrylates, which can be further photopolymerized to generate a higher modulus skin layer in the presence of a

photoabsorber. In employing photopolymerization, I demonstrate spatiotemporal control of the wrinkle formation while maintaining the ability to orient the wrinkles in a variety of configurations. Lastly, I can also independently control the geometry of the material, facilitating lamination of these films in coating applications.

## **2.2 Materials and Methods**

### **2.2.1 Materials**

Pentaerythritol tetramercaptopropionate (PETMP) was kindly supplied from Evans Chemetics. Tetraethyleneglycol diacrylate (TEGDA) was purchased from TCI America. The base catalyst, triethylamine (TEA), was purchased from Sigma Aldrich. The photoinitiators, Irgacure 184 (1-hydroxy-cyclohexyl-phenyl-ketone) and Irgacure 819 (bis(2,4,6-trimethylbenzoyl)-phenylphosphineoxide), and the photo-absorber, Tinuvin 328 (2-(2H-benzotriazol-2-yl)-4,6-ditertpentylphenol), were donated from BASF-CIBA. All chemicals were used without purification.

### **2.2.2 Elastomer formulation**

Resins were formulated with PETMP and TEGDA at a functional group ratio of 1:2 (thiol to acrylate) with 0.5 wt% Tinuvin 328 (T328) and 0.5 wt% Irgacure 184 (I184). T328 was mixed with TEGDA and vortexed until fully dissolved. I184 was mixed with PETMP and heated slightly to increase the rate photoinitiator dissolution. The TEGDA-T328 mixture was subsequently poured into the PETMP-I184 mixture and vortexed. If bubbles were present after mixing, the mixtures were degassed for up to 5 minutes. Finally, 2.5 wt% TEA was added to each sample to catalyze the first-stage Michael-addition polymerization, and mixed for an additional 20 seconds before pouring the mixture into a gasket mold (0.16 cm thickness). For the uniaxial stretching

experiments, the gasket molds were cut into 4 cm x 2 cm rectangle. For the biaxial stretching experiments, the mold dimensions were 4 cm x 4 cm. All samples were used within 24 hours of curing.

To lock in the shape of the wrinkled polymer in an arbitrary geometry, 0.5 wt% Irgacure 819 (I819) was added to the formulation and vortexed. Once the wrinkles were formed using the aforementioned procedure, tape was used to hold the substrate in a specific geometry and exposed to 405 nm light ( $60 \text{ W/m}^2$ , 16 minutes).

### **2.2.3 AFM Modulus Measurements**

The modulus was determined by a Bruker Bioscope Catalyst AFM mounted on a ZEISS Axiovert 2000 using an unmodified Scanasyst Air AFM tip. The moduli obtained were relative to a 2.5 MPa PDMS calibration sample.  $5 \mu\text{m} \times 5 \mu\text{m}$  areas were scanned in tapping mode at 0.501 Hz. Elastomer samples dosed with UV light for 5, 10, and 20 seconds were created and moduli measurements were taken on both the skin and foundation sides.

### **2.2.4 Wrinkle Formation**

The stretching apparatus was constructed using manually controlled micrometer linear stages attached to an optical breadboard (Figure 2.1). Samples were affixed onto each stage by taping the bottom side of the film with double-sided tape and the top of the film with single-sided tape. All samples were irradiated under 20% strain.

The modulus mismatch was created using the aforementioned second-stage radical polymerization using 365 nm light (Exfo, Omnicure Series 2000 UV lamp) at  $80 \text{ W/m}^2$ . Experiments were conducted at discrete exposure times (5 to 40 seconds) and constant strain. Glass coverslips were overlaid atop half the samples to determine

the effects of oxygen inhibition. The coverslip was placed on top of the polymer film with intimate contact, which served as an oxygen barrier between the atmosphere and the surface of the polymer film during the radical polymerization.

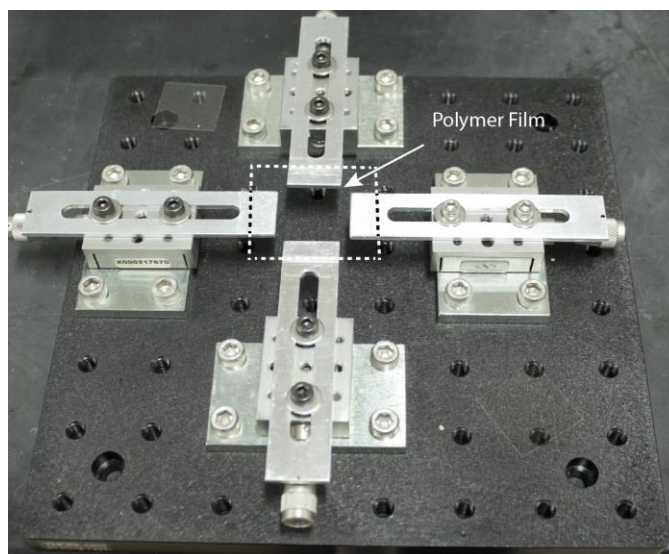


**Figure 2.1** Linear stage set up for uniaxial and biaxial strain. Polymers were cut, centered, and held in place with tape. Samples were then strained and released in a sequential manner.

### 2.2.5 Wrinkle gradients and photopatterning

Gradient experiments were conducted by covering strained samples with an opaque polyester sheet prior to second-stage polymerization. The opaque sheet was attached to a syringe pump apparatus and pulled across the sample at a constant rate, slowly exposing the sample to the irradiating source.

Wrinkle confinement experiments were conducted by irradiating the sample through a transparency photomask. Prior to second-stage polymerization, the photomasks were placed on top of polymer samples (ca. 1mm above the surface).

### 2.3 Results and Discussion

Here, I employ a two-stage polymerization strategy similar to that of Nair et al. [146,147], where an elastomer is formed via one polymerization mechanism, but the second photopolymerization, which increases crosslink density, is restricted to the elastomer's surface. In the first polymerization, a base elastomer is synthesized using a stoichiometric imbalance of tetra-thiol and di-acrylate monomers, yielding a polymer network with excess acrylate functional groups (see Figure 2.2). Note that the initial thiol-ene polymerization is not inhibited by oxygen and cure times are significantly shorter than that of, for example, PDMS [119]. The second-stage, photopolymerization of the pendent acrylates is confined to a thin "skin" layer by introducing a photo-absorber (T328) into the formulation. Combining this approach with mechanical deformation (i.e., mechanophotopatterning) [97], enables wrinkle formation and confinement through photopatterning, rather than through physical defects or stencils, to design intricate patterns and facilitate local control over wrinkle wavelength.

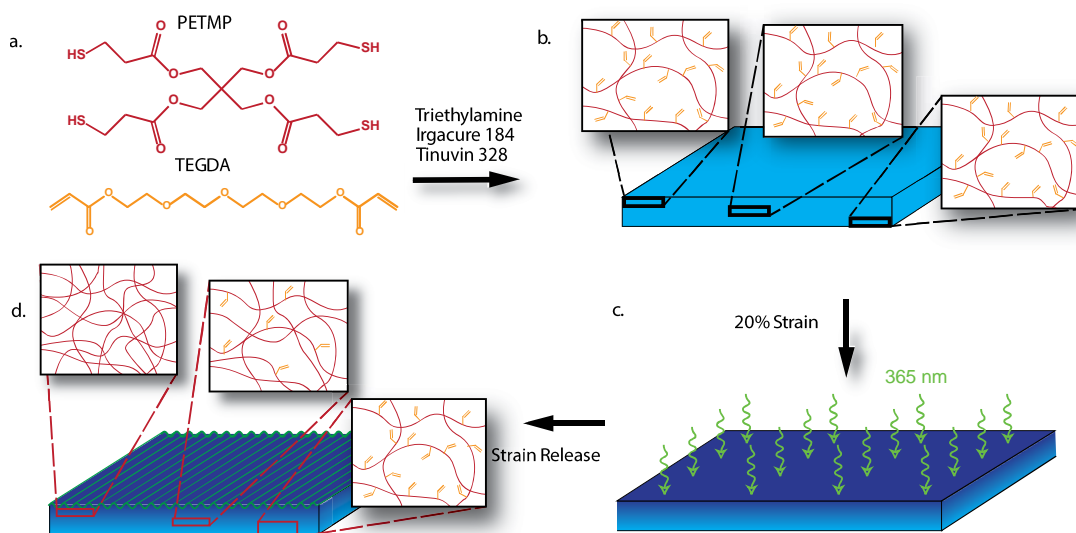


**Figure 2.2 Method of Generating Wrinkles on a thiol-ene surface.** Monomers **a)** pentaerythritol tetramercaptopropionate (PETMP) and tetraethylene glycol diacrylate (TEGDA) were reacted with triethylamine, photoinitiator (I184), and photoabsorber (T328) to produce a **(b)** thiol-ene network with a uniform crosslink density and excess pendant acrylates (first-stage polymerization). **(c)** Applying strain and 365 nm light induces radical polymerization of the acrylates (second stage polymerization). The photoabsorber confines the light to a thin skin layer at the surface. **(d)** Upon releasing the strain on the film, wrinkles are formed with a crosslink density (modulus) gradient

To generate wrinkles, the elastomer is mechanically stretched using linear stages. A skin layer is formed via photoinitiated radical homopolymerization of the pendant acrylate groups in the thiol-ene network in as little as 5 seconds, even in the presence of oxygen. As the second polymerization occurs within a very thin layer at the substrate surface, both irradiation time and oxygen exposure can be used to control the modulus and thickness of the skin layer. Oxygen can readily and continually diffuse into the matrix and will inhibit the acrylate polymerization. To further interrogate the effects of oxygen inhibition, samples with and without an oxygen barrier (i.e., coverslip) were examined with stylus profilometry. As shown in Figure 2.3a, samples employing

a coverslip have significantly increased wrinkling wavelength owing to a higher modulus in the skin layer. As the irradiation dosage is increased, the wrinkle wavelength increases with both the skin thickness and modulus (i.e.,  $\lambda_c \sim h(E_s/E_f)^{1/3}$ ), where  $\lambda_c$  is the wrinkle wavelength,  $h$  is the height of the skin layer, and  $E$  is elastic moduli and subscripts  $s$  and  $f$  denote the skin and foundation, respectively. [43,46]

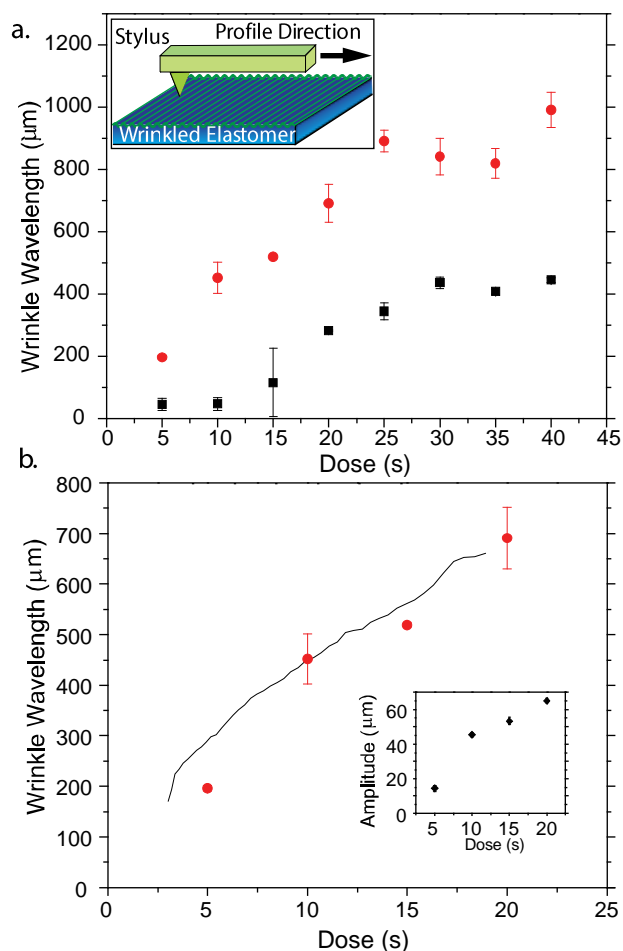


**Figure 2.3 Stylus profilometry of wrinkle wavelength versus dosage.** a) Films with a coverslip (red circles) and without a coverslip oxygen barrier (black squares) were irradiated for 5 to 40 seconds using 365nm light at  $80 \text{ W/m}^2$ . Wrinkle wavelength increased as a function of increasing irradiation duration. Samples masked with a coverslip exhibited larger wrinkles than the unmasked samples due to the absence of oxygen inhibition. Inset: Stylus profilometry schematic. b) Profilometry from wrinkle gradients (solid black line) shows good agreement with discrete wavelength data (red circles) (0 to 20 seconds, 365 nm at  $80 \text{ W/m}^2$  with coverslip). Accompanying amplitude data (inset) are consistent with scaling equation (see supporting information for profilometry setup).

It should be noted that our system does not have a well-defined foundation-skin interface, but rather a gradient in properties due to the attenuation of light with increasing depth into the elastomer. Using tapping mode AFM, I was able to approximate  $E_s$  and  $E_f$ , and thus, calculate an ‘effective’ skin thicknesses of 80  $\mu\text{m}$  at 20 second UV exposure. As expected, this thickness is a function of irradiation dose. In the absence of inhibition, the polymerization rate is highest at the surface but decreases exponentially according to the Beer–Lambert law (i.e.,  $R_p \sim I^{1/2} \sim I_0 e^{-A/2}$ , where  $I_0$  is the incident intensity and  $A$  is absorption) [123]. At longer cure times, the acrylates at the surface reach maximum conversion while the acrylates within the elastomer continue to photopolymerize. In this manner, a controlled frontal polymerization proceeds into the elastomer. The ‘effective’ skin thickness is limited by the penetration depth of the light, which is dictated by the incident intensity and concentration of photoabsorber (i.e., T328). As a consequence, the wrinkle wavelength, shown in Figure 2.3a, increases with increasing dosage, but eventually plateaus for longer dose times. In contrast to the samples with coverslips, which show immediate increase in wrinkle wavelength with dosage time, samples without coverslips show no significant change for the first 10 seconds, which I attribute to oxygen inhibition at the interface [148,149]. Our approach of using photopolymerization to form wrinkles enables spatioselective control of the wrinkle wavelength. As a demonstration, I have created a wrinkled surface with a linear gradient wrinkle wavelength (Figure 2b). After the first-stage polymerization, samples with a coverslip oxygen barrier were strained and covered with an opaque photomask that was subsequently removed at a constant rate during irradiation over a 20 second period.

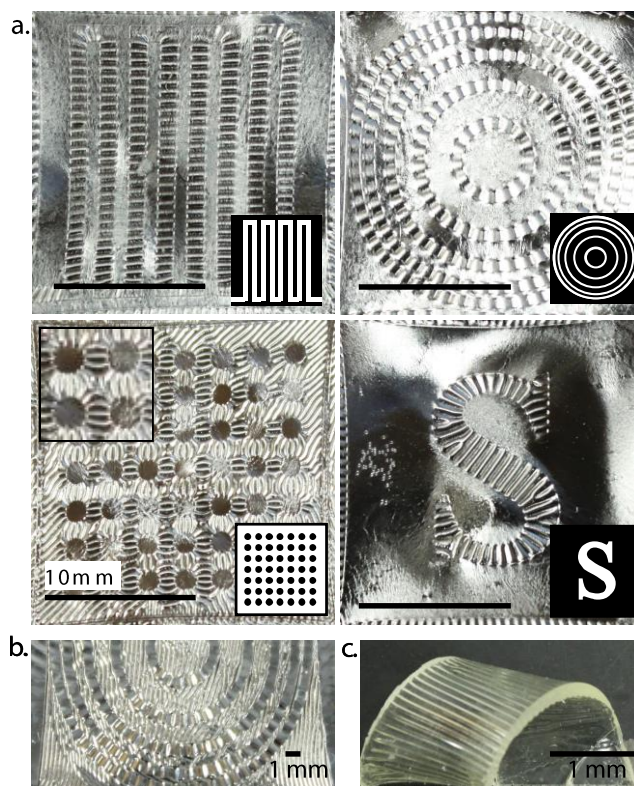


**Figure 2.4 Wrinkle formation via photopatterning on a biaxially stretched specimen.** a) Photolithography guides the alignment of the wrinkles perpendicular to the low stress regions of the thiol-ene elastomer. Samples were irradiated for 20 seconds under 365 nm light at  $80 \text{ W/m}^2$ . Scale bar represents 10 mm (inset: corresponding photomasks) b) Photopolymerized sample showing alternating wrinkle wavelengths. This pattern is created by stepwise dosing, first with a coverslip only ( $80 \text{ W/m}^2$ , 5 seconds) followed by two photomasks ( $80 \text{ W/m}^2$ , 5 seconds and  $80 \text{ W/m}^2$ , 10 seconds). c) Employing two different photoinitiators allows for wrinkle formation and shape memory. Wrinkles were formed using a procedure similar to (a). The coil shape was held in place using tape and exposed to 405 nm light ( $60 \text{ W/m}^2$ , 16 minutes).

Profilometry data of the gradient wrinkles plotted in Figure 2.3b (solid black line) shows the local wrinkle topology is in good agreement with experiments performed at the corresponding, uniform irradiation doses (red circles). These gradient wrinkles

will facilitate experiments to probe surface interactions over a continuum of length scales on the same sample. Wrinkle amplitudes (Figure 2.3b (inset)) are on the micron scale and increase with increasing dosage.

Our method also presents a novel approach to direct wrinkling using a photomask (Figure 2.4a). The regions of the polymer substrate that are exposed to light undergo the second-stage polymerization while the masked areas remain unchanged, thereby creating well-defined boundaries for wrinkle confinement. The low modulus regions allow the high modulus regions to relieve in-plane stresses, aligning the wrinkles perpendicular to the boundary of the mask. This is particularly advantageous because no additional chemical treatments are required nor are extra physical defects introduced into the polymer foundation. This approach provides a rapid method for generating wrinkles on an untreated thiol-ene foundation with excellent pattern fidelity. Moreover, by overlaying photomasks and irradiating the substrates in a stepwise manner, I can form several distinct wavelengths Figure 2.4b. This sequential masking introduces a pattern with controlled variations in irradiation on the elastomer, resulting in the novel wrinkle patterns shown in Figure 2.4b. The longer wavelengths are a consequence of longer exposure times, while the second alternating pattern contains smaller wrinkles.

Last, I illustrate the ability to use two photo-orthogonal photoinitiators to independently control surface wrinkling and increase the bulk modulus of the material. As the photoabsorber, T328, is transparent above 400 nm, a second, visible light photoinitiator can be utilized to trigger polymerization of acrylates in the bulk. A visible light photoinitiator, I819, which absorbs above 400 nm, was added to the monomer mixture prior to the first-stage polymerization. Wrinkles were created using the

aforementioned procedures with 365 nm light. The film was held in a coil shape and exposed to 405 nm light (Figure 2.4c). The resulting bulk polymerization creates new crosslinks, significantly increasing the modulus and thus “locking” the shape whilst maintaining the wrinkle structures. Thus, the final modulus of the material as well as its shape is controlled independently of the modulus of the surface layer and the wrinkle topography. This may have benefits for engineering surface-wrinkled materials with a broader range of surface and bulk moduli.

## **2.4 Conclusion**

Photopolymerization is a novel approach to spatioselectively control wrinkle formation, including gradients and complex patterns. Our system is highly tunable; modifying the types and amounts of photoabsorber, photoinitiator, and thiol–ene monomers as well as utilizing different light wavelengths and intensities provides multiple controls over the mechanical properties, shape, and surface topography of the material. Photo-orthogonality not only allows wrinkle formation but also enables the bulk polymer to be molded into desired geometries. The implementation of surface confined polymerization in a thiol–ene elastomer presents an attractive alternative to PDMS and other elastomers for the exploration of wrinkling phenomenon and ultimately for the a priori design and engineering of surface topography.

## Chapter 3

### CHEMICAL SURFACE FUNCTIONALIZATION OF WRINKLED THIOL-ENE ELASTOMERS

All cell seeding experiments and confocal image analysis were performed in collaboration with Eden Ford and Dr. April M. Kloxin.

#### 3.1 Introduction

Wrinkling or buckling on polymer surfaces presents a fast, cost-effective approach to generating surface topography. To generate wrinkles, a high modulus thin film is mounted on a strained, thicker lower modulus substrate. Upon destraining the elastomer, lateral compressive stress on the thin film results in spontaneous formation of wrinkle structures with wrinkle wavelength,  $\lambda \sim h(E_f/E_s)^{1/3}$ , where  $h$  is the film thickness and  $E_f$  and  $E_s$  are the film and substrate modulus, respectively. Through this approach, topography can be rapidly generated over large surface areas of material, and has led to numerous applications including optical and photovoltaic coatings, [66,67] switchable wetting surfaces, [144,150,151] tunable diffraction grating, [152] antifouling coatings[68], substrates for directed cell-alignment, [64,77,78,82] and flexible optoelectronics, [153,154] among many others. Despite the versatility of wrinkling, the majority of studies are performed on poly(dimethylsiloxane) (PDMS) polymers, [52,53,56-58,65,68,126,130,132] which lack facile methods to confine and align wrinkle features. Moreover, control over surface chemistry, an important handle for enhancing material performance, is limited.

To achieve functionalization, the PDMS surface is typically treated with plasma or ultraviolet oxidation (UVO), which transforms the naturally hydrophobic surface hydrophilic, [155-163] which occurs due to the formation of a nanometer-thick  $\text{SiO}_x$  surface. Unfortunately, this is a short-lived effect, as PDMS undergoes hydrophobic recovery, a process which restores the hydrophobic state of the PDMS surface over long times. [155,156,160] Hydrophobic recovery occurs due to inversion of polar groups from the surface into the bulk, diffusion of low molecular weight PDMS chains to the surface, and condensation of any free silanol groups. [155-157,164] Recent attempts have been made to stabilize the hydrophilicity through post-functionalization. [20,159,162,163,165,166] However, these protocols require long surface chemical treatment times, lack spatial control, [167] and require the use of plasma treatments, all of which limit the commercial viability of wrinkling technology for material applications. Extended plasma treatments have also been shown to induce crack formation in the PDMS surface. [168] On wrinkled PDMS substrates, functionalization has been introduced through physical adsorption of surface moieties, which also lack spatial control over chemical modification and results in a less mechanically robust coating. [87]

To address these limitations, we employ a two-tiered polymerization approach to generate wrinkled materials, with surface functional handles that can be modified after wrinkle formation. [124] The two-tiered polymerization scheme employs a thiol-Michael reaction of tetrathiol with excess diacrylates to generate an elastomer substrate with excess pendant acrylates in the network backbone. Through strained irradiation of the elastomer, free radical polymerization of the excess pendant acrylate moieties enables formation of the higher modulus skin layer. Light intensity and irradiation time

control the size of wrinkle features and through photopatterning, topography can be spatially confined and aligned.

To achieve surface functionalization of this wrinkled material, we leverage the oxygen inhibition associated with the radical photopolymerization used to form the skin layer. Specifically, unreacted acrylate moieties (due to O<sub>2</sub> inhibition) at the surface can be post-functionalized using the rapid efficiency of thiol-ene click reactions. By first coupling thiols to the surface acrylates, we demonstrate the ability to spatially control functionalization through radical mediated thiol-ene chemistry. To demonstrate the efficacy of our method, we employ our materials as cell culture substrates for directed cell-alignment of human mesenchymal stem cells (hMSCs), a cell line that exhibits alignment in the presence of wrinkled topography, which may promote a particular differentiation pathway (i.e., osteogenesis). [38,64,81,169,170] We establish that the material cannot only be modified with chemical cues (i.e., RGDS) to promote cell adhesion and spreading on the surface, but also induces cellular response to the topography through alignment with the troughs of the wrinkled structures.

## **3.2 Materials and Methods**

### **3.2.1 Materials**

Pentaerythritol tetramercaptopropionate (PETMP) was donated by Bruno Bock. Tetraethyleglycol diacrylate (TEGDA, >90%), 1,3,5-trimethylbenzene (TMB), 1,8-diazabicyclo[5.4.0]undec-7ene (DBU), quinine, 3-allyloxy-1,2-propanediol (APD), and methanesulfonic acid (MsOH, >99.0%) were purchased from TCI America. Photoinitiator, Irgacure 651 (I651) (2,2-dimethoxy-1,2-diphenylethan-1-one) and Irgacure 819 (I819) (Bis(2,4,6-trimethylbenzoyl)-phenylphosphineoxide), and

photoabsorber, Tinuvin 479 (T479) were donated by BASF. Triphenylphosphine (TPP, 99%) was purchased from Acros Organics. Diisopropylethylamine (DIPEA), hydroxy ethyl acrylate (HEA), 1H-1H-2H-2H-perfluorodecane thiol (PFDT) and dimethylphosphine (DMPP) was purchased from Sigma Aldrich. Acetonitrile (ACS Certified), dimethylformamide (DMF), methanol, and tetrahydrofuran (THF) were purchased from Fisher Scientific. Deuterated acetonitrile, methanol, and water were also purchased from Fisher Scientific. Amino acids, including alloc-protected lysine (K(alloc)), used in peptide sequencing were purchased from Chem-Impex or Chempep. Fluorescent label, Alexafluor 647 was purchased from Life Technologies Corporation. Trifluoroacetic acid (TFA) and triisopropylsilane (TIPS) was purchased from Chem-Impex. All chemicals were used without further purification.

### **3.2.2 Generation of wrinkled elastomers**

Photoinitiator I651 (0.5wt%), I819 (0.1wt%) and photoabsorber T479 (1.0wt%) were added to TEGDA in a scintillation vial and stirred at 1000 RPM until all components were fully dissolved. TPP (1.0 wt%) and MsOH (0.3 wt%) were then added to the mixture and stirred for 15 minutes. PETMP was then added to the mixture in a 1:2 thiol:acrylate stoichiometry and stirred for 3 additional minutes. The mixture was then cast between two glass slides with 1/16 inch spacer and allowed to cure overnight. All films were irradiated and wrinkled roughly 14.5 hours after casting.

Elastomer samples were placed on a custom made stretching apparatus and strained 20% uniaxially. A glass coverslip was placed atop the elastomer, which was then irradiated with 365 UV light (1 mW/cm<sup>2</sup>) (Omnigure S2000, equipped with a liquid light guide) for a preset amount of time. Samples are held in the strained position for five minutes after irradiation is complete, then destrained to yield wrinkles.

Photopatterned samples were processed similarly, with a photopattern placed on top prior to 365nm irradiation. Gradient samples were created by covering elastomers with a mask, which was slowly withdrawn over the irradiation duration. After 365 nm irradiation, samples were held in the strain position for 5 minutes. All samples were then destrained, placed on a glass slide, and irradiated with 405 nm light (2 mW/cm<sup>2</sup>, 10 minutes) without a coverslip to react the remaining free acrylates in the bulk. Samples were cut into 6mm x 6mm squares for functionalization.

### **3.2.3 Peptide Synthesis**

Pendant RGDS-containing peptides were synthesized as a functional handle to promote cell adhesion on the elastomer surface. Briefly, a sequence AhxWGRGDSK(alloc)G (RGDS) was synthesized using standard Fmoc solid phase peptide synthesis techniques. [171-173] After final deprotection of the Ahx monomer, 2 mg of the Alexa Fluor 647 (AF647) carboxylic acid succinimidyl ester was dissolved with 0.5 mmoles of peptide in 8 mL of DMF with 100  $\mu$ L of DIPEA overnight. Following this reaction, the peptide was cleaved from the resin using a solution of TFA/TIPS/deionized water (95/2.5/2.5) for three hours and precipitated from diethyl ether. The crude peptide was purified via HPLC, lyophilized, and analyzed by mass spectrometry.

### **3.2.4 LAP Synthesis**

The LAP photoinitiator was synthesized according to previously established protocols. [173, 174] Briefly, 2,4,6-trimethylbenzoyl chloride (1.6 g, 0.009 mol) was reacted with an equimolar amount of dimethyl phenylphosphonite (1.5 g, 0.009 mol). The solution was stirred for 18 hours at room temperature under argon, and subsequently

lithium bromide in 2-butanone was added to the solution at a 4x molar excess and heated to 50 °C for 10 minutes. After cooling, the solid precipitate was filtered and rinsed 3 times with 2-butanone to remove unreacted reagents. The remaining product was dried and analyzed using <sup>1</sup>H NMR.

### 3.2.5 Functionalization

Solutions containing PETMP in acetonitrile (15 mg/mL) were prepared in 20 mL scintillation vials. Catalyst, DMPP was then added (0.15mol %) and the mixture was vortexed for 30 seconds. Elastomer squares were submerged into the thiol containing solution for 60 seconds to functionalize the surface. After functionalization, the elastomer squares were removed and sonicated a 4 mL of acetonitrile for an additional 60 seconds.

HEA solutions were prepared by adding 0.5 mol% DBU to 2 mL of pure HEA. Freshly prepared thiol-functionalized elastomers were submerged into the HEA solution for 60 seconds. Samples were then removed and sonicated in 4 mL of deionized water for 60 seconds.

To prepare RGDS-functionalize samples, 25 μL of RGDS solution (40 mg/mL in deionized water, 22 mM LAP) were added to the surface of thiol-functionalized elastomers placed between two 1/16" Teflon spacers. A glass coverslip was immediately placed on top of the sample to ensure even coverage of the RGDS on the surface. Samples were irradiated with 365 nm UV light (10 mW/cm<sup>2</sup>, 60 seconds). Samples were subsequently sonicated in 3 mL of deionized water for one minute.

All samples were sonicated in an additional 4 mL of DI water for 60 minutes and dried under high vacuum at room temperature overnight.

### 3.2.6 Contact Angle Goniometry

Static contact angle measurements were performed by depositing 2 mL of water (purified with a Milli-Q water purification system) on the various functionalized samples (native, thiol, PETMP/HEA, and PETMP/RGDS) and analyzed using a Krüss GmbH FM41 Easy Drop goniometer under ambient conditions. Images were taken 1 second after droplet deposition and analyzed using the accompanying Drop Shape Analysis software. All measurements were performed in triplicate.

### 3.2.7 X-ray photoelectron spectroscopy (XPS)

To determine the appropriate operating solution concentrations for surface functionalization, XPS experiments were conducted using a Thermo Fisher K-Alpha+ XPS on PFDT-functionalized elastomer substrates, at varying PFDT solution concentrations between 0 mg/mL to 70 mg/mL. PFDT was selected due to the high fluorine signals observed in XPS. Surveys were conducted using 100 eV pass energy, 1 eV step size and 10 ms dwell time. For high resolution fluorine data, 20 eV pass energy, 0.1 eV step size and 50 ms dwell time were used. All experiments were conducted using the flood gun for charge compensation.

### 3.2.8 Fourier Transform Infrared Spectroscopy (FTIR)

Kinetic data was obtained out using a Nicolet iS350 FTIR in transmission mode. All experiments were performed in near-IR. Time-dependent conversions,  $\rho(t)$ , were taken as  $1 - \text{Peak Area}(t)/\text{Peak Area}(t=0)$  for both thiols ( $2612\text{-}2509\text{ cm}^{-1}$ ) and the C=C ene bond ( $6131\text{-}6265\text{ cm}^{-1}$ ). Formulations were casted between two glass slides, separated by 0.635 mm PVC shims. Long-time experiments (4 hours) for the thiol-Michael reaction were conducted using a room temperature DTGS detector, with a spectral resolution of  $4\text{ cm}^{-1}$ , averaging over 32 spectra. To characterize the free radical

polymerization, which is significantly faster, FTIR spectra was obtained using the MCT detector, averaging over 8 spectra with a spectral resolution of  $4\text{ cm}^{-1}$ . Conversion data was collected for 3 minutes, with the irradiation of the films starting 30 seconds after FTIR data collection began in order to obtain a baseline.

### **3.2.9 Nuclear Magnetic Resonance (NMR) spectroscopy**

To probe reactions of various monomer couplings for surface functionalization, <sup>1</sup>H-NMR studies were performed using a Bruker AVIII 400 or AVIII 600 NMR spectrometer. Excluding PETMP/K(alloc), which was dissolved in 70/10 acetonitrile-d<sub>2</sub>O due to solubility issues, all other reactions were performed in deuterated acetonitrile. Solutions were prepared with equimolar thiol and ene, with 1,3,5-TMB was added as an internal reference in a 1:3 molar ratio to the ene.

For thiol-Michael reaction, NMR spectra was collected with and without the addition of catalyst, representative of pre- and post-reaction. For radical-thiol ene reactions, all components, including photoinitiator, were mixed and spectra taken before and after UV irradiation. To conserve peptide material, Fmoc-protected K(alloc) was substituted for the RGDS peptide to monitor the reaction of the radical thiol-ene reaction.

### **3.2.10 Human mesenchymal stem cell culture and seeding**

Bone marrow-derived human mesenchymal stem cells (hMSCs) were expanded on tissue culture treated polystyrene in low glucose Dulbecco's Modified Eagle's Medium (DMEM) supplemented with 50 U/mL penicillin, 50 µg/mL streptomycin, 0.2% v/v Amphotericin B, 10% v/v fetal bovine serum, and 1 ng/mL basic fibroblast

growth factor (bFGF). Cells were fed every 2-3 days and were passaged at approximately 85% confluency.

Prior to cell seeding, all material samples were sterilized via germicidal UV light irradiation (254nm) for 30 minutes and placed into non-tissue culture treated 48 well plates. Cells were trypsinized from the tissue culture treated plates, centrifuged, and counted with a hemocytometer. Cells were then suspended in phenol red- and serum-free DMEM (supplemented with 50 U/mL penicillin, 50 µg/mL streptomycin, 0.2% Amphotericin B), and were seeded on top of the materials at 10,000 cells cm<sup>-2</sup>. After 12 hours of culture the media was switched out for 10% fetal bovine serum-containing phenol red-free DMEM (in addition to 50 U/mL penicillin, 50 µg/mL streptomycin, 0.2% Amphotericin B).

### **3.2.11 Confocal Microscopy**

Cells were washed with Dulbecco's phosphate-buffered saline (DPBS) after 3 days of culture on the substrates and fixed with 4% paraformaldehyde for 15 minutes at room temperature. After washing 1 x 5 min. with DPBS and 2 x 5 min. with 3% w/v bovine serum albumin (BSA) + 0.05% v/v Triton-X in DPBS, cells were blocked and permeablized (5% w/v BSA + 0.1% v/v Triton-X in DPBS) at room temperature for 1 hour. Cells were then incubated with Phalloidin Tetramethylrhodamine B isothiocyanate (Phalloidin-TRITC) solution (1:250 dilution, 5% w/v BSA, 0.1% v/v Triton-X in DPBS) for 3 hours at room temperature, followed by 1 x 5 min. DPBS wash and staining with DAPI (700 nM in DPBS, 30 minutes at room temperature). The substrates were washed 3x in DPBS prior to imaging.

Samples were imaged on a Zeiss LSM 880 confocal microscope (z-stacks, 80 images per stack, 2 µm spacing). For quantification of nuclear orientation relative to

wrinkles, average cell area, and cell density, fluorescent images (nuclei and F-actin) were processed and analyzed using NIH ImageJ software (Figure 3.1).

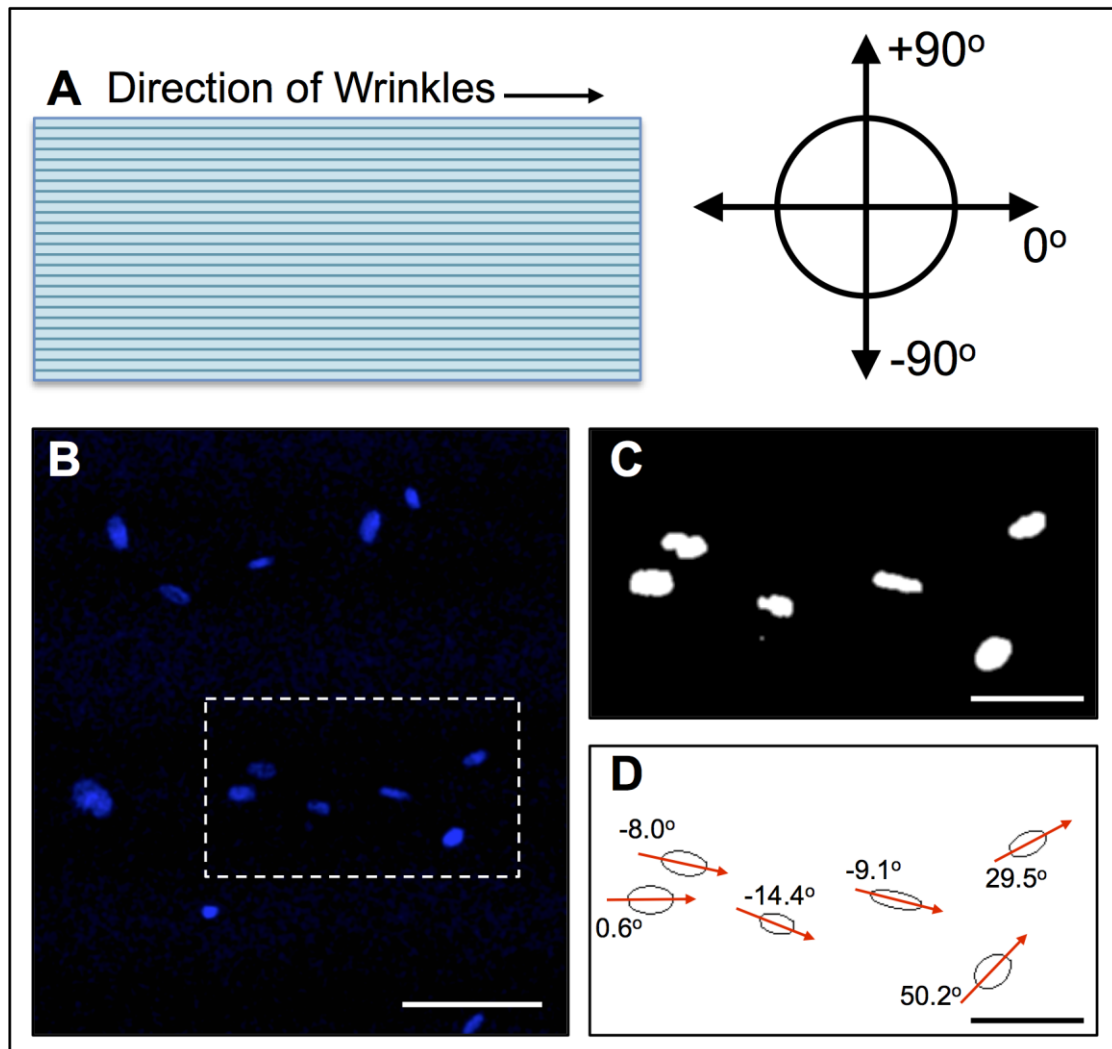


**Figure 3.1 Nuclear alignment quantification.** (A) The direction of wrinkles was assigned as  $0^\circ$  and nuclei direction was determined as the angle relative to the wrinkle direction. (B) Nuclei were stained with DAPI for visualization. Scale bar  $100\ \mu\text{m}$ . (C-D) Nuclei images were processed and each nucleus fitted with an ellipse, from which the angle of orientation was determined. Scale bar =  $50\ \mu\text{m}$ .

### **3.3 Results and Discussion**

To generate wrinkled materials, tetrathiol and excess diacrylate were mixed with photoinitiators (Irgacure 651 and Irgacure 819), photoabsorber (Tinuvin 479) and a catalytic amount of triphenylphosphine to form a homogeneous base elastomer (Figure 3.2). Methanesulfonic acid (MsOH) was added to create a reaction inhibition time allowing the thiol and ene components to be mixed and casted as films before polymerization occurs, as previously demonstrated in literature. [122]

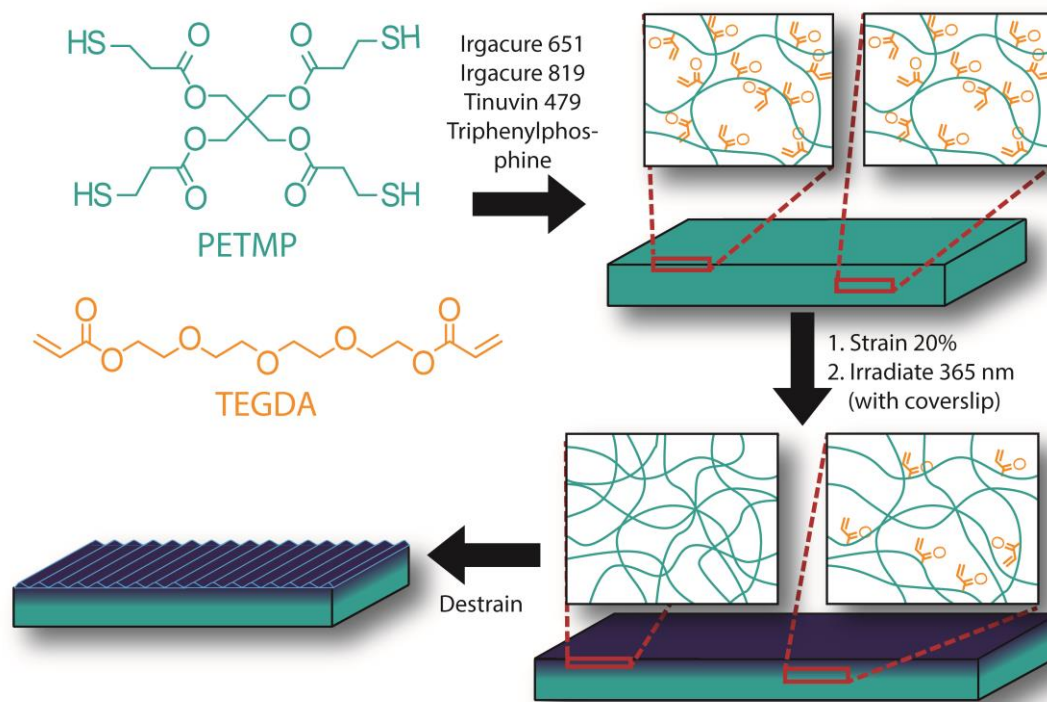


**Figure 3.2 Two-tiered polymerization for wrinkle formation.** Tetrathiol, PETMP, and excess diacrylate, TEGDA, were mixed with photoinitiators (Irg 651 and Irg 819), photoabsorber (T479), and TPP to generate an acrylate-rich elastomeric substrate. Straining and irradiating the elastomer with 365nm UV light triggers radical polymerization of the pendant acrylates. The photoabsorber, which absorbs 365 nm light, prevents light penetration into the bulk, thus confining the second polymerization to the surface. Upon destaining the material, wrinkles are generated due to the elastic moduli mismatch between the film and substrate.

Because of the self-limiting nature of the thiol-Michael reaction, the thiols reached full conversion, leaving behind excess pendant acrylates that were attached to the crosslinked network backbone. Consistent with the 1:2 thiol:ene stoichiometry used to form the elastomer, *in situ* FTIR spectra of conversion vs time for the thiol-Michael

reaction (Figure 3.3) confirms quantitative thiol conversion and roughly 50% acrylate conversion.

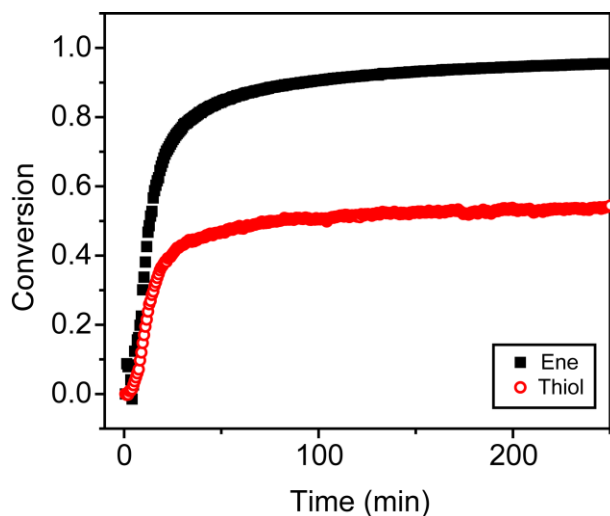


**Figure 3.3 Conversion data of thiol and ene during elastomer formation.** In situ FTIR measurements of the 1:2 PETMP:TEGDA system confirms quantitative conversion of thiol and roughly 50% conversion of the acrylates, which is consistent with the thiol:ene stoichiometry used in formulation.

The thiol-ene elastomer is then strained above the critical strain necessary for wrinkle formation, with a coverslip placed directly on top, which creates an oxygen barrier at the surface and prevents oxygen inhibition of the second free radical polymerization, which is employed to form the film. Through timed irradiation with 365 nm UV light and the presence of a UV photoabsorber, which creates an optically thick material to the 365 nm light source, acrylate homopolymerization is confined to the very surface of the material, resulting in the formation of a high modulus film layer. Samples were held in the strained state for over a minute after irradiation since dark

polymerization occurs in the material. As seen in Figure 3.4, ene conversion continues to increase for roughly 30 seconds after the initial UV irradiation.

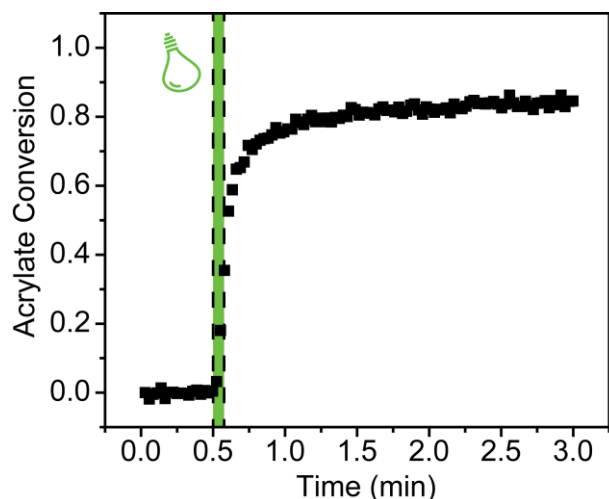


**Figure 3.4 Dark polymerization observed in the free radical polymerization.** Despite irradiating the thin film elastomer substrate for only 5 seconds (green highlighted region), acrylate conversion continues to rise for another 30 seconds before hitting a plateau conversion. This dark polymerization is likely due to diffusion limited radical termination.

This dark polymerization is most likely due to limited diffusion of radical species in the elastomer network generated during the photoirradiation, which hinders radical termination. The coverslip is subsequently removed and the elastomer destrained to yield wrinkles. Wrinkle features can be controlled through irradiation time and intensity (Figure 3.5), with larger wavelengths observed at higher intensity and longer irradiation times due to increasing crosslink density of the film layer.

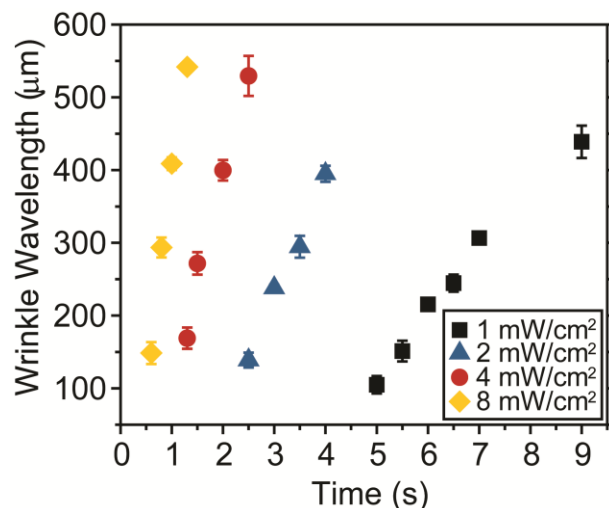


**Figure 3.5 Wrinkle wavelength vs Time and Intensity.** As light controls the film formation necessary to generate wrinkles, both light intensity and irradiation time dictate the size of wrinkle features. Increasing both the intensity and time will lead to increasing wrinkle wavelengths.

The surface chemical functionalization procedure is shown in Figure 3.6. In short, the wrinkled polymer was subjected to 405 nm irradiation (without coverslip) to further crosslink the acrylates in the bulk of the elastomer, increasing the crosslink density and mitigating diffusion of solvent into the network during the functionalization procedure. Because this irradiation step was carried out in the presence of oxygen, free radical polymerization is inhibited at the air/polymer interface, ensuring pendant acrylates were available for post functionalization.

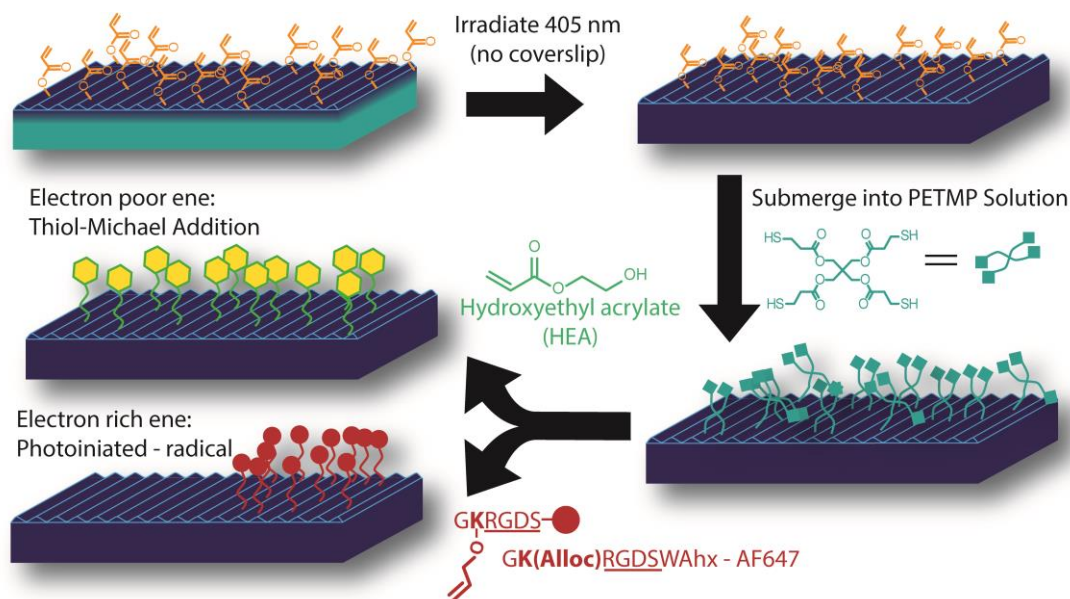


**Figure 3.6 Chemical modification of the acrylate-rich elastomer surface.** Wrinkled surfaces are irradiated with 405 nm light to induce bulk radical polymerization of the remaining acrylates. This post-processed material is then submerged into a solution of tetrathiol, PETMP, which converts the acrylate-rich surface into a thiol-rich surface via the thiol-Michael reaction. In generating the thiol-rich surface, a second modification can be carried out. In the presence of a nucleophile or base catalyst, the pendant thiols will undergo a second thiol-Michael reaction with electron-poor enes (i.e., hydroxyethyl acrylate). Alternatively, thiols can react with electron-rich enes (i.e., allyl) through a photoinitiated radical thiol-ene mechanism. Because this latter reaction is light-triggered, spatial control over chemical functionalization is possible. A RGDS containing peptide was synthesized with an alloc-protected lysine amino acid residue, which contains the electron rich ene that can be coupled to the thiol-rich elastomer.

The acrylate-rich surface was modified using a tetrathiol, PETMP, to produce a thiol-rich interface. High thiol solution concentration ensures excess thiols are present after reaction at the surface, which can be further modified through additional thiol-ene couplings. X-ray photoelectron spectroscopy (XPS) experiments were performed on a

surface functionalized with a monofunctional thiol, perfluorodecanethiol (PFDT), revealed that PFDT concentrations as low as 15 mg/mL (0.31 M) in solvent were sufficient to approach the saturation limit at the polymer surface (Figure 3.7). Thus, using PETMP (MW = 488 g/mol), which has four times the number of thiols as the PFDT (MW = 480 g/mol) at the same mass concentration (i.e., 15 mg/mL), is sufficient to create a thiol-rich elastomer surface.

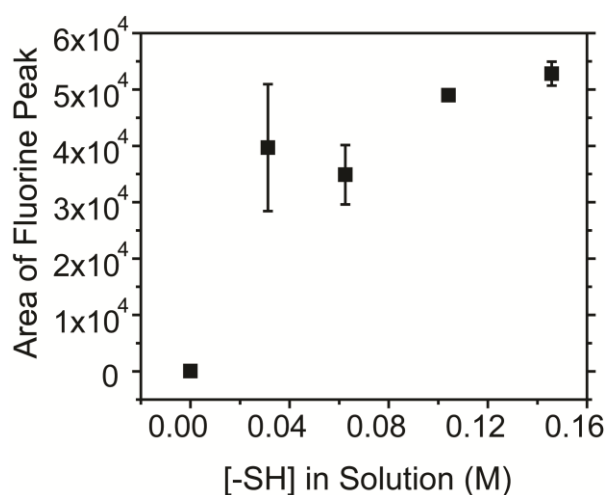


**Figure 3.7 XPS spectra of fluorine peak area versus PFDT solution concentration.** XPS data confirms that even at 0.31 M (15 mg/mL) of the PFDT in solution, the amount of fluorine approaches saturation. Further increases in solution concentration does not increase the surface concentration of the PFDT. Using a tetrathiol, PETMP (MW = 488 g/mol), to do the actual surface modifications yields roughly four times the amount of thiol at the same mass concentration as the PFDT (MW = 480 g/mol), which ensures excess thiol functionality at the surface of the polymer.

The thiol-rich surfaces can be functionalized further through a second thiol-ene reaction (Figure 3.6). In the presence of an electron-deficient ene (i.e., acrylates) and phosphine catalyst, the excess surface thiols can react via the same thiol-Michael

reaction that was used to form the network and to attach the thiols to the surface acrylates. As hydrophilic surfaces exhibit antifouling properties, [175-177] hydroxyethyl acrylate (HEA) was selected for the second thiol-Michael functionalization to impart hydrophilicity to the surface of the elastomer. Alternatively, with an electron-donating ene (i.e., allyl), the reaction will proceed through a radical-mediated reaction, in the presence of a photoinitiator. Through photopatterned UV light, this latter thiol-ene reaction introduces spatial control over chemical modification of the polymer surface. Peptide, AF647-AhxWGRGDSK(alloc)G (AF647-RGDS) was synthesized (Figure 3.8) not only as an electron-donating ene through the allyl of the alloxycarbonyl protecting group on the Lysine residue K(alloc), but also to promote cell adhesion of human mesenchymal stem cells (hMSCs) through integrin binding of the RGDS sequence. [178]

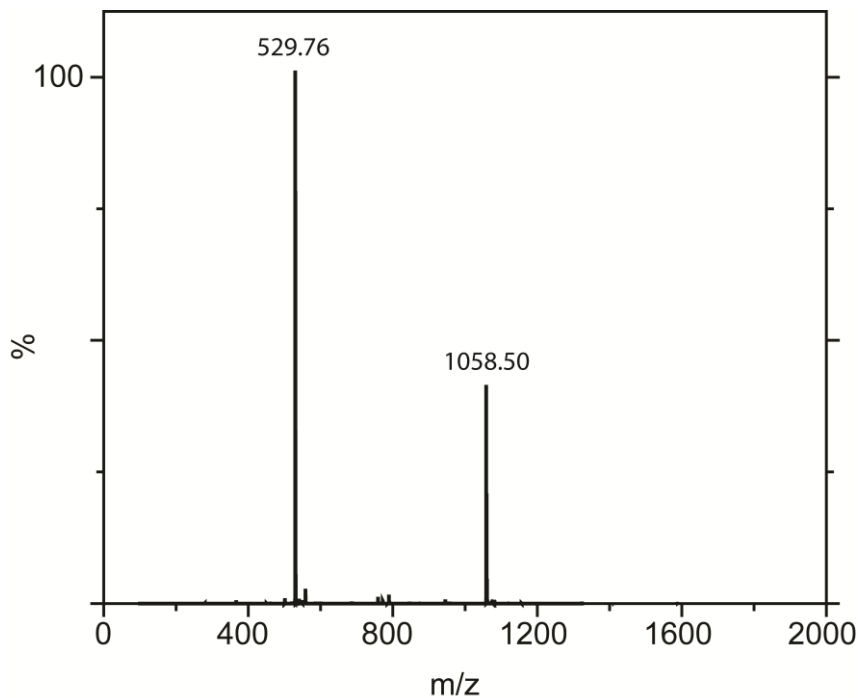


**Figure 3.8 ESI MS of AF647-RGDS peptide.** Calculated mass:  $[m+1, H^+] = 1059$  Da,  $[m+2H^+] = 1060$  Da. Measured  $[m+1, H^+] = 1058.5$  Da,  $[m+2H^+] = 529.76 \times 2 = 1059.52$  Da

Prior to surface functionalization for cell seeding experiments, NMR studies were conducted on the various equimolar thiol-ene combinations. PETMP/TEGDA, which simulates thiol attachment to the acrylate surface, was previously characterized using FTIR (Figure 3.3) and was not analyzed in the NMR studies. To mimic the attachment of HEA to the thiol-modified surface, PETMP/HEA was reacted in the presence of either a phosphine (DMPP) or nucleophilic (DBU) catalyst (Figure 3.9 – 3.10).

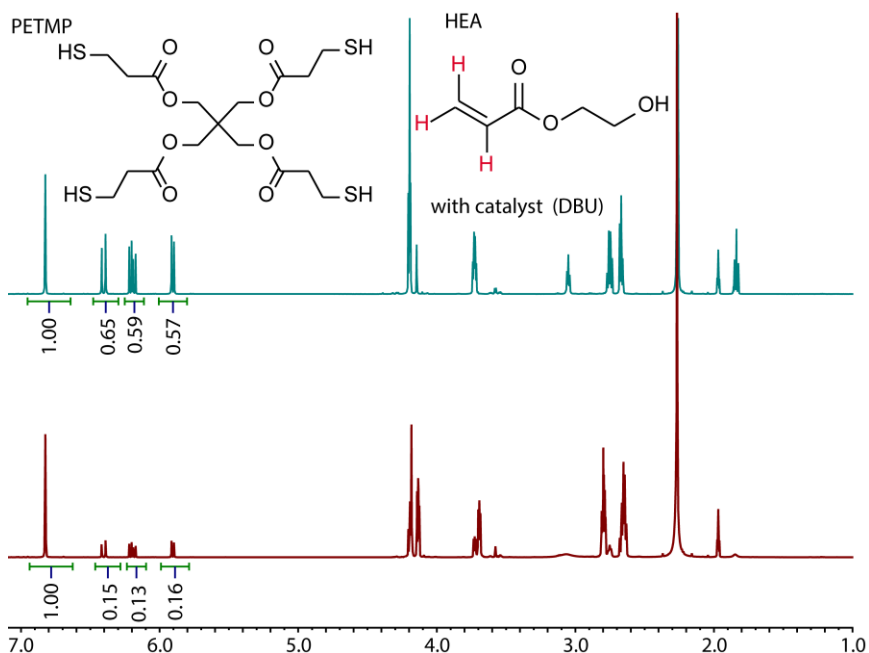


**Figure 3.9** NMR Spectra of PETMP/HEA with base catalyst DBU in Acetonitrile-*d* before (top) and after (bottom) reaction. Reaction achieves roughly 80% conversion as determined by the peaks located between 5.5-6.5 ppm associated with the C=C acrylate moieties of the HEA (red hydrogens). The peak at 6.8 ppm is the trimethylbenzene reference peak.

To conserve peptide material for the radical thiol-ene system, the Fmoc-protected K(alloc) was used in place of the AF647-RGDS, since both molecules undergo the radical thiol-ene reaction through allyl moiety on the K(alloc). Solutions of PETMP/K(alloc) were irradiated with UV light to induce thiol-ene coupling. Due to solubility issues with the photoinitiator, lithium phenyl-2,4,6-trimethylbenzoylphosphinate (LAP), a 70/10 acetonitrile-*d*/D<sub>2</sub>O solvent mixtures was used (Figure 3.10). It is important to note, that while ene conversion in the PETMP/K(alloc) can be measured exactly one minute after starting the reaction by turning off the UV light, NMR spectra for the post-thiol-Michael reactions were taken

roughly five minutes after catalyst addition due to a lack of temporal control over the reaction.

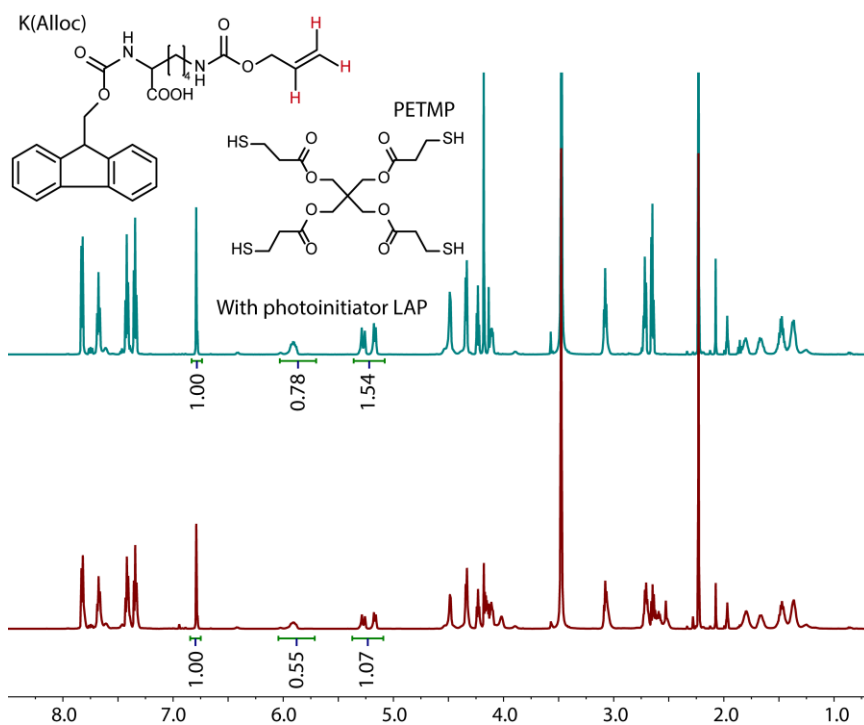


**Figure 3.10** NMR Spectra of PETMP/K(alloc) with photoinitiator LAP in 70/10 Acetonitrile-*d*/D<sub>2</sub>O before (top) and after (bottom) reaction. Reaction achieves roughly 30% conversion as determined by the peaks located between 5.5-6.5 ppm associated with the C=C acrylate moieties of the HEA (red hydrogens). The peak at 6.8 ppm is the trimethylbenzene reference peak.

As seen in Figures 3.9 and 3.10, ene conversion is monitored the three peaks in the 5.5 – 6.5 ppm range, corresponding to the three hydrogens on the alkene. The thiol-Michael reactions proceeded quantitatively while PETMP/K(alloc) approaches roughly 30% ene conversion.

The functionalized surfaces were further characterized using contact angle goniometry (Figure 3.11). Native (acrylate-rich) samples exhibited a contact angle of  $32.1 \pm 1.8^\circ$ . The thiol-rich surfaces, created by reacting a hydrophobic PETMP to the acrylate-rich surface showed a commiserate increase in contact angle ( $75.5 \pm 4.3^\circ$ ). With further coupling of the excess surface thiols to hydrophilic monomers (i.e., hydroxyethyl acrylate, AF647-RGDS), the surfaces are rendered more hydrophilic, thus lowering the contact angle.

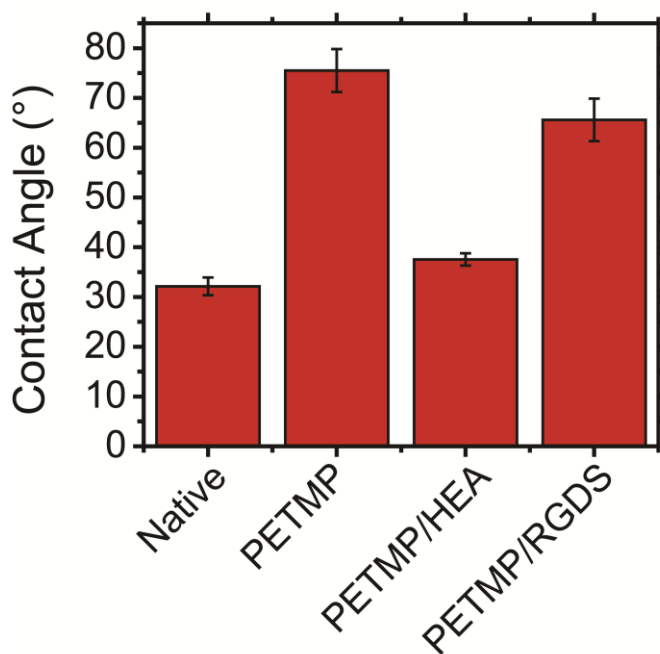


**Figure 3.11 Static Contact angle measurements on functionalize elastomer surfaces.** Native surfaces exhibited a contact angle of  $32 \pm 1.8^\circ$ . When functionalized with hydrophobic PETMP, the contact angle rises to  $75.5 \pm 4.3^\circ$ . With further modification of the thiols with either hydrophilic hydroxyethyl acrylate (HEA) or AF647-RGDS, the contact angle of the surfaces decrease again to  $37.5 \pm 1.2^\circ$  and  $65.6 \pm 4.3^\circ$ , respectively.

Having established chemical reaction of functional moieties, the polymer materials were modified with the various functional handles for cell culture experiments using human mesenchymal stem cells (hMSCs). hMSCs are multipotent progenitor cells that can differentiate into a variety of tissues, including bone and connective tissues, that require cellular alignment for proper morphology and function. [38,83,179,180] Elastomer surfaces, fully treated with both 365 and 405 nm irradiation, were functionalized with PETMP, PETMP/HEA or PETMP/RGDS (Figure 3.12a). hMSCs were seeded on flat, chemically modified surfaces to determine surface chemistry effects on cell density and spreading (Figure 3.12b and c). As expected, PETMP/RGDS functionalized elastomers significantly promoted both cell attachment and spreading (Figure 3.12b and c) compared to the native and PETMP/HEA surfaces. Thiol-rich surfaces also facilitated hMSC attachment and spreading but to a lesser extent. It is worth noting that acrylate-rich elastomers phototreated with just the AF647-RGDS (with LAP) also facilitated similar cell density and spreading as PETMP surfaces. We suspect this may be due to some homopolymerization occurring between the acrylate surface and the allyl group on the RGDS peptide in the presence of photoinitiator both in solution (LAP) as well as in the polymer (Irgacure 651, Irgacure 819).

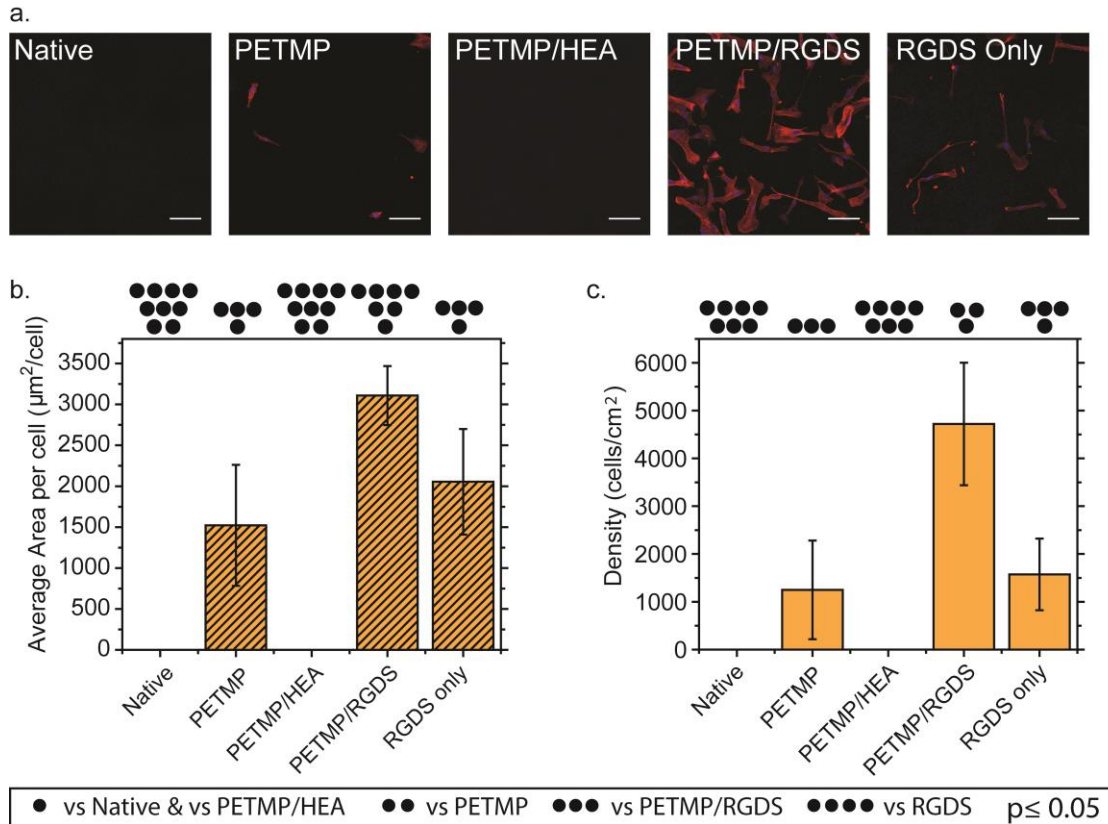
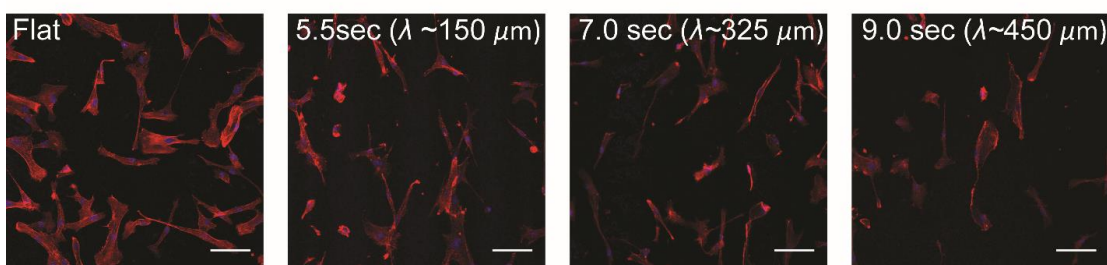


**Figure 3.12 hMSCs seeded on flat functionalized surfaces.** a) Representative confocal microscopy images of hMSCs seeded on various functionalized surfaces (Native, PETMP (thiol-rich), PETMP/HEA (hydrophilic), PETMP/RGDS, and RGDS only). Scale bar represents 100  $\mu\text{m}$ . Cell nuclei are stained blue, while the cytoskeleton is shown in red. hMSCs seeded on PETMP/RGDS-functionalized surfaces exhibited significant improvements in cell spreading (b) and cell density (c) as compared to other functionalization conditions. For PETMP-functionalized samples, hMSCs attached and spread to a lesser degree, possibly due to nonspecific interactions with the free thiol moieties. Homopolymerization of the allyl moiety in the AF647-RGDS sequence (RGDS only) to the free acrylates may also promote hMSC attachment.

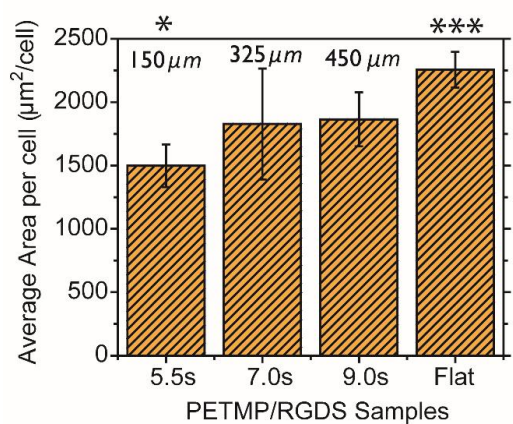
With notable differences observed on the functionalized materials, hMSCs were seeded on PETMP/RGDS-functionalized wrinkled elastomers prepared using three

different 365 nm irradiation times (5.5, 7.0 and 9.0 seconds) corresponding to three distinct wrinkle wavelengths ( $\lambda \sim 150, 325, 450 \mu\text{m}$ , respectively) (Figure 3.13a).

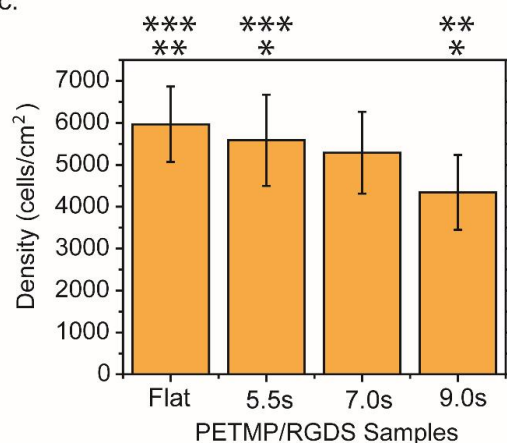
a.



b.



c.



\* vs Flat    \*\* vs 5.5s    \*\*\* vs 9.0s     $p \leq 0.05$

**Figure 3.13 hMSCs seeded on PETMP/RGDS-functionalized wrinkled substrates with increasing wrinkle wavelength.** a) Representative confocal microscopy images of hMSCs seeded on wrinkled substrates reveal alignment of cells with the troughs of wrinkles structures versus a flat PETMP/RGDS-functionalized flat substrate. Scale bar represents  $100 \mu\text{m}$ . Cell nuclei are stained in blue while the cytoskeleton is stained red. b) As the cells tend to settle and spread along the troughs of the wrinkle structures, increasing the wrinkle wavelengths increase the accessible surface area in the troughs for the cells to spread. c) Cell density decreases with increasing 365 nm irradiation time.

Cell spreading increases with increasing wrinkle wavelengths (Figure 3.13b), due to the cells' preference to settle in the troughs of the wrinkle structures. As wrinkle wavelengths increase, the troughs of the structures widen and the curvature near the trough begins to flatten, increasing the surface area of the troughs for cells to settle and spread. Consistent with this trend, flat samples, which can be thought of as an infinitely large wrinkle, have the largest degree of cell spreading associated with the largest degree of accessible surface for cell deposition.

In contrast, the cell density of hMSCs decreases with increasing wrinkle wavelength (Figure 3.13c). One reason for this may be due to variations in PETMP/RGDS density. Since the wrinkle formation process is carried out with a coverslip (i.e., negligible O<sub>2</sub> inhibition), some acrylate conversion is expected at the very surface of the elastomer. As wrinkle wavelength increases with increasing 365 nm irradiation, the amount of remaining pendant acrylates available for post modification should decrease, thus lowering the final RGDS surface concentration.

Cell nuclear alignment was also analyzed based on previously established protocols [87] with aligned cells taken within  $\pm 15^\circ$  off the axis parallel to the wrinkle wavelength direction (Figure 3.14). All nuclei (>30 nuclei per image) not in contact with the edge of the image were analyzed. In comparison to flat PETMP-RGDS samples, wrinkled samples exhibit a two-fold increase in nuclear alignment, with no statistical difference in nuclear alignment between the three wrinkle wavelength conditions ( $\lambda \sim 150\text{-}450 \mu\text{m}$ ). It should be noted the wrinkle sizes used in this study were an order of magnitude larger than wrinkle features used in previous studies, [87] which analyzed hMSC alignment on topographic features that were roughly 20 – 30  $\mu\text{m}$ .

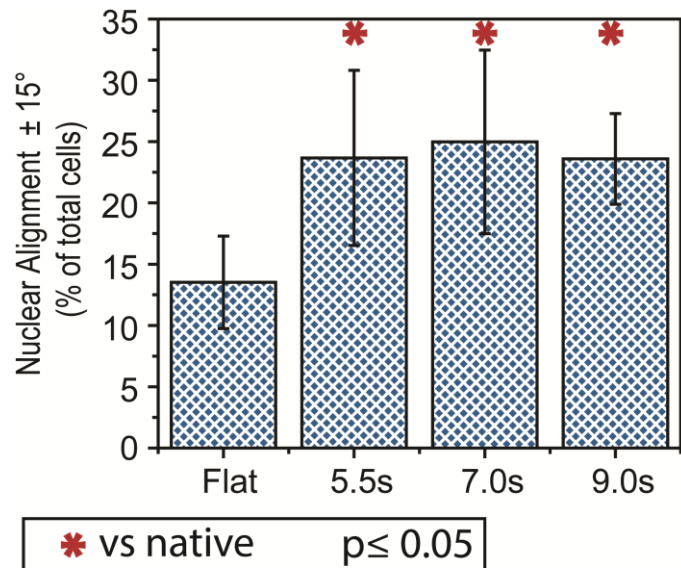


**Figure 3.14 Nuclear Alignment vs wrinkle wavelength on PETMP/RGDS surfaces.**

Cell alignment measurements, taken as  $\pm 15^\circ$  parallel to the wrinkle wavelength, demonstrated two-fold increase in nuclear alignment of hMSCs on PETMP/RGDS-functionalized wrinkle substrates as compared to a flat substrate. Red stars denote significance as compared to flat PETMP/RGDS functionalized sample.

### 3.4 Conclusion

Thiol-ene photowrinkle systems present a powerful tool for controlling surface interactions of polymer materials. Through stoichiometrically controlled thiol-ene formulations, two-tiered polymerization schemes can be implemented towards rapid generation of wrinkles. Importantly, this topography can be further enhanced through post-chemical functionalization, by leveraging oxygen inhibition associated with the free radical photopolymerization. By employing thiol-ene chemistry to chemically modify wrinkle surfaces, it is possible to independently tailor the topography and the surface chemistry towards a targeted application. While in this study we implemented a two-step functionalization protocol to adapt the elastomer for cell culture experiments,

due to the modular nature of thiol-ene ‘click’ chemistry, many commercially available and synthesizable multifunctional thiols and enes can be utilized. In conjunction with the ability to rapidly form spatially aligned and confined topography, the versatility of this approach to controlling surface properties will enable the development of next generation functional coating materials.

## Chapter 4

### PHOTO-WRINKLE FORMATION VIA FLOWCOATING – SUB-MICRON WAVELENGTHS WITH INDEPENDENT CONTROL OVER MODULUS AND CHEMISTRY

#### 4.1 Introduction

Material wrinkling or buckling on polymer substrates offers a rapid low-cost method for generating topography over large surface areas, for applications in optical lenses [57, 130], adhesives [69-71], antifouling coatings [68], cell culture [64, 77, 87] and flexible electronics [153, 154], among many others. To form wrinkles, a thick low modulus substrate exerts lateral compressive stresses on an attached thin, high modulus film. Above a critical stress (or strain), periodic sinusoidal wrinkle structures spontaneously develop in the film layer, resulting from a minimization in the film's bending energy and the elastomer's strain energy (Equation 1.1)

There are several approaches to develop controlled wrinkled surfaces on elastomeric substrates. [52, 53, 56, 57, 59, 64, 65, 68, 124, 130] One of the first examples of deliberate wrinkling on a polymer substrate was by Bowden and coworkers, in which a thin layer of metal was coated on top of a poly(dimethylsiloxane) (PDMS) elastomer. [52] Later work utilized UV ozone (UVO) or plasma oxidation to convert the surface of a strained PDMS elastomer into nanometer-thick silicate thin film. [53, 56, 65] Upon releasing the strain on the PDMS, wrinkles were introduced into the silicate layer. Alternatively, a number of groups have coated thin films from a polymer solution, which were subsequently transferred onto an elastomeric substrate. [59, 125,

181] This method facilitates generation of nanometer-thick polymer films, producing submicron wrinkle structures. Additionally, films with gradient thicknesses have been generated through flowcoating by controlling the coating acceleration. Stafford and coworkers used this procedure to develop SIEBIMM (strain-induced elastic buckling instability for mechanical measurements), a measurement technique that extracts the elastic modulus of the thin film from the wrinkling wavelength using equation (1) (after experimentally determining the film thickness and elastomer modulus). [59, 88]

Despite these advances to create wrinkled topography using flowcoating, several challenges remain. Specifically, because the thin films are not covalently attached to the elastomer foundation, delamination and cracking has been observed, particularly under large elastomer deformations. [125] Additionally, flowcoating or spincoating generates a continuous film, and thus wrinkles are formed across the entire surface. While the introduction of photoreversible moieties, such as azobenzene, can be used to spatially modulate wrinkling, these structures are not permanent and relax over time. [62] Finally, the majority of bilayer wrinkle systems lack the ability to tune the modulus of the thin films; typically, the films are glassy (with an elastic modulus  $>1$  GPa), resulting in a large modulus mismatch between the film and elastomer and setting a lower limit on the wrinkle wavelength (see Equation 1).

To address these limitations, we present a new approach to polymer wrinkling using flowcoating of thiol-ene ‘click’ monomers [114, 115, 121, 182, 183] to target submicron wrinkle structures. The versatility of the thiol-ene reaction, [114, 115, 121] characterized by rapid kinetics under ambient conditions, high reaction selectivity, and spatiotemporal control, has led to the development of chemically-crosslinked polymers networks with tunable modulus [from  $<0.1$  kPa (i.e., hydrogels [18, 184, 185]) to  $>1$

GPa (i.e., dental composites[186])). With the incorporation of specially-designed monomers, stimuli-responsive characteristics, including self-healing[187-189] and light-triggered mechanical actuation (i.e., liquid crystal elastomers), [190] among others, can also be imparted into the network.

Using a model system, we establish thiol-ene formulations to independently control the modulus of each layer to produce nanometer-sized features. Through thiol-to-ene stoichiometric control, we also develop ene-rich films that are covalently bonded to complementary thiol-rich elastomers. Employing photopatterning, we demonstrate spatial control over wrinkle formation and wrinkle alignment. Finally, by flowcoating multiple patterned layers, we spatially control the size of wrinkles, as the wrinkle wavelength is dictated by film thickness.

## **4.2 Materials and Methods**

### **4.2.1 Materials**

Triallyl-1,3,5-triazine-2,4,6-trione (TATATO) and triethylene glycol divinyl ether (TEGDVE) was purchased from Sigma Aldrich. 3,6-dioxa-1,8-octanedithiol (DOODT) was purchased from TCI America. Pentaerythritol tetramercaptopropionate (PETMP) was kindly supplied by Evans Chemetics. Irgacure 651 (2,2-Dimethoxy-1,2-diphenylethan-1-one) was donated from BASF-CIBA. All chemicals were used without further purification.

### **4.2.2 Thiol-rich Elastomer formulation:**

Photoinitiator, Irgacure 651 (0.1wt%), was mixed with TEGDVE and vortexed until fully dissolved. Next, tetrathiol, PETMP, and dithiol, DOODT, were added to the TEGDVE and vortexed for 30 seconds. The PETMP:DOODT:TEGDVE functional

group stoichiometry was 1.5:2:3. This ratio ensures a thiol-rich elastomer. The mixture was then casted between two glass slides with 1.58 mm Teflon spacers and irradiated with 365 nm UV light (EXFO S2000) at 1 mW/cm<sup>2</sup> for five minutes to initiate radical-mediated thiol-ene polymerization to yield an elastomer.

#### **4.2.3 Flowcoating Ene-rich films:**

All glass slides were triple rinsed with acetone, isopropanol, and distilled water prior to use. All glass slides and silicon wafers were then placed in a UVO cleaner (model 342, Jelight Co., Inc.) for at least 1 hour prior to film casting to remove residual organic contaminants. After removal from the UVO chamber, all substrates were rinsed with toluene and dried with nitrogen three times before casting.

Thiol-ene monomers, PETMP and TATATO were added in a 1:1.1 thiol: ene stoichiometry and dissolved in toluene (10wt% monomers in toluene) with 0.5 wt% Irgacure 651 based on monomer weight. Cleaned glass substrates (or silicon wafers) were mounted on a motorized stage and monomer solution (75  $\mu$ L) was injected between substrate and a 1.6 cm coating blade (200  $\mu$ m gap height). The motorized stage was then moved unidirectionally at a constant velocity to generate a uniform monomer thin film. After casting, the films were irradiated with 365 nm UV light (10 mW cm<sup>-2</sup>, 90s) to crosslink the thiol-ene monomers.

To photopattern the films, a photomask was placed over a monomer thin film, prior to UV irradiation. After curing, the films were rinsed with toluene and dried with nitrogen three times to remove any unreacted monomers. All films were heated at 100°C for 2 hours to remove any residual toluene.

#### **4.2.4 Measuring film thickness:**

Films were casted on silicon wafers at the same conditions as on glass slides. Wrinkles generated from both silicon wafers and glass slides showed similar wrinkle wavelengths, indicating the two substrates a similar with respect to flowcoating

All samples were photocured for 90 seconds at  $10 \text{ mW/cm}^2$ , and post-heated for 2 hours at  $100^\circ\text{C}$  to remove any residual solvent. The final crosslinked polymer film thickness was measured using a spectral reflectometer (Filmetrics, F20-UV).

#### **4.2.5 Transferring films to the elastomers**

The ene-rich flowcoated film was brought in contact with a thiol-rich elastomer, which was strained 4% on a custom-built stretching apparatus using manually controlled micrometer linear stages attached to an optical breadboard. Elastomers were affixed using clamps. Wetting was observed between the elastomer and film surfaces. The system was subsequently irradiated with 365 nm UV light ( $10 \text{ mW cm}^{-2}$ , 60s) to covalently attach the film to the elastomer. The entire set up was then submerged into water to delaminate the glass slide from the bilayer polymer system for a few hours. Upon removal from water, the system was vacuum dried overnight. After destraining, wrinkles were imaged under optical microscopy or scanning electron microscopy.

#### **4.2.6 Dynamic Mechanical Analysis (DMA)**

Modulus of bulk thiol-ene polymers were measured using a TA Q800 DMA in tensile mode, using a strain of 1% at a frequency of 1 Hz. Moduli values were taken in triplicate.

#### **4.2.7 Optical Microscopy**

Optical microscopy images were collected in transmittance mode using a Nikon Eclipse LV100, 5 MP CCD camera. Images were taken using 20x, 50x and 100x objective lenses.

#### **4.2.8 Scanning electron microscopy**

For wrinkle wavelengths below the resolution of the optical microscope, a Zeiss Auriga 60 Field Emission Scanning Electron Microscope was employed. Prior to obtaining microscopy images, all wrinkled samples were coated with a thin layer of Au/Pd alloy using a Denton Vacuum Desk IV Cold Sputterer.

#### **4.2.9 Thermogravimetric Analysis (TGA)**

TGA was performed on a TA Discovery TGA. Thin film PETMP:TATATO samples were heated at 10°C/min to 100°C under nitrogen atmosphere, and held isothermally for 2 hours.

#### **4.2.10 Atomic Force Microscopy (AFM) Modulus**

The modulus of thin films were obtained on a Bruker Catalyst AFM with a BioScope II Controller in peak force tapping mode. A Bruker AFM Probe (Model TAP525A – MPP13120) with spring constant,  $k = 200 \text{ N/m}$  was used.  $1\mu\text{m}$  by  $1\mu\text{m}$  scans (256 x 128 modulus data points) were taken on three separate films. The modulus data was fitted to a Gaussian and the mean value was taken as the film modulus. Measurements indicate the modulus of thin films were  $>1 \text{ GPa}$  (Figure 4.1), which is consistent with bulk DMA measurements.

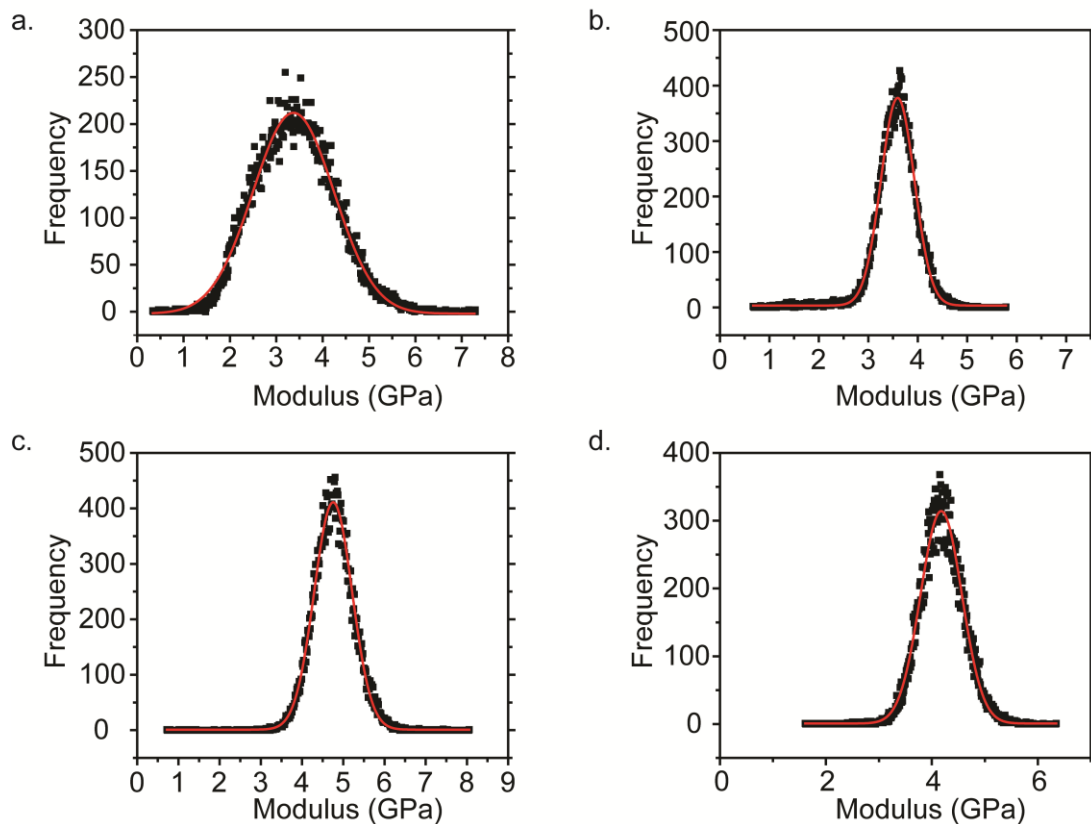


**Figure 4.1 Modulus of thin films.** Modulus histograms for AFM peak force tapping measurements of PETMP/TATATO (1:1.1) thin films. A) Poly(styrene) standard with a mean of 3.37 GPa and a standard deviation of 0.87. b) PETMP:TATATO thin film with a mean of 3.59 GPa and a standard deviation of 0.34. C) Second replicate of PETMP:TATATO film with an average of 4.75 and a standard deviation of 0.46. D) Third replicate of the PETMP:TATATO thin film with an average of 4.17 and a standard deviation of 0.39. These data indicate that these film thicknesses of the PETMP:TATATO films retain their glassy bulk modulus.

### 4.3 Results

The thiol and ene monomers used to formulate the elastomer and thin film were selected based on their molecular structure (i.e., number of functional groups per molecule, backbone flexibility, thiol and ene reactivity, etc.), which directly influences the mechanical properties of the final crosslinked material. For the ene-rich flowcoated film, a 1:1.1 PETMP:TATATO mixture was used (monomers shown in Figure 4.2a). The combination of monomer functionality (tetrathiol and triene) and rigid backbone (specifically of TATATO) is known produce a glassy material at room temperature ( $1.9 \pm 0.05$  GPa). [186] The film is formed using flowcoating, where a monomer solution of the PETMP/TATATO and photoinitiator (Irgacure 651) is injected between a coating blade and a precleaned glass substrate. The glass substrate is actuated using a linear motorized stage, resulting in a thin uniform coating of monomer on the glass. This coating is subsequently crosslinked through a radical mediated thiol-ene photopolymerization. Unlike traditional photopolymerizations that employ meth(acrylate) type monomers, thiol-ene chemistry is insensitive to oxygen, which enables the photopolymerization of the nanometer-thick films under ambient conditions. Films are subsequently heated for two hours at 100°C to completely remove excess solvent in the films, which was confirmed using thermogravimetric analysis (TGA).

Three monomers were used to formulate the elastomer foundation: tetrathiol (PETMP), dithiol (DOODT), and diene (TEGDVE) (Figure 4.2b). The tetrathiol-to-dithiol monomer ratio is used to tune the molecular weight between crosslinks, and correspondingly the elastomer modulus. The elastomer formulation was cast between two glass slides, separated by 1.6 mm spacers and irradiated with 365 nm UV light. A fully cured thiol-rich elastomer with a monomer functional group stoichiometry of

1.5:2:3 (PETMP:DOODT:TEGDVE) possessed a modulus of  $2.5 \pm 0.2$  MPa and was capable of reversible strains of  $>4\%$ .

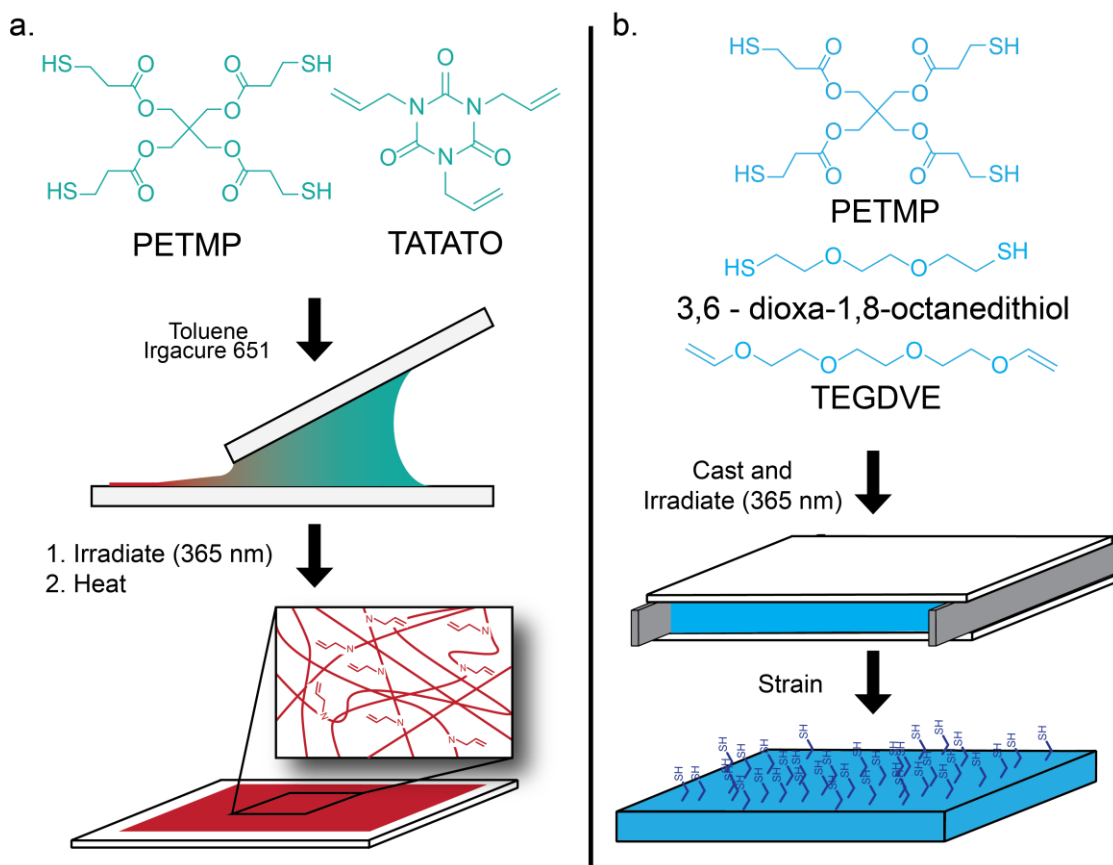


**Figure 4.2 Thiol-ene Film and Elastomer Formulation for Polymer Wrinkling.**

Two independent thiol-ene formulations are employed to generate the thick elastomeric substrate and the thin, high modulus film necessary for wrinkling. A) Tetrathiol and triene (1:1.1 thiol:vinyl functional group stoichiometry) are mixed with photoinitiator (Irgacure 651) and dissolved in toluene. This solution is used to flowcoat nanometer thick films on a glass slide, which are subsequently crosslinked to form a high modulus polymer with excess vinyl functional groups and post-heated to remove residual solvent. B) Separately, tetrathiol, dithiol, and diene (1.5:2:3 thiol:thiol:vinyl functional group stoichiometry, respectively) are mixed with photoinitiator and photocured between two glass slides to generate a thicker low modulus elastomer with excess thiol functional groups.

A wrinkled bilayer was created by transferring and covalently attaching the flowcoated film to the pre-stretched elastomer as shown in Figure 4.3. In this illustrative example, the flowcoated film exhibited a continuous dark blue color on a silicon wafer, indicating a uniform thickness of roughly 100 nm (Figure 4.3a). The film was then brought into contact with a thiol-ene elastomer under 4% strain and irradiated to promote covalent attachment at the film–elastomer interface. Upon removing the silicon wafer, only the parts of the film in contact with the elastomer delaminated (Scheme 2c), leaving behind a discontinuity in the original coated film on the silicon wafer. This film transfer only occurred upon UV irradiation. If the film was contacted to the elastomer without irradiation, the film remained adhered to the silicon wafer upon removing the wafer from the strained elastomer, verifying that the ene-rich film was reacting to the thiol-rich elastomer interface. As a result of the covalent bonding of the film to the elastomer, the elastomer broke when we attempted to delaminate the silicon wafer from the thin film; the section of the elastomer that was in contact with the silicon wafer/thin film remained bonded to the wafer after the elastomer fractured. To successfully remove the wafer from the bilayer system, the entire system (bilayer polymer + stretching apparatus) was submerged into distilled water. The water infiltrates between the silicon wafer and the ene-rich film, which enables removal of the coating substrate without damaging the bilayer. It should be noted that similar wrinkle features are obtained when using a glass slide rather than a silicon wafer.

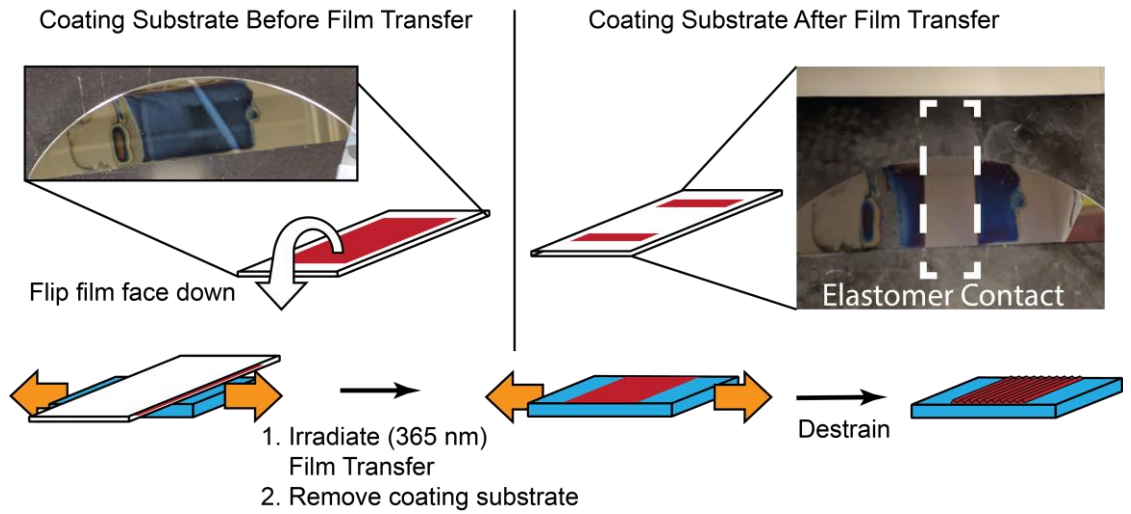


**Figure 4.3 Film Transfer of Flowcoated Film onto a Thiol-ene Elastomer for Wrinkle Formation.** a) Thin films are flowcoated and polymerized on a silicon wafer (or glass slide) and before they are placed in contact with a strained thiol-ene elastomer (b). Irradiation initiates reaction of the excess vinyls at the film interface with the excess thiols at the elastomer interface, to form a covalently attached laminate. The coating substrate is subsequently removed by submerging the entire

Research on flowcoating using linear polymer chains identified several key parameters for controlling film thickness, [191, 192] including polymer concentration and coating velocity. As established by the Landau-Levich theory (Equation 4.2), the film thickness,  $t_{wet}$ , is a function of a constant  $c_1$  ( $=1.34$ ), the characteristic length scale (radius of the rear meniscus of the coating solution),  $L$ , the solution viscosity ( $\mu$ ), the plate velocity ( $U$ ), and the solution surface tension ( $\gamma$ ):

$$\frac{t_{wet}}{L} = c_1 \left( \frac{\mu U}{\gamma} \right)^{\frac{2}{3}} \quad (4.2)$$

In this theory, it is assumed that evaporation of the solvent is negligible during the coating process; previous investigations on flowcoating polymer solutions revealed that an evaporation front formed after the blade during the coating process.

As expected from Equation 4.2, thiol-ene thin films (after crosslinking and post-heating) exhibit an increase in thickness with increasing velocity (Figure 4.4a), which is consistent with previous flowcoating experiments performed on dilute polymer solutions.[192] Similar to increasing velocity, increasing monomer concentration (while maintaining constant thiol:ene stoichiometry) also displays increased coating thickness (Figure 4.4b). These experiments indicate that coating with monomer solutions is comparable to coating with polymer solutions since the flowcoating phenomenon is based on the solution viscosity. Since the monomer solution viscosities are lower than polymer solutions at a given concentration, higher monomer concentrations may be coated using this method. For example, 20wt% monomer solutions are readily coated in contrast to previously reported 10wt% using 50K poly(styrene). [192]

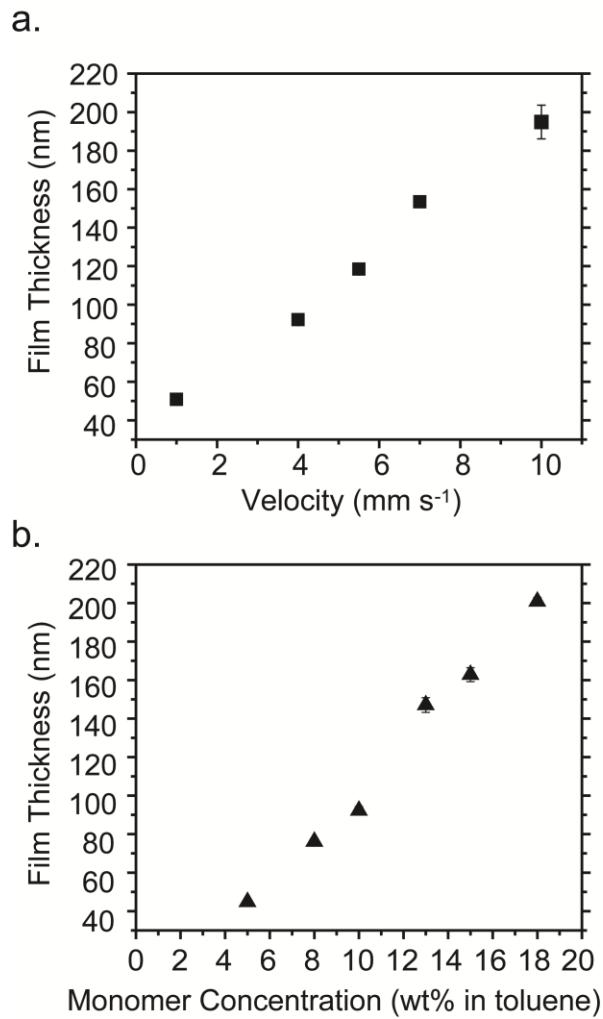


**Figure 4.4 Film thickness versus coating velocity and monomer concentration** A) Film thickness plotted as a function of velocity shows a linear increasing trend. As velocity increases, more monomer is left behind on the flowcoated substrate, thereby increasing the film thickness. B) The film thickness increases with increasing monomer concentration.

Furthermore, it was confirmed for polymer solutions that the velocity and Capillary number ( $\mu U/\gamma$ ) followed the  $2/3$  scaling dictated by the Landau-Levich Theory.[191] As seen in Figure 4.5, in which the logarithm of the film thickness is

plotted against the logarithm of velocity, a slope of  $0.62 \pm 0.06$  is obtained, consistent with the Landau-Levich theory.

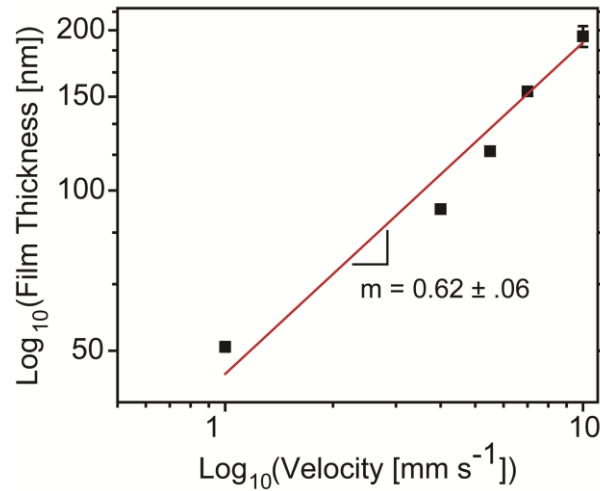


**Figure 4.5**  $\text{Log}_{10}(\text{Film Thickness})$  plotted as a function of  $\text{Log}_{10}(\text{Velocity})$  yields an 0.62 scaling, consistent with the Landau-Levich theory.

The wrinkle wavelength decreases with decreasing film thickness, as expected from the wrinkle wavelength equation. However, as shown in Figure 4.6 the wrinkle wavelength scales with  $h$  to the  $1.20 \pm 0.06$  power, which is a slight deviation from the expected value of 1.

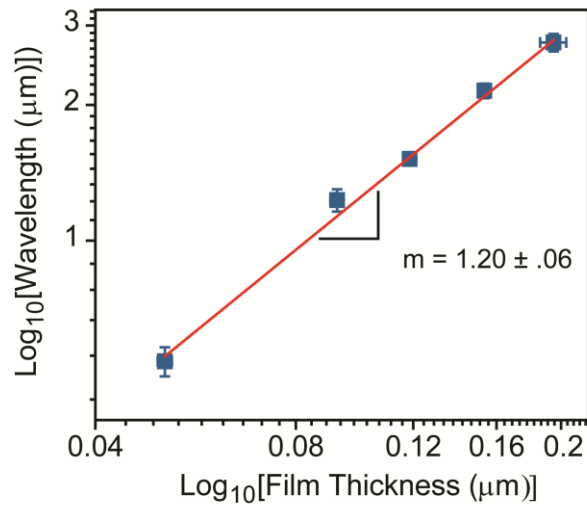


**Figure 4.6** As predicted by Equation 2, wrinkle wavelength scales with  $h$ .

The deviation is more pronounced when wavelengths of film thicknesses approaching 40 nm are included in the fit (Figure 4.7), resulting in the wavelength scaling of  $h^{1.43}$ . The scaling indicates that as film thicknesses decrease below roughly 40 nm, the apparent modulus of these films are lower than the bulk modulus, resulting in a wrinkle wavelength that is lower than expected. This modulus-depression phenomenon has been reported in literature. [88]

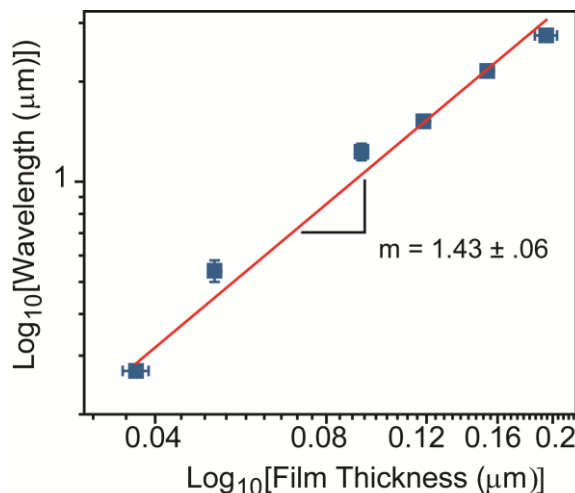


**Figure 4.7 Observed thickness scaling deviations of the wrinkle wavelength as film thickness approaches 40 nm; the wavelength scaling on thickness becomes  $\lambda \sim h^{1.43}$  instead of the expected  $h^1$ .**

Unlike other flowcoated wrinkle systems, the wrinkle wavelength of the thiol-ene system is readily tuned by changing the solution formulation. By controlling the monomer formulation and thiol:ene stoichiometry, the crosslink density is modulated. As shown in Figure 4.8, a different PETMP:TATATO formulation (thiol:ene ratio 0.7:1.1, red triangles) was used as the coating solution to generate thin films for wrinkling. As compared with 1:1.1 films, the modulus of 0.7:1.1 films is lower, resulting in lower wrinkle wavelengths at the same film thicknesses, while retaining the same scaling as the 1:1.1 wrinkle systems. With further formulation optimization, such as using dithiols instead of tetrathiols in the film formulation, the film modulus could be further reduced to achieve even smaller wrinkle features.

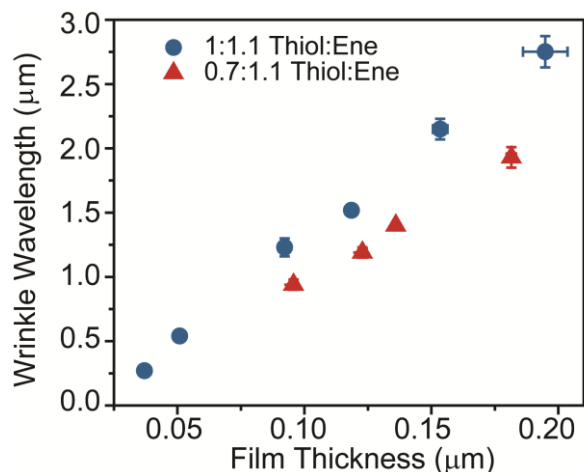


**Figure 4.8 Wrinkle wavelength vs film thickness for films of different moduli.** Wrinkle wavelength can be tuned through modulus of the thin films via monomer structure and/or thiol:ene stoichiometry. Thiol:ene formulations using 1:1.1 (modulus = 1.9 GPa) yield larger wrinkle wavelengths as compared to 0.7:1.1 formulations (modulus = 1.5 GPa). A similar concept can be applied to the elastomer substrate as well.

While flowcoating polymer solutions results in a continuous film, the use of UV irradiation enables spatial deposition of polymer via subsequent photopatterning and rinsing steps. By placing a photomask over the flowcoated film (Figure 4.9a) and irradiating the materials with UV light, crosslinking only occurs in the exposed areas of the film. The unexposed areas remain in monomer form, and are readily rinsed away without damaging the crosslinked polymer. Consequently, once the films are transferred onto the strained elastomer, wrinkle patterns are also confined. As an example, a flowcoated film was transferred to the uniaxially-strained thiol-ene elastomer and was irradiated through a flower photomask (Figure 4.9b). The unexposed regions of the film were then rinsed away and the strained elastomer was released to reveal a photopatterned iridescent film. Optical microscopy of the wrinkle patterns show high pattern fidelity in the photopatterned films, as the wrinkle structures

have clearly defined boundaries. Moreover, the wrinkles themselves align perpendicular to the direction of strain (Figure 4.9b).

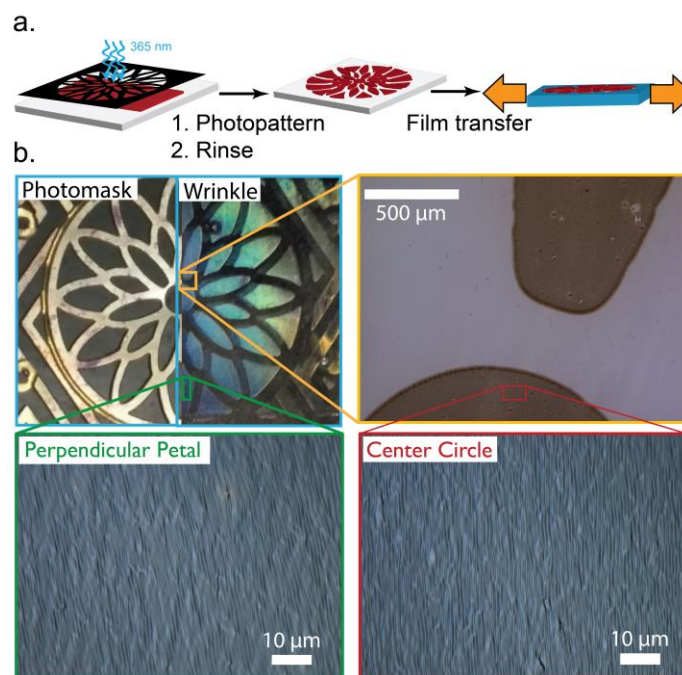


**Figure 4.9 Spatial Control over Wrinkle Formation using Flow-coated Photopolymerization.** A) After flowcoating monomer thin films, a photomask is overlaid on top of the preirradiated film, separated by a thin spacer (1 mm). Exposure to UV irradiation spatiotemporally crosslinks the materials, after which the unexposed, unreacted monomer is rinsed away with toluene. The photopatterned film is transferred to the strain elastomer (as described in Scheme 1). Releasing the strain produces wrinkles approaching submicron wavelengths, resulting in iridescent films. B) Patterned films reveal very distinct boundaries (yellow box – scale bar 500 μm). Unidirectional strain generates aligned wrinkles perpendicular to the strain direction, regardless of the pattern orientation (green and red boxes – scale bar is 5 μm).

Flowcoating and photopatterning provides a rapid route towards wrinkle confinement with multiple distinct wavelengths. By coating and photopatterning

multiple layers of thiol-ene polymer, it is possible to introduce step-changes in film thickness spatially, which upon transfer onto the elastomer will yield different wrinkle wavelengths in accordance with Equation 1.1. A thin film ( $h \sim 130$  nm) was flowcoated, transferred to and irradiated with photopatterned UV light on a thiol-ene elastomer. This process was repeated a second time under the same conditions, leaving behind a second film ( $h \sim 190$  nm) with two different distinct thicknesses (Figure 4.10). After transferring the film to an elastomer, the two photopatterned layers generate areas with distinct wrinkle wavelengths due to the height variation in the film itself. Regions that were not irradiated (i.e., no crosslinked film) exhibited no wrinkles (Figure 4.10b). In regions that retain only one coating (Figure 4.10c, right image), the wrinkle wavelengths were roughly  $1.75 \mu\text{m}$ . Only in regions where both layers were photoirradiated were the largest wrinkle wavelengths ( $\lambda \sim 2.75 \mu\text{m}$ ) observed (Figure 4.10c, left image), owing to the increased film thickness in those regions. While only two layers were coated in this demonstration, it is possible to coat multiple layers, photopatterning each layer to generate spatially controlled discrete wrinkle wavelengths.

#### 4.4 Conclusion

Flowcoating photopolymerizable monomer systems presents an alternative approach to realize sub-micron wrinkled surface topography. The mechanical properties of both the film and the elastomer substrate are highly tunable – with the appropriate thiol and ene monomer selection and stoichiometry, a wide range of moduli can be achieved for both layers. Though the film-to-elastomer modulus ratio in this specific system is 1900:2.5 MPa, thin films with moduli in the MPa regime can be easily achieved with thiol-ene chemistry, which can reduce the film-to-elastomer modulus ratio, thereby driving the wrinkle wavelength even smaller.

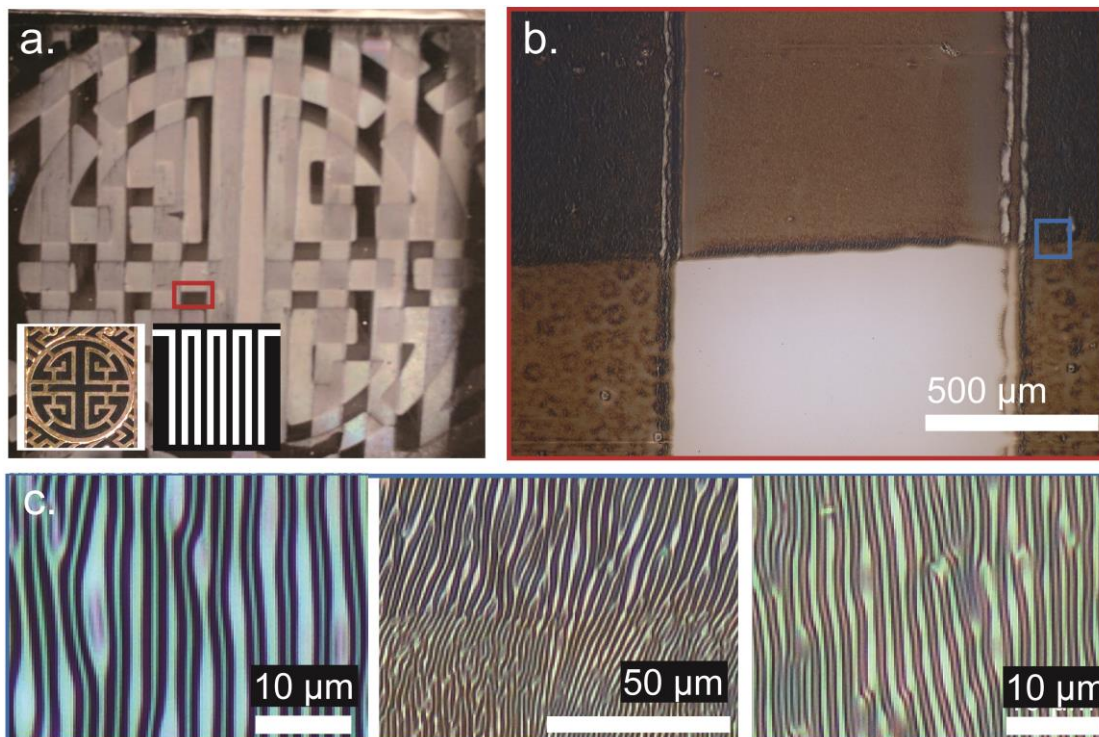


**Figure 4.10 Spatially Confined Formation of Multi-Wavelength Wrinkle Patterns**

A) Two layers of monomer were flowcoated with 10 wt% monomers in toluene at 7 mm/s and photopatterned using the two patterns shown in the inset. Unreacted monomers were rinsed away between each coating step. B) Upon film transfer, three distinct regions are observed – larger wrinkles associated with two layers, small wrinkles corresponding to one layer of crosslinked polymer, and areas with no wrinkles where the unreacted monomers were rinsed away. C) Corresponding large ( $h \sim 190$  nm,  $\lambda \sim 2.75$   $\mu\text{m}$ ) and small wrinkle ( $h \sim 130$  nm,  $\lambda \sim 1.75$   $\mu\text{m}$ ) regions (left and right images, respectively), with the transition region shown in the center image.

Based on the velocity vs film thickness experiments, it is also possible to flowcoat under constant acceleration, which will facilitate development of gradient wrinkle structures as well. Last, through photopatterned UV irradiation, confinement of wrinkled features is easily achievable as well as distinct wrinkle wavelength control through sequential flowcoating and photopatterning. Ultimately, with the modularity

of 'click' chemistry, the monomers in this study can be exchanged with specially synthesized monomers, which will enable development of stimuli responsive wrinkle systems as well as new functional thin film materials.

## Chapter 5

### CONCLUSION AND FUTURE DIRECTIONS

Wrinkled polymer surfaces present a rapid approach to generating long range surface topography for potential applications. To address some of the shortcomings of the widely popular PDMS-type wrinkle systems, which include slow polymerization rates, lack of facile tunability over surface chemistry, and poor alignment/confinement over wrinkle structures, two separate photodirected wrinkle systems have been developed in this thesis as well as methods to control the modulus and chemistry at the interface of the polymer material.

#### 5.1 Conclusions

In Chapter 2, a new wrinkle system was introduced using two orthogonal polymerizations on the same material. The first polymerization, the thiol-Michael reaction, was used to create the elastomeric substrate with excess acrylate moieties, while a photoinitiated free radical polymerization of the remaining acrylates was used to generate the higher modulus film, thereby generating the necessary modulus mismatch to form wrinkles. Wrinkles were formed in seconds under ambient conditions, compared to the 30 to >60 minutes it took with previous methods on PDMS elastomers. More significantly, through photolithography, gradient and aligned wrinkles are easily created, enabling facile production of more complex wrinkle configurations. The tools and techniques developed in Chapter 2, which include commercially available monomers, photoinitiators, and photoabsorbers and industrially relevant techniques

(i.e., photolithography), enable the potential commercial scale up of wrinkling technology.

In Chapter 3, oxygen inhibition of the free radical polymerization is exploited in the two-tiered wrinkling system to introduce chemical functionality to the material surface. Due to oxygen quenching of radicals at the surface of the elastomer, acrylates remain unreacted near the air-solid interface of the elastomer, enabling post chemical functionalization using thiol-Michael and thiol-ene type reactions. In this chapter, directed cell alignment of human mesenchymal stem cells (hMSCs) is also demonstrated towards potential tissue engineering applications. To chemically modify the material, the surface is exposed to tetrathiol in acetonitrile in the presence of a phosphine catalyst to trigger a thiol-Michael reaction. The acetonitrile, a good solvent for the polymer, ensures the thiols can access and react with the free acrylates in the polymer. The tetrathiol was selected to densify the surface functionality while introducing spatial control over the final functionalization step. Further reaction with an alloc-protected RGDS peptide introduced markers necessary for hMSCS to adhere to surfaces. Alternatively, other functional groups, such as hydroxyethyl acrylate (HEA), was introduced to passivate the surface and prevent cell adhesion. Upon cell seeding, cell density and spreading is significantly increased on RGDS-functionalized surfaces as compared to the native, thiol and HEA functionalized materials, indicating functionalization was successful. Because thiols are introduced in the first functionalization step, the alloc-RGDS can also be spatially controlled through a photoinitiated thiol-ene reaction, dictating where cells can adhere to the surface. Moreover, when cultured on functionalized wrinkles substrates, cells also exhibit increased cellular alignment as compared with the flat substrate. Through the work in

Chapter 3, chemical functionalization was shown to enhance material functionality, allowing independent control over the topography and chemistry.

In Chapter 4, an alternative approach to wrinkle formation was introduced using flowcoating to generate higher modulus thin films. The flowcoating approach to wrinkle formation enabled the generation of nanometer-thick films, which upon transfer to a softer elastomer, yields sub-micron wrinkle wavelengths. Although flowcoating/spincoating of long chain polymers (i.e., polystyrene) have been employed in wrinkle formation, this was the first instance of flowcoating with monomers, which were subsequently photocured. While flowcoating controlled the film thickness (i.e.,  $h$  in the wrinkle wavelength equation), utilizing thiol-ene monomers also enabled control over the modulus of the films through careful selection of monomer structure (i.e., ring structures vs linear chains) and through variation in the thiol:ene stoichiometry (i.e., the cross-link density). Thus, this approach introduced an additional control handle in wrinkle formation, which has not been demonstrated in previous flowcoating wrinkle systems. Moreover, similar to the two-tiered wrinkling system, the use of photolithography enabled spatiocontrol over wrinkle formation. By repeated flowcoating and photopatterning steps, stepwise variations in film thicknesses were achieved resulting in multiple distinct wrinkle wavelengths. Through further formulation development of the film and substrate, it is possible to decrease wrinkle wavelengths to below the diffraction limit of light.

Through the work in this thesis, techniques were developed to independently control modulus through thiol-ene formulation, surface chemistry through sequential monomer couplings and spatially confined surface topography through wrinkling using

industrially relevant techniques. Ultimately, these material systems facilitate the development of functional wrinkled materials for commercial applications

## **5.2 Future Directions – Stimuli responsive wrinkles**

The development of flowcoated monomer wrinkle systems presents an avenue towards fabrication of stimuli-responsive surface texture, which have been used in applications such as surfaces with reversible wetting [151], reversible adhesives [71], smart coatings [67], and biomaterials [78].

The methods employed in Chapter 4 can be implemented in designing stimuli-responsive wrinkle systems. Specifically, covalent adaptable networks (CANs) can be employed in creating the high modulus thin films through flowcoating. CANs, as the name implies, are covalently crosslinked polymers that contain functional moieties in the network backbone that are capable of breaking and reforming under external stimuli such as light or heat. CANs possess the structural integrity associated with thermosets, but also retain the reprocessibility of thermoplastics. This ability to reversibly break and reform chemical crosslinks has led to the development of interesting material properties such as stress relaxation [97,193], reversible adhesives [194], and material recycling/self-healing [98,100,103,195,196], among others. Importantly, CANS that employ reversible exchange reactions (e.g., transesterification reactions) undergo concomitant bond breaking and bond-reforming such that the crosslink density, and consequently the modulus, of the material is preserved.

While a variety of stimuli can be used to trigger polymer wrinkling, including humidity/solvent-swelling, [136, 197] pH, [198, 199] temperature, [200] and electricity, [67] light offers the unique advantage of spatiotemporal control as demonstrated in Chapters 2-4. A variety of different types of light triggered moieties have been

employed in CANs, including isomerizations (i.e., azobenzenes), [201-207] photoreversible cycloadditions (e.g., coumarin, anthracene), [208-215] and bond reshuffling (e.g., trithiocarbonates, allyl sulfides). [97, 98, 100-103, 195, 196, 216] Because of the modular nature of thiol-ene chemistry, it is possible to exchange either the thiol or ene species for monomers that contain any of the aforementioned functional moieties. In developing responsive wrinkling systems, synthesis of ene monomers with stimuli-responsive moieties would be an ideal starting point, as the synthetic schemes for both electron-rich and electron poor enes are typically less involved than synthesis of thiols. It is important to note that while a variety of different wrinkle material systems have been developed with the aforementioned functional moieties, [125, 199, 215, 217] the ability to synthesize, flowcoat and react these monomers in step-growth thiol-ene polymerizations offer greater tunability over the thermomechanical properties, and consequently the wrinkle wavelength of the final material.

Figure 5.1 shows the schematic of potential photoresponsive moieties that can be incorporated into the thiol-ene thin films. Figure 5.1a demonstrates the incorporation of azobenzene moieties in a thiol-ene thin film. Azobenzene molecules exhibit trans-to-cis isomerization under photoirradiation, which changes the polarity of the molecule and the length of the molecule. When the thermodynamically stable trans-state is aligned, liquid crystalline domains are formed. Upon irradiation with light, the aligned azobenzene will undergo the trans-to-cis conformational change, resulting in macroscopic deformation. If this molecule is incorporated into a thin film and laminated on a thicker elastomer substrate, the macroscopic deformations can result in wrinkle formation. [62, 125]

Molecules capable of undergoing reversible cycloadditions can also be used in the generating photoreversible wrinkles. In Figure 5.1b, coumarin is incorporated in a partially crosslinked thiol-ene thin film. Upon transferring the film onto a strained elastomer backing and irradiating, the coumarin will undergo a [2+2] cycloaddition reaction, resulting in the formation of a four-membered ring. This four member ring structure will increase the modulus of the film, thereby creating sufficient modulus mismatch for wrinkle formation. Further irradiation with 254 nm light source will reversibly break the [2+2] cycloproduct back into its monomer form, thus erasing the wrinkle structures.

Since stress is inherently introduced into the high modulus thin films during wrinkling, incorporation of bond shuffling moieties can create stress relaxation to erase wrinkle structures. Thiol-ene thin films containing trithiocarbonate moieties can be photocured and transferred onto strained elastomers. Wrinkles will form upon strain release. Radical initiators, which can be triggered using light, will attack the S=C bond, creating the bond reshuffling necessary to reduce stress in the thin film, which will effectively remove wrinkle structures. If the material is restrained and irradiated, the stress of the straining process on the thin film may be sufficient to cause stress relaxation in the elongated state. Because the bond reshuffling does not alter the crosslink density, the elastic mismatch between the film and substrate is maintained and thus after destraining the elastomer the wrinkles are recovered. In all three of the above examples, the use of light enables spatial control over wrinkle formation, which ultimately affords the same advantages of wrinkle confinement and alignment as the previous systems developed in this thesis.

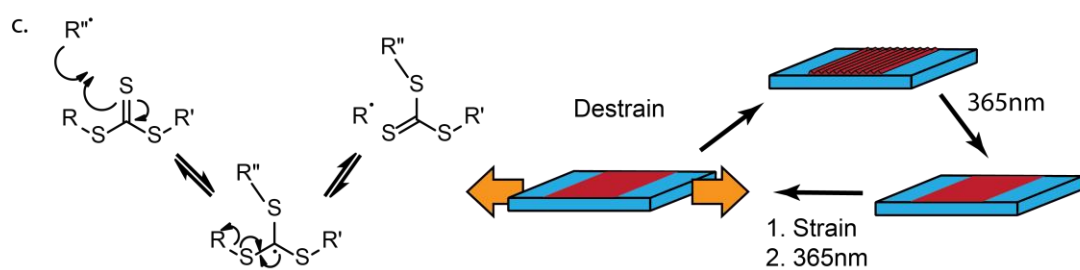
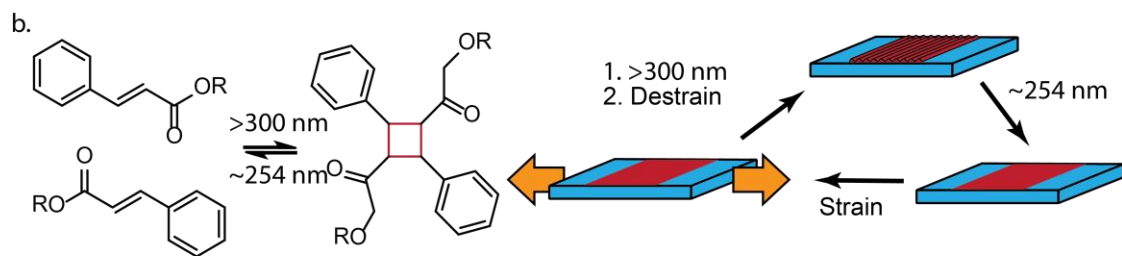
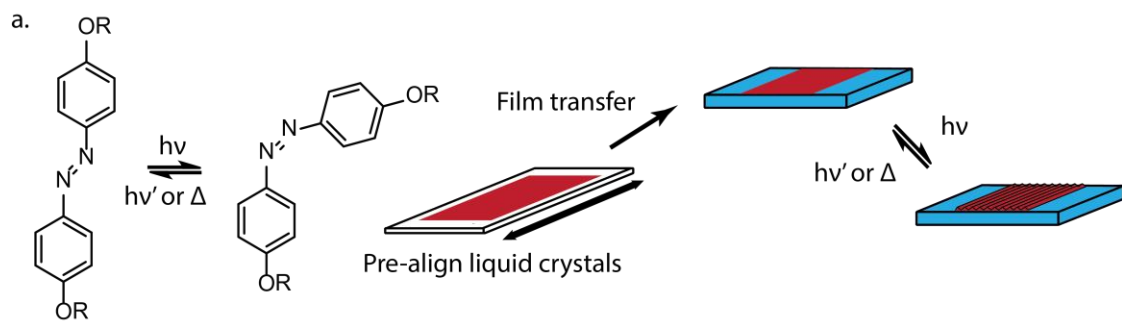


**Figure 5.1 Various photoresponsive moieties and their incorporation into flowcoated thin films.** a) Ene monomers containing azobenzene molecules can be synthesized and reacted with thiols on a flowcoating substrate. Prealignment of the liquid crystal molecules must be induced prior to photopolymerization to ensure liquid crystallinity. Upon transfer to an elastomer substrate (no strain required) and irradiation with a 365 nm light source, the film can undergo macroscopic shrinkage due to trans-cis isomerization of the azobenzene moiety, thus causing shrinkage. Exposure to heat or blue light will return the surface to the original flat state. b) Partially crosslinked thiol-ene films containing coumarin in the network backbone can be transferred onto a strained elastomer. Upon irradiation with >300 nm light, [2+2] dimerization is induced in the coumarin, forming a four-membered ring and increasing the modulus of the film. Upon strain release, wrinkles are formed. Irradiation with 254 nm light will restore the surface to a flat state. c) High modulus thiol-ene films containing trithiocarbonate moieties and photoinitiator can be created and transferred onto a strained elastomer, which upon destrain will form wrinkles. Irradiation with 365 nm light (or a light source matching photoinitiator absorbance) will create bond reshuffling, relaxing the stress in the thin film that was introduced during the wrinkle process, thus regenerating a flat surface. If the bilayer is restrained, and the surface irradiated with light, the thin film will relax in the elongated state, and upon destrain will wrinkle again. The generic functional group, R, denotes attachment to a thiol-ene network.

Another viable approach is to utilize photoinitiated copper catalyzed azide alkyne (CuAAC) reactions to generate the thin films. The CuAAC reaction, which is also a ‘click’ reaction owing to high selectivity, mild reaction conditions, and minimal byproducts, has been applied in a variety of polymer applications, such as shape-memory materials, [218-221] biomaterials and bioconjugation, [222-225] and dental materials. [226-228] The CuAAC reaction scheme is depicted in Figure 5.2. Through photoirradiation, a radical initiator species is generated, which reduces copper(II) to copper(I). This copper(I) species can then trigger the azide-alkyne reaction, generating a rigid triazole ring structure. [219,229-231]

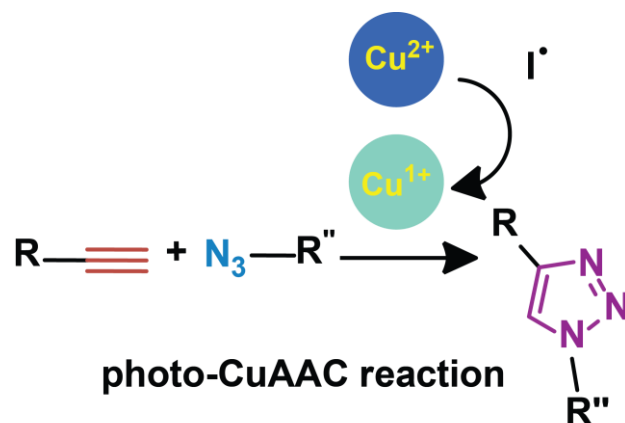


**Figure 5.2 Photo-Copper Catalyzed Azide Alkyne Reaction.** A photoinitiator radical reduces copper(II) to copper(I) which will trigger reaction between the azide ( $-N_3$ ) and alkyne ( $-C\equiv C$ ) resulting in the formation of the triazole ring.

To date, photo-CuAAC has only been implemented in a single wrinkle system. [232] This system, which also employed a two-tiered polymerization scheme, used a thiol-Michael addition to form the underlying elastomer and a photo-CuAAC reaction to form the high modulus thin film. Solvent containing a copper(II) source was swollen into the thiol-ene elastomer containing photoinitiator, unreacted pendant alkynes and diazide monomers. The swelling of the elastomer provided sufficient deformation on the elastomer, and upon irradiation, reduction of the copper (II) to copper(I) resulted in local CuAAC reactions at the surface of the elastomer, thereby increasing the modulus through formation of additional crosslinks. Once the elastomer deswelled, wrinkles spontaneously formed.

While this system provides a starting point for CuAAC-based wrinkling, two main challenges exist. First, the film thickness was controlled solely through diffusion of the copper(II), which resulted in variability in wrinkle wavelengths. Second,

swelling-based deformations results in isotropic wrinkle patterns, which are difficult to confine and align from an application standpoint.

Flowcoating of photo-CuAAC monomers can be used to address both of these challenges. A unique property of CuAAC films is their high fracture toughness, even in glassy networks, which enable CuAAC materials to reach strains in excess of 100%. Moreover, as demonstrated by previous work in the Kloxin group [233], once strained, these networks actually maintain that strain, though the time scale of this effect is unknown. Only under application of heat above the glass transition temperature of CuAAC network, will the network return to its original length. Preliminary work in the Kloxin group also found that the modulus of the film is conserved after application of strain/heat as compared to the original material.

Using this property of CuAAC networks, flowcoated CuAAC films can be formulated with excess alkyne functionalities or reacted with propargyl acrylates to yield functional handles that can be used to covalently attach films to unstrained elastomer substrates through thiol-yne or thiol-Michael reactions respectively. The elastomer/CuAAC film bilayer can then be strained (uniaxially or biaxially) and held for a duration of time to allow the CuAAC film to relax to the elongated state. Upon releasing the strain, while the elastomer will snap back to its original length, the CuAAC film should maintain its elongated state, thus generating wrinkles. Through heat (i.e., embossing) these wrinkles can be spatially removed, ultimately yielding a thermoresponsive CuAAC wrinkling system.

### **5.3 Future Directions – Wrinkled Particles**

Beyond the development of planar wrinkled materials, extending wrinkling to spherical surfaces, particularly particles, has gained attention in the last decade [234-

250], with some notable applications in increasing photovoltaic efficiency through wrinkled titanium dioxide particles [240], smart surfaces for improved aerodynamics [244], drug delivery [236,239,247], and as biomaterial platforms for cell attachment [243].

Wrinkled particles are developed using similar criterion as wrinkled planar surfaces. Like planar systems, particles must contain a thin, high modulus shell attached to a thicker softer core to create a modulus mismatch. The shell must also be sufficiently deformed under compressive stress (i.e., through deswelling of the particle) to form wrinkled morphologies. The notable exception is how wrinkle wavelength scales with film thickness. Cao and coworkers demonstrated through theory and simulation, that wrinkle wavelength follows a power law scaling,  $\lambda/R = a(R/h)^b$ , where  $\lambda$  is the wrinkle wavelength,  $R$  is the particle radius,  $h$  is the shell thickness and  $a$  and  $b$  are power law constants [234]. Values  $a=3.0$  and  $b=-0.8$  showed reasonable fitting for  $R/h < 100$ . As  $R/h \rightarrow \infty$  (i.e., large particle size), the wavelength scaling will eventually reflect the planar wrinkle wavelength equation.

Though micro- and nanoparticles have been synthesized using ‘click monomer systems via microfluidics and emulsion or suspension polymerizations [251-261], no particle systems have been developed to wrinkle. Using the aforementioned CuAAC reaction, it may be possible to create wrinkles on particle surfaces (Figure 5.3). Multifunctional CuAAC monomers dissolved in an organic solvent can be dispersed in an aqueous media such as water. The monomer/solvent system, being insoluble in water, can be stabilized with a surfactant such as sodium dodecyl sulfate. Catalytic amounts of copper (I) can then be introduced into the mixture. While some copper species are soluble in the organic monomers, others are difficult to disperse in the

organic monomers without a ligand. By selecting a copper source that can only dissolve in the aqueous phase, reaction will only occur at the organic-aqueous interface of the droplets, thereby polymerizing the monomers to form a polymer shell. This shell thickness can be controlled through reaction time via diffusion of copper into the droplet. Once the polymer particles are removed from the aqueous media and dried, the deswelling process will result in wrinkling of the solid shell.

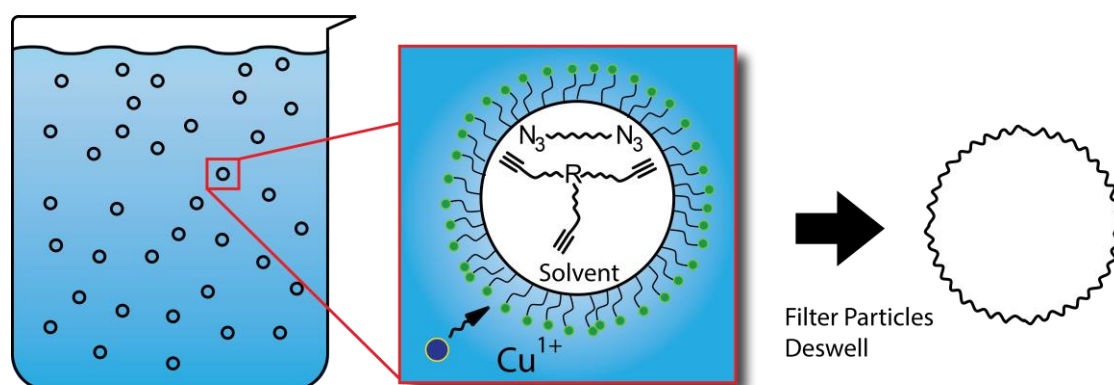


**Figure 5.3. Formation of wrinkled particles using CuAAC ‘click’ chemistry.** Organic multifunctional azide and alkyne monomers and organic solvent are suspended in an aqueous solution containing copper (I) and stabilized at the oil-water droplet interface by surfactant. Because specific species of copper (I) do not readily dissolve in the organic phase, polymerization is limited to the droplet interface, forming a shell. Diffusion of the copper into the droplet will dictate shell thickness. Upon filtering the particles and deswelling the organic solvent, wrinkles will spontaneously form due to the elastic modulus mismatch between the harder shell and the liquid core.

Because the liquid monomer is encapsulated by a solid shell, the modulus mismatch between the core and the shell is several orders of magnitude higher than traditional polymer bilayer systems. The wrinkle wavelength and amplitude are functions of the elastic mismatch and thus it is feasible to produce high aspect radial wrinkle structures by controlling the degree of deswelling, which ultimately can increase the available surface area of these particles.

## REFERENCES

- [1]. Rothmund, P. W. K. Folding DNA to create nanoscale shapes and patterns, *Nature*. **2006**, 440, 297-302
- [2]. Chang, E. P. Viscoelastic properties of pressure-sensitive adhesives, *Journal of Adhesion*. **1997**, 60, 233-248
- [3]. Engler, A. J., Griffin, M. A., Sen, S., Bonnetmann, C. G., Sweeney, H. L. and Discher, D. E. Myotubes differentiate optimally on substrates with tissue-like stiffness: pathological implications for soft or stiff microenvironments, *Journal of Cell Biology*. **2004**, 166, 877-887
- [4]. Jiang, X. F., Yang, K., Yang, X. Q., Liu, Y. F., Cheng, Y. C., Chen, X. Y. and Tu, Y. Elastic modulus affects the growth and differentiation of neural stem cells, *Neural Regeneration Research*. **2015**, 10, 1523-1527
- [5]. Laniel, M., Huq, E., Allen, S., Buttery, L., Williams, P. M. and Alexander, M. R. Substrate induced differentiation of human mesenchymal stem cells on hydrogels with modified surface chemistry and controlled modulus, *Soft Matter*. **2011**, 7, 6501-6514
- [6]. Leipzig, N. D. and Shoichet, M. S. The effect of substrate stiffness on adult neural stem cell behavior, *Biomaterials*. **2009**, 30, 6867-6878
- [7]. Mullen, C. A., Vaughan, T. J., Billiar, K. L. and McNamara, L. M. The Effect of Substrate Stiffness, Thickness, and Cross-Linking Density on Osteogenic Cell Behavior, *Biophysical Journal*. **2015**, 108, 1604-1612
- [8]. Romanazzo, S. Effects of substrate stiffness on myoblasts phenotype and differentiation, *Journal of Tissue Engineering and Regenerative Medicine*. **2012**, 6, 239-239
- [9]. Xu, Q. W., Li, C., Kang, Y. J. and Zhang, Y. L. Long term effects of substrate stiffness on the development of hMSC mechanical properties, *Rsc Advances*. **2015**, 5, 105651-105660

- [10]. Hozumi, A., Ushiyama, K., Sugimura, H. and Takai, O. Fluoroalkylsilane monolayers formed by chemical vapor surface modification on hydroxylated oxide surfaces, *Langmuir*. **1999**, 15, 7600-7604
- [11]. Pester, C. W., Poelma, J. E., Narupai, B., Patel, S. N., Su, G. M., Mates, T. E., Luo, Y. D., Ober, C. K., Hawker, C. J. and Kramer, E. J. Ambiguous Anti-Fouling Surfaces: Facile Synthesis by Light-Mediated Radical Polymerization, *Journal of Polymer Science Part a-Polymer Chemistry*. **2016**, 54, 253-262
- [12]. Lee, H., Alcaraz, M. L., Rubner, M. F. and Cohen, R. E. Zwitter-Wettability and Antifogging Coatings with Frost-Resisting Capabilities, *Acs Nano*. **2013**, 7, 2172-2185
- [13]. Lee, H., Dellatore, S. M., Miller, W. M. and Messersmith, P. B. Mussel-inspired surface chemistry for multifunctional coatings, *Science*. **2007**, 318, 426-430
- [14]. Mussel-Inspired Glue Seals Membranes, *Science*. **2013**, 339, 890-890
- [15]. Li, A. L., Mu, Y. B., Jiang, W. and Wan, X. B. A mussel-inspired adhesive with stronger bonding strength under underwater conditions than under dry conditions, *Chemical Communications*. **2015**, 51, 9117-9120
- [16]. Ahn, B. K., Das, S., Linstadt, R., Kaufman, Y., Martinez-Rodriguez, N. R., Mirshafian, R., Kesselman, E., Talmon, Y., Lipshutz, B. H., Israelachvili, J. N. and Waite, J. H. High-performance mussel-inspired adhesives of reduced complexity, *Nature Communications*. **2015**, 6,
- [17]. Favia, P. and d'Agostino, R. Plasma treatments and plasma deposition of polymers for biomedical applications, *Surface & Coatings Technology*. **1998**, 98, 1102-1106
- [18]. Della Giustina, G., Giulitti, S., Brigo, L., Zanatta, M., Tromayer, M., Liska, R., Elvassore, N. and Brusatin, G. Hydrogel with Orthogonal Reactive Units: 2D and 3D Cross-Linking Modulation, *Macromolecular Rapid Communications*. **2017**, 38,
- [19]. Krishnan, S., Ayothi, R., Hexemer, A., Finlay, J. A., Sohn, K. E., Perry, R., Ober, C. K., Kramer, E. J., Callow, M. E., Callow, J. A. and Fischer, D. A. Anti-biofouling properties of comblike block copolymers with amphiphilic side chains, *Langmuir*. **2006**, 22, 5075-5086
- [20]. Kuddannaya, S., Chuah, Y. J., Lee, M. H. A., Menon, N. V., Kang, Y. J. and Zhang, Y. L. Surface Chemical Modification of Poly(dimethylsiloxane) for the Enhanced Adhesion and Proliferation of Mesenchymal Stem Cells, *Acs Applied Materials & Interfaces*. **2013**, 5, 9777-9784

- [21]. Saha, K., Keung, A. J., Irwin, E. F., Li, Y., Little, L., Schaffer, D. V. and Healy, K. E. Substrate Modulus Directs Neural Stem Cell Behavior, *Biophysical Journal*. **2008**, 95, 4426-4438
- [22]. Barthlott, W. and Neinhuis, C. Purity of the sacred lotus, or escape from contamination in biological surfaces, *Planta*. **1997**, 202, 1-8
- [23]. Feng, L., Li, S. H., Li, Y. S., Li, H. J., Zhang, L. J., Zhai, J., Song, Y. L., Liu, B. Q., Jiang, L. and Zhu, D. B. Super-hydrophobic surfaces: From natural to artificial, *Advanced Materials*. **2002**, 14, 1857-1860
- [24]. Bhushan, B. Bioinspired Structured Surfaces, *Langmuir*. **2012**, 28, 1698-1714
- [25]. Szyndler, M. W., Haynes, K. F., Potter, M. F., Corn, R. M. and Loudon, C. Entrapment of bed bugs by leaf trichomes inspires microfabrication of biomimetic surfaces, *Journal of the Royal Society Interface*. **2013**, 10,
- [26]. Autumn, K., Liang, Y. A., Hsieh, S. T., Zesch, W., Chan, W. P., Kenny, T. W., Fearing, R. and Full, R. J. Adhesive force of a single gecko foot-hair, *Nature*. **2000**, 405, 681-685
- [27]. Autumn, K., Sitti, M., Liang, Y. C. A., Peattie, A. M., Hansen, W. R., Sponberg, S., Kenny, T. W., Fearing, R., Israelachvili, J. N. and Full, R. J. Evidence for van der Waals adhesion in gecko setae, *Proceedings of the National Academy of Sciences of the United States of America*. **2002**, 99, 12252-12256
- [28]. Hansen, W. R. and Autumn, K. Evidence for self-cleaning in gecko setae, *Proceedings of the National Academy of Sciences of the United States of America*. **2005**, 102, 385-389
- [29]. Tian, Y., Pesika, N., Zeng, H. B., Rosenberg, K., Zhao, B. X., McGuiggan, P., Autumn, K. and Israelachvili, J. Adhesion and friction in gecko toe attachment and detachment, *Proceedings of the National Academy of Sciences of the United States of America*. **2006**, 103, 19320-19325
- [30]. Northen, M. T., Greiner, C., Arzt, E. and Turner, K. L. A Gecko-Inspired Reversible Adhesive, *Advanced Materials*. **2008**, 20, 3905-+
- [31]. Boesel, L. F., Greiner, C., Arzt, E. and del Campo, A. Gecko-Inspired Surfaces: A Path to Strong and Reversible Dry Adhesives, *Advanced Materials*. **2010**, 22, 2125-2137
- [32]. Jin, K., Tian, Y., Erickson, J. S., Puthoff, J., Autumn, K. and Pesika, N. S. Design and Fabrication of Gecko-Inspired Adhesives, *Langmuir*. **2012**, 28, 5737-5742

- [33]. Schumacher, J. F., Aldred, N., Callow, M. E., Finlay, J. A., Callow, J. A., Clare, A. S. and Brennan, A. B. Species-specific engineered antifouling topographies: correlations between the settlement of algal zoospores and barnacle cyprids, *Biofouling*. **2007**, 23, 307-317
- [34]. Schumacher, J. F., Carman, M. L., Estes, T. G., Feinberg, A. W., Wilson, L. H., Callow, M. E., Callow, J. A., Finlay, J. A. and Brennan, A. B. Engineered antifouling microtopographies - effect of feature size, geometry, and roughness on settlement of zoospores of the green alga *Ulva*, *Biofouling*. **2007**, 23, 55-62
- [35]. Wooh, S., Koh, J. H., Lee, S., Yoon, H. and Char, K. Trilevel-Structured Superhydrophobic Pillar Arrays with Tunable Optical Functions, *Advanced Functional Materials*. **2014**, 24, 5550-5556
- [36]. Lopez-Bosque, M. J., Tejada-Montes, E., Cazorla, M., Linacero, J., Atienza, Y., Smith, K. H., Llado, A., Colombelli, J., Engel, E. and Mata, A. Fabrication of hierarchical micro-nanotopographies for cell attachment studies, *Nanotechnology*. **2013**, 24,
- [37]. Engelmayr, G. C., Cheng, M. Y., Bettinger, C. J., Borenstein, J. T., Langer, R. and Freed, L. E. Accordion-like honeycombs for tissue engineering of cardiac anisotropy, *Nature Materials*. **2008**, 7, 1003-1010
- [38]. Wang, P. Y., Li, W. T., Yu, J. S. and Tsai, W. B. Modulation of osteogenic, adipogenic and myogenic differentiation of mesenchymal stem cells by submicron grooved topography, *Journal of Materials Science-Materials in Medicine*. **2012**, 23, 3015-3028
- [39]. Hagberg, E. C., Malkoch, M., Ling, Y. B., Hawker, C. J. and Carter, K. R. Effects of modulus and surface chemistry of thiol-ene photopolymers in nanoimprinting, *Nano Letters*. **2007**, 7, 233-237
- [40]. Johnson, B. N., Lancaster, K. Z., Zhen, G. H., He, J. Y., Gupta, M. K., Kong, Y. L., Engel, E. A., Krick, K. D., Ju, A., Meng, F. B., Enquist, L. W., Jia, X. F. and McAlpine, M. C. 3D Printed Anatomical Nerve Regeneration Pathways, *Advanced Functional Materials*. **2015**, 25, 6205-6217
- [41]. Derby, B. Printing and Prototyping of Tissues and Scaffolds, *Science*. **2012**, 338, 921-926
- [42]. Groenewold, J. Wrinkling of plates coupled with soft elastic media, *Physica A*. **2001**, 298, 32-45

- [43]. Genzer, J. and Groenewold, J. Soft matter with hard skin: From skin wrinkles to templating and material characterization, *Soft Matter*. **2006**, 2, 310-323
- [44]. Thurlimann, B. Column Buckling - Historical and Actual Notes, *Journal of Constructional Steel Research*. **1990**, 17, 95-111
- [45]. Cerda, E. and Mahadevan, L. Geometry and physics of wrinkling, *Physical Review Letters*. **2003**, 90,
- [46]. Yang, S., Khare, K. and Lin, P.-C. Harnessing Surface Wrinkle Patterns in Soft Matter, *Advanced Functional Materials*. **2010**, 20, 2550-2564
- [47]. Jiang, H. Q., Khang, D. Y., Song, J. Z., Sun, Y. G., Huang, Y. G. and Rogers, J. A. Finite deformation mechanics in buckled thin films on compliant supports, *Proceedings of the National Academy of Sciences of the United States of America*. **2007**, 104, 15607-15612
- [48]. Wang, S., Song, J., Kim, D.-H., Huang, Y. and Rogers, J. A. Local versus global buckling of thin films on elastomeric substrates, *Applied Physics Letters*. **2008**, 93, 023126
- [49]. Wang, S. D., Song, J. Z., Kim, D. H., Huang, Y. G. and Rogers, J. A. Local versus global buckling of thin films on elastomeric substrates, *Applied Physics Letters*. **2008**, 93,
- [50]. Wang, Q. M. and Zhao, X. H. A three-dimensional phase diagram of growth-induced surface instabilities, *Scientific Reports*. **2015**, 5,
- [51]. Wang, Q. and Zhao, X. A three-dimensional phase diagram of growth-induced surface instabilities, *Sci Rep*. **2015**, 5, 8887
- [52]. Bowden, N., Brittain, S., Evans, A. G., Hutchinson, J. W. and Whitesides, G. M. Spontaneous formation of ordered structures in thin films of metals supported on an elastomeric polymer, *Nature*. **1998**, 393, 146-149
- [53]. Bowden, N., Huck, W. T. S., Paul, K. E. and Whitesides, G. M. The controlled formation of ordered, sinusoidal structures by plasma oxidation of an elastomeric polymer, *Applied Physics Letters*. **1999**, 75, 2557-2559
- [54]. Chua, D. B. H., Ng, H. T. and Li, S. F. Y. Spontaneous formation of complex and ordered structures on oxygen-plasma-treated elastomeric polydimethylsiloxane, *Applied Physics Letters*. **2000**, 76, 721-723

- [55]. Chen, X. and Hutchinson, J. W. Herringbone buckling patterns of compressed thin films on compliant substrates, *Journal of Applied Mechanics-Transactions of the Asme.* **2004**, 71, 597-603
- [56]. Efimenko, K., Rackaitis, M., Manias, E., Vaziri, A., Mahadevan, L. and Genzer, J. Nested self-similar wrinkling patterns in skins, *Nature Materials.* **2005**, 4, 293-297
- [57]. Chandra, D., Yang, S. and Lin, P.-C. Strain responsive concave and convex microlens arrays, *Applied Physics Letters.* **2007**, 91,
- [58]. Watanabe, M. and Hashimoto, R. Area-Selective Microwrinkle Formation on Poly(dimethylsiloxane) by Treatment with Strong Acid, *Journal of Polymer Science Part B-Polymer Physics.* **2015**, 53, 167-174
- [59]. Stafford, C. M., Harrison, C., Beers, K. L., Karim, A., Amis, E. J., Vanlandingham, M. R., Kim, H. C., Volksen, W., Miller, R. D. and Simonyi, E. E. A buckling-based metrology for measuring the elastic moduli of polymeric thin films, *Nature Materials.* **2004**, 3, 545-550
- [60]. Imburgia, M. J. and Crosby, A. J. Rolling wrinkles on elastic substrates, *Extreme Mechanics Letters.* **2016**, 6, 23-30
- [61]. Kim, J., Yoon, J. and Hayward, R. C. Dynamic display of biomolecular patterns through an elastic creasing instability of stimuli-responsive hydrogels, *Nature Materials.* **2010**, 9, 159-164
- [62]. Takeshima, T., Liao, W., Nagashima, Y., Beppu, K., Hara, M., Nagano, S. and Seki, T. Photoresponsive Surface Wrinkle Morphologies in Liquid Crystalline Polymer Films, *Macromolecules.* **2015**, 48, 6378-6384
- [63]. Chan, E. P. and Crosby, A. J. Spontaneous formation of stable aligned wrinkling patterns, *Soft Matter.* **2006**, 2, 324-328
- [64]. Guvendiren, M. and Burdick, J. A. The control of stem cell morphology and differentiation by hydrogel surface wrinkles, *Biomaterials.* **2010**, 31, 6511-6518
- [65]. Lin, P. C. and Yang, S. Spontaneous formation of one-dimensional ripples in transit to highly ordered two-dimensional herringbone structures through sequential and unequal biaxial mechanical stretching, *Applied Physics Letters.* **2007**, 90,
- [66]. Kim, J. B., Kim, P., Pegard, N. C., Oh, S. J., Kagan, C. R., Fleischer, J. W., Stone, H. A. and Loo, Y. L. Wrinkles and deep folds as photonic structures in photovoltaics, *Nature Photonics.* **2012**, 6, 327-332

- [67]. van den Ende, D., Kamminga, J. D., Boersma, A., Andritsch, T. and Steeneken, P. G. Voltage-Controlled Surface Wrinkling of Elastomeric Coatings, *Advanced Materials*. **2013**, 25, 3438-3442
- [68]. Efimenko, K., Finlay, J., Callow, M. E., Callow, J. A. and Genzer, J. Development and Testing of Hierarchically Wrinkled Coatings for Marine Antifouling, *Acs Applied Materials & Interfaces*. **2009**, 1, 1031-1040
- [69]. Lin, P.-C., Vajpayee, S., Jagota, A., Hui, C.-Y. and Yang, S. Mechanically tunable dry adhesive from wrinkled elastomers, *Soft Matter*. **2008**, 4, 1830-1835
- [70]. Davis, C. S., Martina, D., Creton, C., Lindner, A. and Crosby, A. J. Enhanced Adhesion of Elastic Materials to Small-Scale Wrinkles, *Langmuir*. **2012**, 28, 14899-14908
- [71]. Jeong, H. E., Kwak, M. K. and Suh, K. Y. Stretchable, Adhesion-Tunable Dry Adhesive by Surface Wrinkling, *Langmuir*. **2010**, 26, 2223-2226
- [72]. Charest, J. L., Eliason, M. T., Garcia, A. J. and King, W. P. Combined microscale mechanical topography and chemical patterns on polymer cell culture substrates, *Biomaterials*. **2006**, 27, 2487-2494
- [73]. Chua, J. S., Chng, C. P., Moe, A. A. K., Tann, J. Y., Goh, E. L. K., Chiam, K. H. and Yim, E. K. F. Extending neurites sense the depth of the underlying topography during neuronal differentiation and contact guidance, *Biomaterials*. **2014**, 35, 7750-7761
- [74]. Chuah, Y. J., Koh, Y. T., Lim, K., Menon, N. V., Wu, Y. and Kang, Y. Simple surface engineering of polydimethylsiloxane with polydopamine for stabilized mesenchymal stem cell adhesion and multipotency, *Scientific Reports*. **2015**, 5,
- [75]. Clark, P., Connolly, P., Curtis, A. S. G., Dow, J. A. T. and Wilkinson, C. D. W. Cell Guidance by Ultrafine Topography In vitro, *Journal of Cell Science*. **1991**, 99, 73-77
- [76]. Dalby, M. J., Riehle, M. O., Yarwood, S. J., Wilkinson, C. D. W. and Curtis, A. S. G. Nucleus alignment and cell signaling in fibroblasts: response to a micro-grooved topography, *Experimental Cell Research*. **2003**, 284, 274-282
- [77]. Greco, F., Fujie, T., Ricotti, L., Taccola, S., Mazzolai, B. and Mattoli, V. Microwrinkled Conducting Polymer Interface for Anisotropic Multicellular Alignment, *Acs Applied Materials & Interfaces*. **2013**, 5, 573-584

- [78]. Kiang, J. D., Wen, J. H., del Alamo, J. C. and Engler, A. J. Dynamic and reversible surface topography influences cell morphology, *Journal of Biomedical Materials Research Part A*. **2013**, 101A, 2313-2321
- [79]. Lim, J. Y. and Donahue, H. J. Cell sensing and response to micro- and nanostructured surfaces produced by chemical and topographic patterning, *Tissue Engineering*. **2007**, 13, 1879-1891
- [80]. Luna, J. I., Ciriza, J., Garcia-Ojeda, M. E., Kong, M., Herren, A., Lieu, D. K., Li, R. A., Fowlkes, C. C., Khine, M. and McCloskey, K. E. Multiscale Biomimetic Topography for the Alignment of Neonatal and Embryonic Stem Cell-Derived Heart Cells, *Tissue Engineering Part C-Methods*. **2011**, 17, 579-588
- [81]. Wang, Z. Y., Teo, E. Y., Chong, M. S. K., Zhang, Q. Y., Lim, J., Zhang, Z. Y., Hong, M. H., Thian, E. S., Chan, J. K. Y. and Teoh, S. H. Biomimetic Three-Dimensional Anisotropic Geometries by Uniaxial Stretch of Poly(epsilon-Caprolactone) Films for Mesenchymal Stem Cell Proliferation, Alignment, and Myogenic Differentiation, *Tissue Engineering Part C-Methods*. **2013**, 19, 538-549
- [82]. Yang, P., Baker, R. M., Henderson, J. H. and Mather, P. T. In vitro wrinkle formation via shape memory dynamically aligns adherent cells, *Soft Matter*. **2013**, 9, 4705-4714
- [83]. Yim, E. K. F., Darling, E. M., Kulangara, K., Guilak, F. and Leong, K. W. Nanotopography-induced changes in focal adhesions, cytoskeletal organization, and mechanical properties of human mesenchymal stem cells, *Biomaterials*. **2010**, 31, 1299-1306
- [84]. Zahor, D., Radko, A., Vago, R. and Gheber, L. A. Organization of mesenchymal stem cells is controlled by micropatterned silicon substrates, *Materials Science & Engineering C-Biomimetic and Supramolecular Systems*. **2007**, 27, 117-121
- [85]. Zhu, H. B., Cao, B. R., Zhen, Z. P., Laxmi, A. A., Li, D., Liu, S. R. and Mao, C. B. Controlled growth and differentiation of MSCs on grooved films assembled from monodisperse biological nanofibers with genetically tunable surface chemistries, *Biomaterials*. **2011**, 32, 4744-4752
- [86]. Vandeparre, H., Gabriele, S., Brau, F., Gay, C., Parker, K. K. and Damman, P. Hierarchical wrinkling patterns, *Soft Matter*. **2010**, 6, 5751-5756
- [87]. Guvendiren, M. and Burdick, J. A. Stem Cell Response to Spatially and Temporally Displayed and Reversible Surface Topography, *Advanced Healthcare Materials*. **2013**, 2, 155-164

- [88]. Stafford, C. M., Vogt, B. D., Harrison, C., Julthongpiput, D. and Huang, R. Elastic moduli of ultrathin amorphous polymer films, *Macromolecules*. **2006**, 39, 5095-5099
- [89]. Anseth, K. S., Newman, S. M. and Bowman, C. N. Polymeric dental composites: Properties and reaction behavior of multimethacrylate dental restorations, *Biopolymers li*. **1995**, 122, 177-217
- [90]. Cook, W. D. PHOTOPOLYMERIZATION KINETICS OF DIMETHACRYLATES USING THE CAMPHORQUINONE AMINE INITIATOR SYSTEM, *Polymer*. **1992**, 33, 600-609
- [91]. Cramer, N. B., Stansbury, J. W. and Bowman, C. N. Recent Advances and Developments in Composite Dental Restorative Materials, *Journal of Dental Research*. **2011**, 90, 402-416
- [92]. Sideridou, I., Tserki, V. and Papanastasiou, G. Effect of chemical structure on degree of conversion in light-cured dimethacrylate-based dental resins, *Biomaterials*. **2002**, 23, 1819-1829
- [93]. Sideridou, I., Tserki, V. and Papanastasiou, G. Study of water sorption, solubility and modulus of elasticity of light-cured dimethacrylate-based dental resins, *Biomaterials*. **2003**, 24, 655-665
- [94]. Stansbury, J. W. and Dickens, S. H. Determination of double bond conversion in dental resins by near infrared spectroscopy, *Dental Materials*. **2001**, 17, 71-79
- [95]. Tumbleston, J. R., Shirvanyants, D., Ermoshkin, N., Januszewicz, R., Johnson, A. R., Kelly, D., Chen, K., Pinschmidt, R., Rolland, J. P., Ermoshkin, A., Samulski, E. T. and DeSimone, J. M. Continuous liquid interface production of 3D objects, *Science*. **2015**, 347, 1349-1352
- [96]. Wagner, C. and Harned, N. EUV LITHOGRAPHY Lithography gets extreme, *Nature Photonics*. **2010**, 4, 24-26
- [97]. Kloxin, C. J., Scott, T. F., Park, H. Y. and Bowman, C. N. Mechanophotopatterning on a Photoresponsive Elastomer, *Advanced Materials*. **2011**, 23, 1977-1981
- [98]. Amamoto, Y., Otsuka, H., Takahara, A. and Matyjaszewski, K. Self-Healing of Covalently Cross-Linked Polymers by Reshuffling Thiuram Disulfide Moieties in Air under Visible Light, *Advanced Materials*. **2012**, 24, 3975-3980

- [99]. Bowman, C. N. and Kloxin, C. J. Covalent Adaptable Networks: Reversible Bond Structures Incorporated in Polymer Networks, *Angewandte Chemie-International Edition*. **2012**, 51, 4272-4274
- [100]. Kloxin, C. J., Scott, T. F., Adzima, B. J. and Bowman, C. N. Covalent Adaptable Networks (CANS): A Unique Paradigm in Cross-Linked Polymers, *Macromolecules*. **2010**, 43, 2643-2653
- [101]. Ryu, J., D'Amato, M., Cui, X., Long, K. N., Qi, H. J. and Dunn, M. L. Photo-origami-Bending and folding polymers with light, *Applied Physics Letters*. **2012**, 100,
- [102]. Stuart, M. A. C., Huck, W. T. S., Genzer, J., Muller, M., Ober, C., Stamm, M., Sukhorukov, G. B., Szleifer, I., Tsukruk, V. V., Urban, M., Winnik, F., Zauscher, S., Luzinov, I. and Minko, S. Emerging applications of stimuli-responsive polymer materials, *Nature Materials*. **2010**, 9, 101-113
- [103]. Wu, D. Y., Meure, S. and Solomon, D. Self-healing polymeric materials: A review of recent developments, *Progress in Polymer Science*. **2008**, 33, 479-522
- [104]. Chatani, S., Kloxin, C. J. and Bowman, C. N. The power of light in polymer science: photochemical processes to manipulate polymer formation, structure, and properties, *Polymer Chemistry*. **2014**, 5, 2187-2201
- [105]. Maruo, S. and Kawata, S. Two-photon-absorbed photopolymerization for three-dimensional microfabrication, *Mems 97, Proceedings - Ieee the Tenth Annual International Workshop on Micro Electro Mechanical Systems*. **1997**, 169-174
- [106]. Maruo, S., Nakamura, O. and Kawata, S. Three-dimensional microfabrication with two-photon-absorbed photopolymerization, *Optics Letters*. **1997**, 22, 132-134
- [107]. LaFratta, C. N., Fourkas, J. T., Baldacchini, T. and Farrer, R. A. Multiphoton fabrication, *Angewandte Chemie-International Edition*. **2007**, 46, 6238-6258
- [108]. Scott, T. F., Kloxin, C. J., Forman, D. L., McLeod, R. R. and Bowman, C. N. Principles of voxel refinement in optical direct write lithography, *Journal of Materials Chemistry*. **2011**, 21, 14150-14155
- [109]. Scott, T. F., Kloxin, C. J., Draughon, R. B. and Bowman, C. N. Nonclassical dependence of polymerization rate on initiation rate observed in thiol-ene photopolymerizations, *Macromolecules*. **2008**, 41, 2987-2989

- [110]. Gan, Z. S., Cao, Y. Y., Evans, R. A. and Gu, M. Three-dimensional deep sub-diffraction optical beam lithography with 9 nm feature size, *Nature Communications*. **2013**, 4,
- [111]. Muller, T., Schumann, C. and Kraegeloh, A. STED Microscopy and its Applications: New Insights into Cellular Processes on the Nanoscale, *Chemphyschem*. **2012**, 13, 1986-2000
- [112]. Kolb, H. C., Finn, M. G. and Sharpless, K. B. Click chemistry: Diverse chemical function from a few good reactions, *Angewandte Chemie-International Edition*. **2001**, 40, 2004-+
- [113]. Sharpless, K. B. and Kolb, H. C. Click chemistry. A concept for merging process and discovery chemistry., *Abstracts of Papers of the American Chemical Society*. **1999**, 217, U95-U95
- [114]. Hoyle, C. E., Lowe, A. B. and Bowman, C. N. Thiol-click chemistry: a multifaceted toolbox for small molecule and polymer synthesis, *Chemical Society Reviews*. **2010**, 39, 1355-1387
- [115]. Hoyle, C. E. and Bowman, C. N. Thiol-Ene Click Chemistry, *Angewandte Chemie-International Edition*. **2010**, 49, 1540-1573
- [116]. Xi, W. X., Peng, H. Y., Aguirre-Soto, A., Kloxin, C. J., Stansbury, J. W. and Bowman, C. N. Spatial and Temporal Control of Thiol-Michael Addition via Photocaged Superbase in Photopatterning and Two-Stage Polymer Networks Formation, *Macromolecules*. **2014**, 47, 6159-6165
- [117]. Claudino, M., Zhang, X. P., Alim, M. D., Podgorski, M. and Bowman, C. N. Mechanistic Kinetic Modeling of Thiol-Michael Addition Photopolymerizations via Photocaged "Superbase" Generators: An Analytical Approach, *Macromolecules*. **2016**, 49, 8061-8074
- [118]. Cramer, N. B., Reddy, S. K., Cole, M., Hoyle, C. and Bowman, C. N. Initiation and kinetics of thiol-ene photopolymerizations without photoinitiators, *Journal of Polymer Science Part a-Polymer Chemistry*. **2004**, 42, 5817-5826
- [119]. Chan, J. W., Hoyle, C. E., Lowe, A. B. and Bowman, M. Nucleophile-Initiated Thiol-Michael Reactions: Effect of Organocatalyst, Thiol, and Ene, *Macromolecules*. **2010**, 43, 6381-6388
- [120]. Morgan, C. R., Magnotta, F. and Ketley, A. D. THIOL-ENE PHOTO-CURABLE POLYMERS, *Journal of Polymer Science Part a-Polymer Chemistry*. **1977**, 15, 627-645

- [121]. Hoyle, C. E., Lee, T. Y. and Roper, T. Thiol-enes: Chemistry of the past with promise for the future, *Journal of Polymer Science Part a-Polymer Chemistry*. **2004**, 42, 5301-5338
- [122]. Chatani, S., Sheridan, R. J., Podgorski, M., Nair, D. P. and Bowman, C. N. Temporal Control of Thiol-Click Chemistry, *Chemistry of Materials*. **2013**, 25, 3897-3901
- [123]. Odian, G. *Principles of Polymerization*, 4th Edition; John Wiley & Sons: Hoboken, NJ, 4th Edition, **2004**;
- [124]. Ma, S. J., Mannino, S. J., Wagner, N. J. and Kloxin, C. J. Photodirected Formation and Control of Wrinkles on a Thiol-ene Elastomer, *Acs Macro Letters*. **2013**, 2, 474-477
- [125]. Agrawal, A., Luchette, P., Palffy-Muhoray, P., Biswal, S. L., Chapman, W. G. and Verduzco, R. Surface wrinkling in liquid crystal elastomers, *Soft Matter*. **2012**, 8, 7138-7142
- [126]. Bayley, F. A., Liao, J. L., Stavrinou, P. N., Chiche, A. and Cabral, J. T. Wavefront kinetics of plasma oxidation of polydimethylsiloxane: limits for sub-mu m wrinkling, *Soft Matter*. **2014**, 10, 1155-1166
- [127]. Breid, D. and Crosby, A. J. Surface wrinkling behavior of finite circular plates, *Soft Matter*. **2009**, 5, 425-431
- [128]. Breid, D. and Crosby, A. J. Effect of stress state on wrinkle morphology, *Soft Matter*. **2011**, 7, 4490-4496
- [129]. Breid, D. and Crosby, A. J. Curvature-controlled wrinkle morphologies, *Soft Matter*. **2013**, 9, 3624-3630
- [130]. Chan, E. P. and Crosby, A. J. Fabricating microlens arrays by surface wrinkling, *Advanced Materials*. **2006**, 18, 3238
- [131]. Chen, Y. C. and Crosby, A. J. Wrinkling of inhomogeneously strained thin polymer films, *Soft Matter*. **2013**, 9, 43-47
- [132]. Chung, J. Y., Nolte, A. J. and Stafford, C. M. Surface Wrinkling: A Versatile Platform for Measuring Thin-Film Properties, *Advanced Materials*. **2011**, 23, 349-368
- [133]. Davis, C. S. and Crosby, A. J. Wrinkle morphologies with two distinct wavelengths, *Journal of Polymer Science Part B-Polymer Physics*. **2012**, 50, 1225-1232

- [134]. Hyun, D. C. and Jeong, U. Substrate Thickness: An Effective Control Parameter for Polymer Thin Film Buckling on PDMS Substrates, *Journal of Applied Polymer Science*. **2009**, 112, 2683-2690
- [135]. Khare, K., Zhou, J. and Yang, S. Tunable Open-Channel Microfluidics on Soft Poly(dimethylsiloxane) (PDMS) Substrates with Sinusoidal Grooves, *Langmuir*. **2009**, 25, 12794-12799
- [136]. Kim, H. S. and Crosby, A. J. Solvent-Responsive Surface via Wrinkling Instability, *Advanced Materials*. **2011**, 23, 4188-4192
- [137]. Moon, M. W., Lee, S. H., Sun, J. Y., Oh, K. H., Vaziri, A. and Hutchinson, J. W. Wrinkled hard skins on polymers created by focused ion beam, *Proceedings of the National Academy of Sciences of the United States of America*. **2007**, 104, 1130-1133
- [138]. Rodriguez-Hernandez, J. and del Campo, A. Fabrication of hierarchical wrinkled morphologies through sequential UVO treatments, *Journal of Applied Polymer Science*. **2015**, 132,
- [139]. Watanabe, M., Hatano, R. and Koizumi, C. Spontaneous formation of interdigitated array pattern in wrinkled gold films deposited on poly(dimethylsiloxane) elastomer, *Polymer Journal*. **2015**, 47, 320-327
- [140]. Xuan, Y., Guo, X., Cui, Y. S., Yuan, C. S., Ge, H. X., Cui, B. and Chen, Y. F. Crack-free controlled wrinkling of a bilayer film with a gradient interface, *Soft Matter*. **2012**, 8, 9603-9609
- [141]. Yabu, H., Saito, Y., Nakamichi, Y., Hirai, Y., Fujinami, S., Nakajima, K., Nishi, T. and Shimomura, M. Self-assembled porous templates allow pattern transfer to poly(dimethyl siloxane) sheets through surface wrinkling, *Polymer Journal*. **2012**, 44, 573-578
- [142]. Chan, E. P., Lin, Q. and Stafford, C. M. Quantifying the elasticity and viscosity of geometrically confined polymer films via thermal wrinkling, *Journal of Polymer Science Part B-Polymer Physics*. **2012**, 50, 1556-1561
- [143]. Chandra, D. and Crosby, A. J. Self-Wrinkling of UV-Cured Polymer Films, *Advanced Materials*. **2011**, 23, 3441-3445
- [144]. Lin, P.-C. and Yang, S. Mechanically switchable wetting on wrinkled elastomers with dual-scale roughness, *Soft Matter*. **2009**, 5, 1011-1018

- [145]. Huck, W. T. S., Bowden, N., Onck, P., Pardoën, T., Hutchinson, J. W. and Whitesides, G. M. Ordering of spontaneously formed buckles on planar surfaces, *Langmuir*. **2000**, 16, 3497-3501
- [146]. Nair, D. P., Cramer, N. B., Gaipa, J. C., McBride, M. K., Matherly, E. M., McLeod, R. R., Shandas, R. and Bowman, C. N. Two-Stage Reactive Polymer Network Forming Systems, *Advanced Functional Materials*. **2012**, 22, 1502-1510
- [147]. Nair, D. R., Cramer, N. B., McBride, M. K., Gaipa, J. C., Shandas, R. and Bowman, C. N. Enhanced two-stage reactive polymer network forming systems, *Polymer*. **2012**, 53, 2429-2434
- [148]. O'Brien, A. K. and Bowman, C. N. Impact of oxygen on photopolymerization kinetics and polymer structure, *Macromolecules*. **2006**, 39, 2501-2506
- [149]. O'Brien, A. K. and Bowman, C. N. Modeling the effect of oxygen on photopolymerization kinetics, *Macromolecular Theory and Simulations*. **2006**, 15, 176-182
- [150]. Li, Y. Y., Dai, S. X., John, J. and Carter, K. R. Superhydrophobic Surfaces from Hierarchically Structured Wrinkled Polymers, *Acs Applied Materials & Interfaces*. **2013**, 5, 11066-11073
- [151]. Zhang, Z., Zhang, T., Zhang, Y. W., Kim, K.-S. and Gao, H. Strain-Controlled Switching of Hierarchically Wrinkled Surfaces between Superhydrophobicity and Superhydrophilicity, **2012**, 28, 2753-2760
- [152]. Harrison, C., Stafford, C. M., Zhang, W. H. and Karim, A. Sinusoidal phase grating created by a tunably buckled surface, *Applied Physics Letters*. **2004**, 85, 4016-4018
- [153]. Khang, D. Y., Rogers, J. A. and Lee, H. H. Mechanical Buckling: Mechanics, Metrology, and Stretchable Electronics, *Advanced Functional Materials*. **2009**, 19, 1526-1536
- [154]. Ma, Y. J., Jang, K. I., Wang, L., Jung, H. N., Kwak, J. W., Xue, Y. G., Chen, H., Yang, Y. Y., Shi, D. W., Feng, X., Rogers, J. A. and Huang, Y. G. Design of Strain-Limiting Substrate Materials for Stretchable and Flexible Electronics, *Advanced Functional Materials*. **2016**, 26, 5345-5351
- [155]. Kim, B., Peterson, E. T. K. and Papautsky, I. Long-term stability of plasma oxidized PDMS surfaces, *Proceedings of the 26th Annual International Conference of the Ieee Engineering in Medicine and Biology Society, Vols 1-7*. **2004**, 26, 5013-5016

- [156]. Kim, J., Chaudhury, M. K. and Owen, M. J. Hydrophobicity loss and recovery of silicone HV insulation, *Ieee Transactions on Dielectrics and Electrical Insulation*. **1999**, 6, 695-702
- [157]. Morra, M., Occhiello, E., Marola, R., Garbassi, F., Humphrey, P. and Johnson, D. On the Aging of Oxygen Plasma-Treated Polydimethylsiloxane Surfaces, *Journal of Colloid and Interface Science*. **1990**, 137, 11-24
- [158]. Cordeiro, A. L., Nitschke, M., Janke, A., Helbig, R., D'Souza, F., Donnelly, G. T., Willemsen, P. R. and Werner, C. Fluorination of poly(dimethylsiloxane) surfaces by low pressure CF(4) plasma - physicochemical and antifouling properties, *Express Polymer Letters*. **2009**, 3, 70-83
- [159]. Maheshwari, N., Kottantharayil, A., Kumar, M. and Mukherji, S. Long term hydrophilic coating on poly(dimethylsiloxane) substrates for microfluidic applications, *Applied Surface Science*. **2010**, 257, 451-457
- [160]. Mosadegh, B., Tavana, H., Leshner-Perez, S. C. and Takayama, S. High-density fabrication of normally closed microfluidic valves by patterned deactivation of oxidized polydimethylsiloxane, *Lab on a Chip*. **2011**, 11, 738-742
- [161]. Sharma, V., Dhayal, M., Govind, Shivaprasad, S. M. and Jain, S. C. Surface characterization of plasma-treated and PEG-grafted PDMS for micro fluidic applications, *Vacuum*. **2007**, 81, 1094-1100
- [162]. Yao, M. J. and Fang, J. Hydrophilic PEO-PDMS for microfluidic applications, *Journal of Micromechanics and Microengineering*. **2012**, 22,
- [163]. Tan, S. H., Nguyen, N. T., Chua, Y. C. and Kang, T. G. Oxygen plasma treatment for reducing hydrophobicity of a sealed polydimethylsiloxane microchannel, *Biomicrofluidics*. **2010**, 4,
- [164]. Zhang, Z. L., Crozatier, C., Le Berre, M. and Chen, Y. In situ bio-functionalization and cell adhesion in microfluidic devices, *Microelectronic Engineering*. **2005**, 78-79, 556-562
- [165]. Roth, J., Albrecht, V., Nitschke, M., Bellmann, C., Simon, F., Zschoche, S., Michel, S., Luhmann, C., Grundke, K. and Voit, B. Surface Functionalization of Silicone Rubber for Permanent Adhesion Improvement, *Langmuir*. **2008**, 24, 12603-12611
- [166]. Frimat, J. P., Menne, H., Michels, A., Kittel, S., Kettler, R., Borgmann, S., Franzke, J. and West, J. Plasma stencilling methods for cell patterning, *Analytical and Bioanalytical Chemistry*. **2009**, 395, 601-609

- [167]. Hillborg, H., Ankner, J. F., Gedde, U. W., Smith, G. D., Yasuda, H. K. and Wikstrom, K. Crosslinked polydimethylsiloxane exposed to oxygen plasma studied by neutron reflectometry and other surface specific techniques, *Polymer*. **2000**, 41, 6851-6863
- [168]. Wang, P. Y., Yu, H. T. and Tsai, W. B. Modulation of Alignment and Differentiation of Skeletal Myoblasts by Submicron Ridges/Grooves Surface Structure, *Biotechnology and Bioengineering*. **2010**, 106, 285-294
- [169]. Kilian, K. A., Bugarija, B., Lahn, B. T. and Mrksich, M. Geometric cues for directing the differentiation of mesenchymal stem cells, *Proceedings of the National Academy of Sciences of the United States of America*. **2010**, 107, 4872-4877
- [170]. Collins, J. M., Porter, K. A., Singh, S. K. and Vanier, G. S. High-Efficiency Solid Phase Peptide Synthesis (HE-SPPS), *Organic Letters*. **2014**, 16, 940-943
- [171]. Merrifield, R. B. Solid Phase Peptide Synthesis .1. Synthesis of a Tetrapeptide, *Journal of the American Chemical Society*. **1963**, 85, 2149-&
- [172]. Sawicki, L. A. and Kloxin, A. M. Design of thiol-ene photoclick hydrogels using facile techniques for cell culture applications, *Biomaterials Science*. **2014**, 2, 1612-1626
- [173]. Fairbanks, B. D., Schwartz, M. P., Bowman, C. N. and Anseth, K. S. Photoinitiated polymerization of PEG-diacrylate with lithium phenyl-2,4,6-trimethylbenzoylphosphinate: polymerization rate and cytocompatibility, *Biomaterials*. **2009**, 30, 6702-6707
- [174]. Rana, D. and Matsuura, T. Surface modifications for antifouling membranes, *Chem Rev*. **2010**, 110, 2448-71
- [175]. Rufin, M. A., Barry, M. E., Adair, P. A., Hawkins, M. L., Raymond, J. E. and Grunlan, M. A. Protein resistance efficacy of PEO-silane amphiphiles: Dependence on PEO-segment length and concentration, *Acta Biomaterialia*. **2016**, 41, 247-252
- [176]. Sebra, R. P., Reddy, S. K., Masters, K. S., Bowman, C. N. and Anseth, K. S. Controlled polymerization chemistry to graft architectures that influence cell-material interactions, *Acta Biomaterialia*. **2007**, 3, 151-161
- [177]. Frith, J. E., Mills, R. J., Hudson, J. E. and Cooper-White, J. J. Tailored Integrin-Extracellular Matrix Interactions to Direct Human Mesenchymal Stem Cell Differentiation, *Stem Cells and Development*. **2012**, 21, 2442-2456

- [178]. Wong, S. T., Teo, S. K., Park, S., Chiam, K. H. and Yim, E. K. F. Anisotropic rigidity sensing on grating topography directs human mesenchymal stem cell elongation, *Biomechanics and Modeling in Mechanobiology*. **2014**, 13, 27-39
- [179]. Subramony, S. D., Dargis, B. R., Castillo, M., Azeloglu, E. U., Tracey, M. S., Su, A. and Lu, H. H. The guidance of stem cell differentiation by substrate alignment and mechanical stimulation, *Biomaterials*. **2013**, 34, 1942-1953
- [180]. Suzuki, K., Hirai, Y. and Ohzono, T. Oscillating Friction on Shape-Tunable Wrinkles, *Acs Applied Materials & Interfaces*. **2014**, 6, 10121-10131
- [181]. Lowe, A. B. Thiol-ene "click" reactions and recent applications in polymer and materials synthesis: a first update, *Polymer Chemistry*. **2014**, 5, 4820-4870
- [182]. Brei, M. R., Donovan, B. R., Patton, D. L. and Storey, R. F. Synthesis and thiol-ene photopolymerization of (meth)allyl-terminated polysulfides, *Journal of Applied Polymer Science*. **2017**, 134,
- [183]. Gould, S. T., Darling, N. J. and Anseth, K. S. Small peptide functionalized thiol-ene hydrogels as culture substrates for understanding valvular interstitial cell activation and de novo tissue deposition, *Acta Biomaterialia*. **2012**, 8, 3201-3209
- [184]. Chen, T. F., Siow, K. S., Ng, P. Y., Nai, M. H., Lim, C. T. and Majlis, B. Y. Ageing properties of polyurethane methacrylate and off-stoichiometry thiol-ene polymers after nitrogen and argon plasma treatment, *Journal of Applied Polymer Science*. **2016**, 133,
- [185]. Lu, H., Carioscia, J. A., Stansbury, J. W. and Bowman, C. N. Investigations of step-growth thiol-ene polymerizations for novel dental restoratives, *Dental Materials*. **2005**, 21, 1129-1136
- [186]. Resetco, C., Hendriks, B., Badi, N. and Du Prez, F. Thiol-ene chemistry for polymer coatings and surface modification - building in sustainability and performance, *Materials Horizons*. **2017**, 4, 1041-1053
- [187]. Zuo, Y. J., Gou, Z. M., Zhang, C. Q. and Feng, S. Y. Polysiloxane-Based Autonomic Self-Healing Elastomers Obtained through Dynamic Boronic Ester Bonds Prepared by Thiol-Ene "Click" Chemistry, *Macromolecular Rapid Communications*. **2016**, 37, 1052-1059
- [188]. Cheng, C. J., Zhang, X., Chen, X. H., Li, J., Huang, Q. H., Hu, Z. Y. and Tu, Y. M. Self-healing polymers based on eugenol via combination of thiol-ene and thiol oxidation reactions, *Journal of Polymer Research*. **2016**, 23,

- [189]. He, L. R., Szopinski, D., Wu, Y., Luinstra, G. A. and Theato, P. Toward Self-Healing Hydrogels Using One-Pot Thiol-Ene Click and Borax-Diol Chemistry, *Acs Macro Letters*. **2015**, 4, 673-678
- [190]. Ware, T. H., Perry, Z. P., Middleton, C. M., Iacono, S. T. and White, T. J. Programmable Liquid Crystal Elastomers Prepared by Thiol-Ene Photopolymerization, *Acs Macro Letters*. **2015**, 4, 942-946
- [191]. Davis, R. L., Jayaraman, S., Chaikin, P. M. and Register, R. A. Creating Controlled Thickness Gradients in Polymer Thin Films via Flowcoating, *Langmuir*. **2014**, 30, 5637-5644
- [192]. Stafford, C. M., Roskov, K. E., Epps, T. H. and Fasolka, M. J. Generating thickness gradients of thin polymer films via flow coating, *Review of Scientific Instruments*. **2006**, 77,
- [193]. Park, H. Y., Kloxin, C. J., Scott, T. F. and Bowman, C. N. Covalent Adaptable Networks as Dental Restorative Resins: Stress relaxation by addition-fragmentation chain transfer in allyl sulfide-containing resins, *Dental Materials*. **2010**, 26, 1010-1016
- [194]. Michal, B. T., Spencer, E. J. and Rowan, S. J. Stimuli-Responsive Reversible Two-Level Adhesion from a Structurally Dynamic Shape-Memory Polymer, *Acs Applied Materials & Interfaces*. **2016**, 8, 11041-11049
- [195]. Amamoto, Y., Kamada, J., Otsuka, H., Takahara, A. and Matyjaszewski, K. Polymers through Reshuffling of Trithiocarbonate Units, *Angewandte Chemie-International Edition*. **2011**, 50, 1660-1663
- [196]. Nicolay, R., Kamada, J., Van Wassen, A. and Matyjaszewski, K. Responsive Gels Based on a Dynamic Covalent Trithiocarbonate Cross-Linker, *Macromolecules*. **2010**, 43, 4355-4361
- [197]. Tokudome, Y., Suzuki, K., Kitanaga, T. and Takahashi, M. Hierarchical Nested Wrinkles on Silica-Polymer Hybrid Films: Stimuli-Responsive Micro Periodic Surface Architectures, *Scientific Reports*. **2012**, 2,
- [198]. Leocmach, M., Nespoulous, M., Manneville, S. and Gibaud, T. Hierarchical wrinkling in a confined permeable biogel, *Science Advances*. **2015**, 1,
- [199]. Li, F. D., Hou, H. H., Yin, J. and Jiang, X. S. Multi-Responsive Wrinkling Patterns by the Photoswitchable Supramolecular Network, *Acs Macro Letters*. **2017**, 6, 848-853

- [200]. Tokudome, Y., Kuniwaki, H., Suzuki, K., Carboni, D., Poologasundarampillai, G. and Takahashi, M. Thermoresponsive Wrinkles on Hydrogels for Soft Actuators, *Advanced Materials Interfaces*. **2016**, 3,
- [201]. Bandara, H. M. D. and Burdette, S. C. Photoisomerization in different classes of azobenzene, *Chemical Society Reviews*. **2012**, 41, 1809-1825
- [202]. Ichimura, K., Oh, S. K. and Nakagawa, M. Light-driven motion of liquids on a photoresponsive surface, *Science*. **2000**, 288, 1624-1626
- [203]. Klajn, R. Immobilized azobenzenes for the construction of photoresponsive materials, *Pure and Applied Chemistry*. **2010**, 82, 2247-2279
- [204]. Kumar, G. S. and Neckers, D. C. PHOTOCHEMISTRY OF AZOBENZENE-CONTAINING POLYMERS, *Chemical Reviews*. **1989**, 89, 1915-1925
- [205]. Li, C. S., Lo, C. W., Zhu, D. F., Li, C. H., Liu, Y. and Jiang, H. R. Synthesis of a Photoresponsive Liquid-Crystalline Polymer Containing Azobenzene, *Macromolecular Rapid Communications*. **2009**, 30, 1928-1935
- [206]. Natansohn, A. and Rochon, P. Photoinduced motions in azo-containing polymers, *Chemical Reviews*. **2002**, 102, 4139-4175
- [207]. Pace, G., Ferri, V., Grave, C., Elbing, M., von Haenisch, C., Zharnikov, M., Mayor, M., Rampi, M. A. and Samori, P. Cooperative light-induced molecular movements of highly ordered azobenzene self-assembled monolayers, *Proceedings of the National Academy of Sciences of the United States of America*. **2007**, 104, 9937-9942
- [208]. Chen, Y. and Chen, K. H. Synthesis and reversible photocleavage of novel polyurethanes containing coumarin dimer components, *Journal of Polymer Science Part a-Polymer Chemistry*. **1997**, 35, 613-624
- [209]. He, J., Tremblay, L., Lacelle, S. and Zhao, Y. Preparation of polymer single chain nanoparticles using intramolecular photodimerization of coumarin, *Soft Matter*. **2011**, 7, 2380-2386
- [210]. Iliopoulos, K., Krupka, O., Gindre, D. and Salle, M. Reversible Two-Photon Optical Data Storage in Coumarin-Based Copolymers, *Journal of the American Chemical Society*. **2010**, 132, 14343-14345
- [211]. Kaur, G., Johnston, P. and Saito, K. Photo-reversible dimerisation reactions and their applications in polymeric systems, *Polymer Chemistry*. **2014**, 5, 2171-2186

- [212]. Kim, C., Trajkovska, A., Wallace, J. U. and Chen, S. H. New insight into photoalignment of liquid crystals on coumarin-containing polymer films, *Macromolecules*. **2006**, 39, 3817-3823
- [213]. Kiskan, B. and Yagci, Y. Self-Healing of Poly(propylene oxide)-Polybenzoxazine Thermosets by Photoinduced Coumarine Dimerization, *Journal of Polymer Science Part a-Polymer Chemistry*. **2014**, 52, 2911-2918
- [214]. Mal, N. K., Fujiwara, M. and Tanaka, Y. Photocontrolled reversible release of guest molecules from coumarin-modified mesoporous silica, *Nature*. **2003**, 421, 350-353
- [215]. Hou, H. H., Li, F. D., Su, Z. L., Yin, J. and Jiang, X. S. Light-reversible hierarchical patterns by dynamic photo-dimerization induced wrinkles, *Journal of Materials Chemistry C*. **2017**, 5, 8765-8773
- [216]. Lai, J. T., Filla, D. and Shea, R. Functional polymers from novel carboxyl-terminated trithiocarbonates as highly efficient RAFT agents, *Macromolecules*. **2002**, 35, 6754-6756
- [217]. Ware, T. H. and White, T. J. Programmed liquid crystal elastomers with tunable actuation strain, *Polymer Chemistry*. **2015**, 6, 4835-4844
- [218]. McBride, M., Baranek, A. and Bowman, C. Shape memory properties of polymer networks formed using photomediated copper(I)-catalyzed azide alkyne cycloaddition (photo-CuAAC), *Abstracts of Papers of the American Chemical Society*. **2015**, 249,
- [219]. McBride, M. K., Gong, T., Nair, D. P. and Bowman, C. N. Photo-mediated copper(I)-catalyzed azide-alkyne cycloaddition (CuAAC) "click" reactions for forming polymer networks as shape memory materials, *Polymer*. **2014**, 55, 5880-5884
- [220]. Ramdas, M. R., Kumar, K. S. S. and Nair, C. P. R. Click polymerizations: Encouraging route for shape memory polymers, *Materials Letters*. **2016**, 172, 216-221
- [221]. Zhang, H. Y., Zhu, Y., Chen, J. D. and Zhang, S. M. Preparation of polyHIPE via CuAAC "click" chemistry and its application as a highly efficient adsorbent of Cu(II) ions, *Journal of Polymer Science Part a-Polymer Chemistry*. **2017**, 55, 2129-2135
- [222]. Doran, S., Murtezi, E., Barlas, F. B., Timur, S. and Yagci, Y. One-Pot Photo-Induced Sequential CuAAC and Thiol-Ene Click Strategy for Bioactive Macromolecular Synthesis, *Macromolecules*. **2014**, 47, 3608-3613

- [223]. Lallana, E., Sousa-Herves, A., Fernandez-Trillo, F., Riguera, R. and Fernandez-Megia, E. Click Chemistry for Drug Delivery Nanosystems, *Pharmaceutical Research*. **2012**, 29, 1-34
- [224]. Lutz, J. F. and Zarafshani, Z. Efficient construction of therapeutics, bioconjugates, biomaterials and bioactive surfaces using azide-alkyne "click" chemistry, *Advanced Drug Delivery Reviews*. **2008**, 60, 958-970
- [225]. Oyman Eyrilmez, G., Doran, S., Murtezi, E., Demir, B., Demirkol, D. O., Coskunol, H., Timur, S. and Yagci, Y. Selective Cell Adhesion and Biosensing Applications of Bio-Active Block Copolymers Prepared by CuAAC/Thiol-ene Double Click Reactions, *Macromolecular Bioscience*. **2015**, 15, 1233-1241
- [226]. Song, H. B., Baranek, A., McBride, M., Gong, T., Flores, A., Stansbury, J., Kloxin, C. and Bowman, C. Optimizing photo-CuAAC polymerization kinetic for dental restorative materials, *Abstracts of Papers of the American Chemical Society*. **2015**, 249,
- [227]. Song, H. B., Sowan, N., Shah, P. K., Baranek, A., Flores, A., Stansbury, J. W. and Bowman, C. N. Reduced shrinkage stress via photo-initiated copper(I)-catalyzed cycloaddition polymerizations of azide-alkyne resins, *Dental Materials*. **2016**, 32, 1332-1342
- [228]. Song, H. B., Wang, X., Patton, J. R., Stansbury, J. W. and Bowman, C. N. Kinetics and mechanics of photo-polymerized triazole-containing thermosetting composites via the copper(I)-catalyzed azide-alkyne cycloaddition, *Dental Materials*. **2017**, 33, 621-629
- [229]. Adzima, B. J., Tao, Y. H., Kloxin, C. J., DeForest, C. A., Anseth, K. S. and Bowman, C. N. Spatial and temporal control of the alkyne-azide cycloaddition by photoinitiated Cu(II) reduction, *Nature Chemistry*. **2011**, 3, 256-259
- [230]. Bowman, C. N., Gong, T. and Alzahrani, A. Photopolymerizations and polymers based on the CuAAC reaction, *Abstracts of Papers of the American Chemical Society*. **2014**, 248,
- [231]. Gong, T., Adzima, B. J., Baker, N. H. and Bowman, C. N. Photopolymerization Reactions Using the Photoinitiated Copper (I)-Catalyzed Azide-Alkyne Cycloaddition (CuAAC) Reaction, *Advanced Materials*. **2013**, 25, 2024-2028
- [232]. Alzahrani, A. A., Nair, D. P., Smits, D. J., Saed, M., Yakacki, C. M. and Bowman, C. N. Photo-CuAAC Induced Wrinkle Formation in a Thiol-Acrylate Elastomer via Sequential Click Reactions, *Chemistry of Materials*. **2014**, 26, 5303-5309

- [233]. Shete, A. U. and Kloxin, C. J. One-pot blue-light triggered tough interpenetrating polymeric network (IPN) using CuAAC and methacrylate reactions, *Polymer Chemistry*. **2017**, 8, 3668-3673
- [234]. Cao, G. X., Chen, X., Li, C. R., Ji, A. and Cao, Z. X. Self-assembled triangular and labyrinth buckling patterns of thin films on spherical substrates, *Physical Review Letters*. **2008**, 100,
- [235]. Chan, H. K. and Chew, N. Y. K. Novel alternative methods for the delivery of drugs for the treatment of asthma, *Advanced Drug Delivery Reviews*. **2003**, 55, 793-805
- [236]. Chew, N. Y. K. and Chan, H. K. Use of solid corrugated particles to enhance powder aerosol performance, *Pharmaceutical Research*. **2001**, 18, 1570-1577
- [237]. Fogle, C., Rowat, A. C., Levine, A. J. and Rudnick, J. Shape transitions in soft spheres regulated by elasticity, *Physical Review E*. **2013**, 88,
- [238]. Hano, N., Takafuji, M. and Ihara, H. One-pot preparation of polymer microspheres having wrinkled hard surfaces through self-assembly of silica nanoparticles, *Chemical Communications*. **2017**, 53, 9147-9150
- [239]. Ina, M., Zhushma, A. P., Lebedeva, N. V., Vatankeh-Varnoosfaderani, M., Olson, S. D. and Sheiko, S. S. The design of wrinkled microcapsules for enhancement of release rate, *Journal of Colloid and Interface Science*. **2016**, 478, 296-302
- [240]. Kang, J. S., Lim, J., Rho, W. Y., Kim, J., Moon, D. S., Jeong, J., Jung, D., Choi, J. W., Lee, J. K. and Sung, Y. E. Wrinkled silica/titania nanoparticles with tunable interwrinkle distances for efficient utilization of photons in dye-sensitized solar cells, *Scientific Reports*. **2016**, 6,
- [241]. Li, B., Jia, F., Cao, Y. P., Feng, X. Q. and Gao, H. J. Surface Wrinkling Patterns on a Core-Shell Soft Sphere, *Physical Review Letters*. **2011**, 106,
- [242]. Li, M., Joung, D., Hughes, B., Waldman, S. D., Kozinski, J. A. and Hwang, D. K. Wrinkling Non-Spherical Particles and Its Application in Cell Attachment Promotion, *Scientific Reports*. **2016**, 6, 30463
- [243]. Li, M. G., Joung, D. H., Hughes, B., Waldman, S. D., Kozinski, J. A. and Hwang, D. K. Wrinkling Non-Spherical Particles and Its Application in Cell Attachment Promotion, *Scientific Reports*. **2016**, 6,
- [244]. Terwagne, D., Brojan, M. and Reis, P. M. Smart Morphable Surfaces for Aerodynamic Drag Control, *Advanced Materials*. **2014**, 26, 6608-6611

- [245]. Trindade, A. C., Canejo, J. P., Patricio, P., Brogueira, P., Teixeira, P. I. and Godinho, M. H. Hierarchical wrinkling on elastomeric Janus spheres, *Journal of Materials Chemistry*. **2012**, 22, 22044-22049
- [246]. Trindade, A. C., Canejo, J. P., Pinto, L. F. V., Patricio, P., Brogueira, P., Teixeira, P. I. C. and Godinho, M. H. Wrinkling Labyrinth Patterns on Elastomeric Janus Particles, *Macromolecules*. **2011**, 44, 2220-2228
- [247]. Wang, Z. M., Gupta, S. K. and Meenach, S. A. Development and physicochemical characterization of acetalated dextran aerosol particle systems for deep lung delivery, *International Journal of Pharmaceutics*. **2017**, 525, 264-274
- [248]. Zhou, Q. Z., Xiang, H. F., Fan, H. S., Yang, X. L., Zhao, N. and Xu, J. Facile fabrication of golf ball-like hollow microspheres of organic-inorganic silica, *Journal of Materials Chemistry*. **2011**, 21, 13056-13061
- [249]. Hano, N., Takafuji, M. and Ihara, H. One-pot preparation of polymer microspheres having wrinkled hard surfaces through self-assembly of silica nanoparticles, *Chemical Communications*. **2017**, 53,
- [250]. Lee, J., Ku, K. H., Kim, M., Shin, J. M., Han, J., Park, C. H., Yi, G. R., Jang, S. G. and Kim, B. J. Stimuli-Responsive, Shape-Transforming Nanostructured Particles, *Advanced Materials*. **2017**, 29,
- [251]. Cox, L. M., Sun, X. H., Wang, C., Sowan, N., Killgore, J. P., Long, R., Wu, H. A., Bowman, C. N. and Ding, Y. F. Light-Stimulated Permanent Shape Reconfiguration in Cross-Linked Polymer Microparticles, *Acs Applied Materials & Interfaces*. **2017**, 9, 14422-14428
- [252]. Durham, O. Z. and Shipp, D. A. Suspension thiol-ene photopolymerization: Effect of stabilizing agents on particle size and stability, *Polymer*. **2014**, 55, 1674-1680
- [253]. Hessberger, T., Braun, L. and Zentel, R. Microfluidic Synthesis of Actuating Microparticles from a Thiol-Ene Based Main-Chain Liquid Crystalline Elastomer, *Polymers*. **2016**, 8,
- [254]. Jivan, F., Yegappan, R., Pearce, H., Carrow, J. K., McShane, M., Gaharwar, A. K. and Alge, D. L. Sequential Thiol-Ene and Tetrazine Click Reactions for the Polymerization and Functionalization of Hydrogel Microparticles, *Biomacromolecules*. **2016**, 17, 3516-3523

- [255]. Serra, C. A., Khan, I. U., Chang, Z. Q., Bouquey, M., Muller, R., Kraus, I., Schmutz, M., Vandamme, T., Anton, N., Ohm, C., Zentel, R., Knauer, A. and Kohler, M. Engineering Polymer Microparticles by Droplet Microfluidics, *Journal of Flow Chemistry*. **2013**, 3, 66-75
- [256]. Tan, J. J., Li, C. M., Zhou, J., Yin, C. J., Zhang, B. L., Gu, J. W. and Zhang, Q. Y. Fast and facile fabrication of porous polymer particles via thiol-ene suspension photopolymerization, *Rsc Advances*. **2014**, 4, 13334-13339
- [257]. Wang, C., Zhang, X. P., Podgorski, M., Xi, W. X., Stansbury, J. and Bowman, C. N. Monodispersity/Narrow Polydispersity Cross-Linked Microparticles Prepared by Step-Growth Thiol-Michael Addition Dispersion Polymerizations, *Macromolecules*. **2015**, 48, 8461-8470
- [258]. Wang, C., Zieger, M. M., Schenzel, A., Wegener, M., Willenbacher, J., Barner-Kowollik, C. and Bowman, C. N. Photoinduced Tetrazole-Based Functionalization of Off-Stoichiometric Clickable Microparticles, *Advanced Functional Materials*. **2017**, 27,
- [259]. Amato, D., Amato, D., Flynt, A. and Patton, D. Functional polymer nanoparticles via thiol-ene nanoemulsion photopolymerization, *Abstracts of Papers of the American Chemical Society*. **2015**, 249,
- [260]. Amato, D., Amato, D., Brei, M., Storey, R. and Patton, D. Thiol-alkyne photopolymerization in miniemulsion: A facile route to functional polymer nanoparticles, *Abstracts of Papers of the American Chemical Society*. **2015**, 249,
- [261]. Amato, D. V., Amato, D. N., Flynt, A. S. and Patton, D. L. Functional, sub-100 nm polymer nanoparticles via thiol-ene miniemulsion photopolymerization, *Polymer Chemistry*. **2015**, 6, 5625-5632
- [262]. Rothmund, P. W. K. Folding DNA to create nanoscale shapes and patterns, *Nature*. **2006**, 440, 297-302
- [263]. Chang, E. P. Viscoelastic properties of pressure-sensitive adhesives, *Journal of Adhesion*. **1997**, 60, 233-248
- [264]. Engler, A. J., Griffin, M. A., Sen, S., Bonnetmann, C. G., Sweeney, H. L. and Discher, D. E. Myotubes differentiate optimally on substrates with tissue-like stiffness: pathological implications for soft or stiff microenvironments, *Journal of Cell Biology*. **2004**, 166, 877-887

- [265]. Jiang, X. F., Yang, K., Yang, X. Q., Liu, Y. F., Cheng, Y. C., Chen, X. Y. and Tu, Y. Elastic modulus affects the growth and differentiation of neural stem cells, *Neural Regeneration Research*. **2015**, 10, 1523-1527
- [266]. Lanniel, M., Huq, E., Allen, S., Buttery, L., Williams, P. M. and Alexander, M. R. Substrate induced differentiation of human mesenchymal stem cells on hydrogels with modified surface chemistry and controlled modulus, *Soft Matter*. **2011**, 7, 6501-6514
- [267]. Leipzig, N. D. and Shoichet, M. S. The effect of substrate stiffness on adult neural stem cell behavior, *Biomaterials*. **2009**, 30, 6867-6878
- [268]. Mullen, C. A., Vaughan, T. J., Billiar, K. L. and McNamara, L. M. The Effect of Substrate Stiffness, Thickness, and Cross-Linking Density on Osteogenic Cell Behavior, *Biophysical Journal*. **2015**, 108, 1604-1612
- [269]. Romanazzo, S. Effects of substrate stiffness on myoblasts phenotype and differentiation, *Journal of Tissue Engineering and Regenerative Medicine*. **2012**, 6, 239-239
- [270]. Xu, Q. W., Li, C., Kang, Y. J. and Zhang, Y. L. Long term effects of substrate stiffness on the development of hMSC mechanical properties, *Rsc Advances*. **2015**, 5, 105651-105660
- [271]. Hozumi, A., Ushiyama, K., Sugimura, H. and Takai, O. Fluoroalkylsilane monolayers formed by chemical vapor surface modification on hydroxylated oxide surfaces, *Langmuir*. **1999**, 15, 7600-7604
- [272]. Pester, C. W., Poelma, J. E., Narupai, B., Patel, S. N., Su, G. M., Mates, T. E., Luo, Y. D., Ober, C. K., Hawker, C. J. and Kramer, E. J. Ambiguous Anti-Fouling Surfaces: Facile Synthesis by Light-Mediated Radical Polymerization, *Journal of Polymer Science Part a-Polymer Chemistry*. **2016**, 54, 253-262
- [273]. Lee, H., Alcaraz, M. L., Rubner, M. F. and Cohen, R. E. Zwitter-Wettability and Antifogging Coatings with Frost-Resisting Capabilities, *Acs Nano*. **2013**, 7, 2172-2185
- [274]. Lee, H., Dellatore, S. M., Miller, W. M. and Messersmith, P. B. Mussel-inspired surface chemistry for multifunctional coatings, *Science*. **2007**, 318, 426-430
- [275]. Mussel-Inspired Glue Seals Membranes, *Science*. **2013**, 339, 890-890

- [276]. Li, A. L., Mu, Y. B., Jiang, W. and Wan, X. B. A mussel-inspired adhesive with stronger bonding strength under underwater conditions than under dry conditions, *Chemical Communications*. **2015**, 51, 9117-9120
- [277]. Ahn, B. K., Das, S., Linstadt, R., Kaufman, Y., Martinez-Rodriguez, N. R., Mirshafian, R., Kesselman, E., Talmon, Y., Lipshutz, B. H., Israelachvili, J. N. and Waite, J. H. High-performance mussel-inspired adhesives of reduced complexity, *Nature Communications*. **2015**, 6,
- [278]. Favia, P. and d'Agostino, R. Plasma treatments and plasma deposition of polymers for biomedical applications, *Surface & Coatings Technology*. **1998**, 98, 1102-1106
- [279]. Della Giustina, G., Giulitti, S., Brigo, L., Zanatta, M., Tromayer, M., Liska, R., Elvassore, N. and Brusatin, G. Hydrogel with Orthogonal Reactive Units: 2D and 3D Cross-Linking Modulation, *Macromolecular Rapid Communications*. **2017**, 38,
- [280]. Krishnan, S., Ayothi, R., Hexemer, A., Finlay, J. A., Sohn, K. E., Perry, R., Ober, C. K., Kramer, E. J., Callow, M. E., Callow, J. A. and Fischer, D. A. Anti-biofouling properties of comblike block copolymers with amphiphilic side chains, *Langmuir*. **2006**, 22, 5075-5086
- [281]. Kuddannaya, S., Chuah, Y. J., Lee, M. H. A., Menon, N. V., Kang, Y. J. and Zhang, Y. L. Surface Chemical Modification of Poly(dimethylsiloxane) for the Enhanced Adhesion and Proliferation of Mesenchymal Stem Cells, *Acs Applied Materials & Interfaces*. **2013**, 5, 9777-9784
- [282]. Saha, K., Keung, A. J., Irwin, E. F., Li, Y., Little, L., Schaffer, D. V. and Healy, K. E. Substrate Modulus Directs Neural Stem Cell Behavior, *Biophysical Journal*. **2008**, 95, 4426-4438
- [283]. Barthlott, W. and Neinhuis, C. Purity of the sacred lotus, or escape from contamination in biological surfaces, *Planta*. **1997**, 202, 1-8
- [284]. Feng, L., Li, S. H., Li, Y. S., Li, H. J., Zhang, L. J., Zhai, J., Song, Y. L., Liu, B. Q., Jiang, L. and Zhu, D. B. Super-hydrophobic surfaces: From natural to artificial, *Advanced Materials*. **2002**, 14, 1857-1860
- [285]. Bhushan, B. Bioinspired Structured Surfaces, *Langmuir*. **2012**, 28, 1698-1714
- [286]. Szyndler, M. W., Haynes, K. F., Potter, M. F., Corn, R. M. and Loudon, C. Entrapment of bed bugs by leaf trichomes inspires microfabrication of biomimetic surfaces, *Journal of the Royal Society Interface*. **2013**, 10,

- [287]. Autumn, K., Liang, Y. A., Hsieh, S. T., Zesch, W., Chan, W. P., Kenny, T. W., Fearing, R. and Full, R. J. Adhesive force of a single gecko foot-hair, *Nature*. **2000**, 405, 681-685
- [288]. Autumn, K., Sitti, M., Liang, Y. C. A., Peattie, A. M., Hansen, W. R., Sponberg, S., Kenny, T. W., Fearing, R., Israelachvili, J. N. and Full, R. J. Evidence for van der Waals adhesion in gecko setae, *Proceedings of the National Academy of Sciences of the United States of America*. **2002**, 99, 12252-12256
- [289]. Hansen, W. R. and Autumn, K. Evidence for self-cleaning in gecko setae, *Proceedings of the National Academy of Sciences of the United States of America*. **2005**, 102, 385-389
- [290]. Tian, Y., Pesika, N., Zeng, H. B., Rosenberg, K., Zhao, B. X., McGuiggan, P., Autumn, K. and Israelachvili, J. Adhesion and friction in gecko toe attachment and detachment, *Proceedings of the National Academy of Sciences of the United States of America*. **2006**, 103, 19320-19325
- [291]. Northen, M. T., Greiner, C., Arzt, E. and Turner, K. L. A Gecko-Inspired Reversible Adhesive, *Advanced Materials*. **2008**, 20, 3905-+
- [292]. Boesel, L. F., Greiner, C., Arzt, E. and del Campo, A. Gecko-Inspired Surfaces: A Path to Strong and Reversible Dry Adhesives, *Advanced Materials*. **2010**, 22, 2125-2137
- [293]. Jin, K., Tian, Y., Erickson, J. S., Puthoff, J., Autumn, K. and Pesika, N. S. Design and Fabrication of Gecko-Inspired Adhesives, *Langmuir*. **2012**, 28, 5737-5742
- [294]. Schumacher, J. F., Aldred, N., Callow, M. E., Finlay, J. A., Callow, J. A., Clare, A. S. and Brennan, A. B. Species-specific engineered antifouling topographies: correlations between the settlement of algal zoospores and barnacle cyprids, *Biofouling*. **2007**, 23, 307-317
- [295]. Schumacher, J. F., Carman, M. L., Estes, T. G., Feinberg, A. W., Wilson, L. H., Callow, M. E., Callow, J. A., Finlay, J. A. and Brennan, A. B. Engineered antifouling microtopographies - effect of feature size, geometry, and roughness on settlement of zoospores of the green alga *Ulva*, *Biofouling*. **2007**, 23, 55-62
- [296]. Wooh, S., Koh, J. H., Lee, S., Yoon, H. and Char, K. Trilevel-Structured Superhydrophobic Pillar Arrays with Tunable Optical Functions, *Advanced Functional Materials*. **2014**, 24, 5550-5556

- [297]. Lopez-Bosque, M. J., Tejada-Montes, E., Cazorla, M., Linacero, J., Atienza, Y., Smith, K. H., Llado, A., Colombelli, J., Engel, E. and Mata, A. Fabrication of hierarchical micro-nanotopographies for cell attachment studies, *Nanotechnology*. **2013**, 24,
- [298]. Engelmayr, G. C., Cheng, M. Y., Bettinger, C. J., Borenstein, J. T., Langer, R. and Freed, L. E. Accordion-like honeycombs for tissue engineering of cardiac anisotropy, *Nature Materials*. **2008**, 7, 1003-1010
- [299]. Wang, P. Y., Li, W. T., Yu, J. S. and Tsai, W. B. Modulation of osteogenic, adipogenic and myogenic differentiation of mesenchymal stem cells by submicron grooved topography, *Journal of Materials Science-Materials in Medicine*. **2012**, 23, 3015-3028
- [300]. Hagberg, E. C., Malkoch, M., Ling, Y. B., Hawker, C. J. and Carter, K. R. Effects of modulus and surface chemistry of thiol-ene photopolymers in nanoimprinting, *Nano Letters*. **2007**, 7, 233-237
- [301]. Johnson, B. N., Lancaster, K. Z., Zhen, G. H., He, J. Y., Gupta, M. K., Kong, Y. L., Engel, E. A., Krick, K. D., Ju, A., Meng, F. B., Enquist, L. W., Jia, X. F. and McAlpine, M. C. 3D Printed Anatomical Nerve Regeneration Pathways, *Advanced Functional Materials*. **2015**, 25, 6205-6217
- [302]. Derby, B. Printing and Prototyping of Tissues and Scaffolds, *Science*. **2012**, 338, 921-926
- [303]. Groenewold, J. Wrinkling of plates coupled with soft elastic media, *Physica A*. **2001**, 298, 32-45
- [304]. Genzer, J. and Groenewold, J. Soft matter with hard skin: From skin wrinkles to templating and material characterization, *Soft Matter*. **2006**, 2, 310-323
- [305]. Thurlimann, B. Column Buckling - Historical and Actual Notes, *Journal of Constructional Steel Research*. **1990**, 17, 95-111
- [306]. Cerda, E. and Mahadevan, L. Geometry and physics of wrinkling, *Physical Review Letters*. **2003**, 90,
- [307]. Yang, S., Khare, K. and Lin, P.-C. Harnessing Surface Wrinkle Patterns in Soft Matter, *Advanced Functional Materials*. **2010**, 20, 2550-2564

- [308]. Jiang, H. Q., Khang, D. Y., Song, J. Z., Sun, Y. G., Huang, Y. G. and Rogers, J. A. Finite deformation mechanics in buckled thin films on compliant supports, *Proceedings of the National Academy of Sciences of the United States of America*. **2007**, 104, 15607-15612
- [309]. Wang, S. D., Song, J. Z., Kim, D. H., Huang, Y. G. and Rogers, J. A. Local versus global buckling of thin films on elastomeric substrates, *Applied Physics Letters*. **2008**, 93,
- [310]. Wang, S., Song, J., Kim, D.-H., Huang, Y. and Rogers, J. A. Local versus global buckling of thin films on elastomeric substrates, *Applied Physics Letters*. **2008**, 93, 023126
- [311]. Wang, Q. M. and Zhao, X. H. A three-dimensional phase diagram of growth-induced surface instabilities, *Scientific Reports*. **2015**, 5,
- [312]. Wang, Q. and Zhao, X. A three-dimensional phase diagram of growth-induced surface instabilities, *Sci Rep*. **2015**, 5, 8887
- [313]. Bowden, N., Brittain, S., Evans, A. G., Hutchinson, J. W. and Whitesides, G. M. Spontaneous formation of ordered structures in thin films of metals supported on an elastomeric polymer, *Nature*. **1998**, 393, 146-149
- [314]. Bowden, N., Huck, W. T. S., Paul, K. E. and Whitesides, G. M. The controlled formation of ordered, sinusoidal structures by plasma oxidation of an elastomeric polymer, *Applied Physics Letters*. **1999**, 75, 2557-2559
- [315]. Chua, D. B. H., Ng, H. T. and Li, S. F. Y. Spontaneous formation of complex and ordered structures on oxygen-plasma-treated elastomeric polydimethylsiloxane, *Applied Physics Letters*. **2000**, 76, 721-723
- [316]. Chen, X. and Hutchinson, J. W. Herringbone buckling patterns of compressed thin films on compliant substrates, *Journal of Applied Mechanics-Transactions of the Asme*. **2004**, 71, 597-603
- [317]. Efimenko, K., Rackaitis, M., Manias, E., Vaziri, A., Mahadevan, L. and Genzer, J. Nested self-similar wrinkling patterns in skins, *Nature Materials*. **2005**, 4, 293-297
- [318]. Chandra, D., Yang, S. and Lin, P.-C. Strain responsive concave and convex microlens arrays, *Applied Physics Letters*. **2007**, 91,
- [319]. Watanabe, M. and Hashimoto, R. Area-Selective Microwrinkle Formation on Poly(dimethylsiloxane) by Treatment with Strong Acid, *Journal of Polymer Science Part B-Polymer Physics*. **2015**, 53, 167-174

- [320]. Stafford, C. M., Harrison, C., Beers, K. L., Karim, A., Amis, E. J., Vanlandingham, M. R., Kim, H. C., Volksen, W., Miller, R. D. and Simonyi, E. E. A buckling-based metrology for measuring the elastic moduli of polymeric thin films, *Nature Materials*. **2004**, 3, 545-550
- [321]. Imburgia, M. J. and Crosby, A. J. Rolling wrinkles on elastic substrates, *Extreme Mechanics Letters*. **2016**, 6, 23-30
- [322]. Kim, J., Yoon, J. and Hayward, R. C. Dynamic display of biomolecular patterns through an elastic creasing instability of stimuli-responsive hydrogels, *Nature Materials*. **2010**, 9, 159-164
- [323]. Takeshima, T., Liao, W., Nagashima, Y., Beppu, K., Hara, M., Nagano, S. and Seki, T. Photoresponsive Surface Wrinkle Morphologies in Liquid Crystalline Polymer Films, *Macromolecules*. **2015**, 48, 6378-6384
- [324]. Chan, E. P. and Crosby, A. J. Spontaneous formation of stable aligned wrinkling patterns, *Soft Matter*. **2006**, 2, 324-328
- [325]. Guvendiren, M. and Burdick, J. A. The control of stem cell morphology and differentiation by hydrogel surface wrinkles, *Biomaterials*. **2010**, 31, 6511-6518
- [326]. Lin, P. C. and Yang, S. Spontaneous formation of one-dimensional ripples in transit to highly ordered two-dimensional herringbone structures through sequential and unequal biaxial mechanical stretching, *Applied Physics Letters*. **2007**, 90,
- [327]. Kim, J. B., Kim, P., Pegard, N. C., Oh, S. J., Kagan, C. R., Fleischer, J. W., Stone, H. A. and Loo, Y. L. Wrinkles and deep folds as photonic structures in photovoltaics, *Nature Photonics*. **2012**, 6, 327-332
- [328]. van den Ende, D., Kamminga, J. D., Boersma, A., Andritsch, T. and Steeneken, P. G. Voltage-Controlled Surface Wrinkling of Elastomeric Coatings, *Advanced Materials*. **2013**, 25, 3438-3442
- [329]. Efimenko, K., Finlay, J., Callow, M. E., Callow, J. A. and Genzer, J. Development and Testing of Hierarchically Wrinkled Coatings for Marine Antifouling, *Acs Applied Materials & Interfaces*. **2009**, 1, 1031-1040
- [330]. Lin, P.-C., Vajpayee, S., Jagota, A., Hui, C.-Y. and Yang, S. Mechanically tunable dry adhesive from wrinkled elastomers, *Soft Matter*. **2008**, 4, 1830-1835
- [331]. Davis, C. S., Martina, D., Creton, C., Lindner, A. and Crosby, A. J. Enhanced Adhesion of Elastic Materials to Small-Scale Wrinkles, *Langmuir*. **2012**, 28, 14899-14908

- [332]. Jeong, H. E., Kwak, M. K. and Suh, K. Y. Stretchable, Adhesion-Tunable Dry Adhesive by Surface Wrinkling, *Langmuir*. **2010**, 26, 2223-2226
- [333]. Charest, J. L., Eliason, M. T., Garcia, A. J. and King, W. P. Combined microscale mechanical topography and chemical patterns on polymer cell culture substrates, *Biomaterials*. **2006**, 27, 2487-2494
- [334]. Chua, J. S., Chng, C. P., Moe, A. A. K., Tann, J. Y., Goh, E. L. K., Chiam, K. H. and Yim, E. K. F. Extending neurites sense the depth of the underlying topography during neuronal differentiation and contact guidance, *Biomaterials*. **2014**, 35, 7750-7761
- [335]. Chuah, Y. J., Koh, Y. T., Lim, K., Menon, N. V., Wu, Y. and Kang, Y. Simple surface engineering of polydimethylsiloxane with polydopamine for stabilized mesenchymal stem cell adhesion and multipotency, *Scientific Reports*. **2015**, 5,
- [336]. Clark, P., Connolly, P., Curtis, A. S. G., Dow, J. A. T. and Wilkinson, C. D. W. Cell Guidance by Ultrafine Topography In vitro, *Journal of Cell Science*. **1991**, 99, 73-77
- [337]. Dalby, M. J., Riehle, M. O., Yarwood, S. J., Wilkinson, C. D. W. and Curtis, A. S. G. Nucleus alignment and cell signaling in fibroblasts: response to a micro-grooved topography, *Experimental Cell Research*. **2003**, 284, 274-282
- [338]. Greco, F., Fujie, T., Ricotti, L., Taccola, S., Mazzolai, B. and Mattoli, V. Microwrinkled Conducting Polymer Interface for Anisotropic Multicellular Alignment, *Acs Applied Materials & Interfaces*. **2013**, 5, 573-584
- [339]. Kiang, J. D., Wen, J. H., del Alamo, J. C. and Engler, A. J. Dynamic and reversible surface topography influences cell morphology, *Journal of Biomedical Materials Research Part A*. **2013**, 101A, 2313-2321
- [340]. Lim, J. Y. and Donahue, H. J. Cell sensing and response to micro- and nanostructured surfaces produced by chemical and topographic patterning, *Tissue Engineering*. **2007**, 13, 1879-1891
- [341]. Luna, J. I., Ciriza, J., Garcia-Ojeda, M. E., Kong, M., Herren, A., Lieu, D. K., Li, R. A., Fowlkes, C. C., Khine, M. and McCloskey, K. E. Multiscale Biomimetic Topography for the Alignment of Neonatal and Embryonic Stem Cell-Derived Heart Cells, *Tissue Engineering Part C-Methods*. **2011**, 17, 579-588

- [342]. Wang, Z. Y., Teo, E. Y., Chong, M. S. K., Zhang, Q. Y., Lim, J., Zhang, Z. Y., Hong, M. H., Thian, E. S., Chan, J. K. Y. and Teoh, S. H. Biomimetic Three-Dimensional Anisotropic Geometries by Uniaxial Stretch of Poly(epsilon-Caprolactone) Films for Mesenchymal Stem Cell Proliferation, Alignment, and Myogenic Differentiation, *Tissue Engineering Part C-Methods*. **2013**, 19, 538-549
- [343]. Yang, P., Baker, R. M., Henderson, J. H. and Mather, P. T. In vitro wrinkle formation via shape memory dynamically aligns adherent cells, *Soft Matter*. **2013**, 9, 4705-4714
- [344]. Yim, E. K. F., Darling, E. M., Kulangara, K., Guilak, F. and Leong, K. W. Nanotopography-induced changes in focal adhesions, cytoskeletal organization, and mechanical properties of human mesenchymal stem cells, *Biomaterials*. **2010**, 31, 1299-1306
- [345]. Zahor, D., Radko, A., Vago, R. and Gheber, L. A. Organization of mesenchymal stem cells is controlled by micropatterned silicon substrates, *Materials Science & Engineering C-Biomimetic and Supramolecular Systems*. **2007**, 27, 117-121
- [346]. Zhu, H. B., Cao, B. R., Zhen, Z. P., Laxmi, A. A., Li, D., Liu, S. R. and Mao, C. B. Controlled growth and differentiation of MSCs on grooved films assembled from monodisperse biological nanofibers with genetically tunable surface chemistries, *Biomaterials*. **2011**, 32, 4744-4752
- [347]. Vandeparre, H., Gabriele, S., Brau, F., Gay, C., Parker, K. K. and Damman, P. Hierarchical wrinkling patterns, *Soft Matter*. **2010**, 6, 5751-5756
- [348]. Guvendiren, M. and Burdick, J. A. Stem Cell Response to Spatially and Temporally Displayed and Reversible Surface Topography, *Advanced Healthcare Materials*. **2013**, 2, 155-164
- [349]. Stafford, C. M., Vogt, B. D., Harrison, C., Julthongpiput, D. and Huang, R. Elastic moduli of ultrathin amorphous polymer films, *Macromolecules*. **2006**, 39, 5095-5099
- [350]. Anseth, K. S., Newman, S. M. and Bowman, C. N. Polymeric dental composites: Properties and reaction behavior of multimethacrylate dental restorations, *Biopolymers Ii*. **1995**, 122, 177-217
- [351]. Cook, W. D. PHOTOPOLYMERIZATION KINETICS OF DIMETHACRYLATES USING THE CAMPHORQUINONE AMINE INITIATOR SYSTEM, *Polymer*. **1992**, 33, 600-609

- [352]. Cramer, N. B., Stansbury, J. W. and Bowman, C. N. Recent Advances and Developments in Composite Dental Restorative Materials, *Journal of Dental Research*. **2011**, 90, 402-416
- [353]. Sideridou, I., Tserki, V. and Papanastasiou, G. Effect of chemical structure on degree of conversion in light-cured dimethacrylate-based dental resins, *Biomaterials*. **2002**, 23, 1819-1829
- [354]. Sideridou, I., Tserki, V. and Papanastasiou, G. Study of water sorption, solubility and modulus of elasticity of light-cured dimethacrylate-based dental resins, *Biomaterials*. **2003**, 24, 655-665
- [355]. Stansbury, J. W. and Dickens, S. H. Determination of double bond conversion in dental resins by near infrared spectroscopy, *Dental Materials*. **2001**, 17, 71-79
- [356]. Tumbleston, J. R., Shirvanyants, D., Ermoshkin, N., Januszewicz, R., Johnson, A. R., Kelly, D., Chen, K., Pinschmidt, R., Rolland, J. P., Ermoshkin, A., Samulski, E. T. and DeSimone, J. M. Continuous liquid interface production of 3D objects, *Science*. **2015**, 347, 1349-1352
- [357]. Wagner, C. and Harned, N. EUV LITHOGRAPHY Lithography gets extreme, *Nature Photonics*. **2010**, 4, 24-26
- [358]. Kloxin, C. J., Scott, T. F., Park, H. Y. and Bowman, C. N. Mechanophotopatterning on a Photoresponsive Elastomer, *Advanced Materials*. **2011**, 23, 1977-1981
- [359]. Amamoto, Y., Otsuka, H., Takahara, A. and Matyjaszewski, K. Self-Healing of Covalently Cross-Linked Polymers by Reshuffling Thiuram Disulfide Moieties in Air under Visible Light, *Advanced Materials*. **2012**, 24, 3975-3980
- [360]. Bowman, C. N. and Kloxin, C. J. Covalent Adaptable Networks: Reversible Bond Structures Incorporated in Polymer Networks, *Angewandte Chemie-International Edition*. **2012**, 51, 4272-4274
- [361]. Kloxin, C. J., Scott, T. F., Adzima, B. J. and Bowman, C. N. Covalent Adaptable Networks (CANS): A Unique Paradigm in Cross-Linked Polymers, *Macromolecules*. **2010**, 43, 2643-2653
- [362]. Ryu, J., D'Amato, M., Cui, X., Long, K. N., Qi, H. J. and Dunn, M. L. Photo-origami-Bending and folding polymers with light, *Applied Physics Letters*. **2012**, 100,

- [363]. Stuart, M. A. C., Huck, W. T. S., Genzer, J., Muller, M., Ober, C., Stamm, M., Sukhorukov, G. B., Szleifer, I., Tsukruk, V. V., Urban, M., Winnik, F., Zauscher, S., Luzinov, I. and Minko, S. Emerging applications of stimuli-responsive polymer materials, *Nature Materials*. **2010**, 9, 101-113
- [364]. Wu, D. Y., Meure, S. and Solomon, D. Self-healing polymeric materials: A review of recent developments, *Progress in Polymer Science*. **2008**, 33, 479-522
- [365]. Chatani, S., Kloxin, C. J. and Bowman, C. N. The power of light in polymer science: photochemical processes to manipulate polymer formation, structure, and properties, *Polymer Chemistry*. **2014**, 5, 2187-2201
- [366]. Maruo, S. and Kawata, S. Two-photon-absorbed photopolymerization for three-dimensional microfabrication, *Mems 97, Proceedings - Ieee the Tenth Annual International Workshop on Micro Electro Mechanical Systems*. **1997**, 169-174
- [367]. Maruo, S., Nakamura, O. and Kawata, S. Three-dimensional microfabrication with two-photon-absorbed photopolymerization, *Optics Letters*. **1997**, 22, 132-134
- [368]. LaFratta, C. N., Fourkas, J. T., Baldacchini, T. and Farrer, R. A. Multiphoton fabrication, *Angewandte Chemie-International Edition*. **2007**, 46, 6238-6258
- [369]. Scott, T. F., Kloxin, C. J., Forman, D. L., McLeod, R. R. and Bowman, C. N. Principles of voxel refinement in optical direct write lithography, *Journal of Materials Chemistry*. **2011**, 21, 14150-14155
- [370]. Scott, T. F., Kloxin, C. J., Draughon, R. B. and Bowman, C. N. Nonclassical dependence of polymerization rate on initiation rate observed in thiol-ene photopolymerizations, *Macromolecules*. **2008**, 41, 2987-2989
- [371]. Gan, Z. S., Cao, Y. Y., Evans, R. A. and Gu, M. Three-dimensional deep sub-diffraction optical beam lithography with 9 nm feature size, *Nature Communications*. **2013**, 4,
- [372]. Muller, T., Schumann, C. and Kraegeloh, A. STED Microscopy and its Applications: New Insights into Cellular Processes on the Nanoscale, *Chemphyschem*. **2012**, 13, 1986-2000
- [373]. Kolb, H. C., Finn, M. G. and Sharpless, K. B. Click chemistry: Diverse chemical function from a few good reactions, *Angewandte Chemie-International Edition*. **2001**, 40, 2004-+

- [374]. Sharpless, K. B. and Kolb, H. C. Click chemistry. A concept for merging process and discovery chemistry., *Abstracts of Papers of the American Chemical Society*. **1999**, 217, U95-U95
- [375]. Hoyle, C. E., Lowe, A. B. and Bowman, C. N. Thiol-click chemistry: a multifaceted toolbox for small molecule and polymer synthesis, *Chemical Society Reviews*. **2010**, 39, 1355-1387
- [376]. Hoyle, C. E. and Bowman, C. N. Thiol-Ene Click Chemistry, *Angewandte Chemie-International Edition*. **2010**, 49, 1540-1573
- [377]. Xi, W. X., Peng, H. Y., Aguirre-Soto, A., Kloxin, C. J., Stansbury, J. W. and Bowman, C. N. Spatial and Temporal Control of Thiol-Michael Addition via Photocaged Superbase in Photopatterning and Two-Stage Polymer Networks Formation, *Macromolecules*. **2014**, 47, 6159-6165
- [378]. Claudino, M., Zhang, X. P., Alim, M. D., Podgorski, M. and Bowman, C. N. Mechanistic Kinetic Modeling of Thiol-Michael Addition Photopolymerizations via Photocaged "Superbase" Generators: An Analytical Approach, *Macromolecules*. **2016**, 49, 8061-8074
- [379]. Cramer, N. B., Reddy, S. K., Cole, M., Hoyle, C. and Bowman, C. N. Initiation and kinetics of thiol-ene photopolymerizations without photoinitiators, *Journal of Polymer Science Part a-Polymer Chemistry*. **2004**, 42, 5817-5826
- [380]. Chan, J. W., Hoyle, C. E., Lowe, A. B. and Bowman, M. Nucleophile-Initiated Thiol-Michael Reactions: Effect of Organocatalyst, Thiol, and Ene, *Macromolecules*. **2010**, 43, 6381-6388
- [381]. Morgan, C. R., Magnotta, F. and Ketley, A. D. THIOL-ENE PHOTO-CURABLE POLYMERS, *Journal of Polymer Science Part a-Polymer Chemistry*. **1977**, 15, 627-645
- [382]. Hoyle, C. E., Lee, T. Y. and Roper, T. Thiol-enes: Chemistry of the past with promise for the future, *Journal of Polymer Science Part a-Polymer Chemistry*. **2004**, 42, 5301-5338
- [383]. Chatani, S., Sheridan, R. J., Podgorski, M., Nair, D. P. and Bowman, C. N. Temporal Control of Thiol-Click Chemistry, *Chemistry of Materials*. **2013**, 25, 3897-3901
- [384]. Odian, G. *Principles of Polymerization*, 4th Edition; John Wiley & Sons: Hoboken, NJ, 4th Edition, **2004**;

- [385]. Ma, S. J., Mannino, S. J., Wagner, N. J. and Kloxin, C. J. Photodirected Formation and Control of Wrinkles on a Thiol-ene Elastomer, *Acs Macro Letters*. **2013**, 2, 474-477
- [386]. Agrawal, A., Luchette, P., Palffy-Muhoray, P., Biswal, S. L., Chapman, W. G. and Verduzco, R. Surface wrinkling in liquid crystal elastomers, *Soft Matter*. **2012**, 8, 7138-7142
- [387]. Bayley, F. A., Liao, J. L., Stavrinou, P. N., Chiche, A. and Cabral, J. T. Wavefront kinetics of plasma oxidation of polydimethylsiloxane: limits for sub-micron wrinkling, *Soft Matter*. **2014**, 10, 1155-1166
- [388]. Breid, D. and Crosby, A. J. Surface wrinkling behavior of finite circular plates, *Soft Matter*. **2009**, 5, 425-431
- [389]. Breid, D. and Crosby, A. J. Effect of stress state on wrinkle morphology, *Soft Matter*. **2011**, 7, 4490-4496
- [390]. Breid, D. and Crosby, A. J. Curvature-controlled wrinkle morphologies, *Soft Matter*. **2013**, 9, 3624-3630
- [391]. Chan, E. P. and Crosby, A. J. Fabricating microlens arrays by surface wrinkling, *Advanced Materials*. **2006**, 18, 3238
- [392]. Chen, Y. C. and Crosby, A. J. Wrinkling of inhomogeneously strained thin polymer films, *Soft Matter*. **2013**, 9, 43-47
- [393]. Chung, J. Y., Nolte, A. J. and Stafford, C. M. Surface Wrinkling: A Versatile Platform for Measuring Thin-Film Properties, *Advanced Materials*. **2011**, 23, 349-368
- [394]. Davis, C. S. and Crosby, A. J. Wrinkle morphologies with two distinct wavelengths, *Journal of Polymer Science Part B-Polymer Physics*. **2012**, 50, 1225-1232
- [395]. Hyun, D. C. and Jeong, U. Substrate Thickness: An Effective Control Parameter for Polymer Thin Film Buckling on PDMS Substrates, *Journal of Applied Polymer Science*. **2009**, 112, 2683-2690
- [396]. Khare, K., Zhou, J. and Yang, S. Tunable Open-Channel Microfluidics on Soft Poly(dimethylsiloxane) (PDMS) Substrates with Sinusoidal Grooves, *Langmuir*. **2009**, 25, 12794-12799
- [397]. Kim, H. S. and Crosby, A. J. Solvent-Responsive Surface via Wrinkling Instability, *Advanced Materials*. **2011**, 23, 4188-4192

- [398]. Moon, M. W., Lee, S. H., Sun, J. Y., Oh, K. H., Vaziri, A. and Hutchinson, J. W. Wrinkled hard skins on polymers created by focused ion beam, *Proceedings of the National Academy of Sciences of the United States of America*. **2007**, 104, 1130-1133
- [399]. Rodriguez-Hernandez, J. and del Campo, A. Fabrication of hierarchical wrinkled morphologies through sequential UVO treatments, *Journal of Applied Polymer Science*. **2015**, 132,
- [400]. Watanabe, M., Hatano, R. and Koizumi, C. Spontaneous formation of interdigitated array pattern in wrinkled gold films deposited on poly(dimethylsiloxane) elastomer, *Polymer Journal*. **2015**, 47, 320-327
- [401]. Xuan, Y., Guo, X., Cui, Y. S., Yuan, C. S., Ge, H. X., Cui, B. and Chen, Y. F. Crack-free controlled wrinkling of a bilayer film with a gradient interface, *Soft Matter*. **2012**, 8, 9603-9609
- [402]. Yabu, H., Saito, Y., Nakamichi, Y., Hirai, Y., Fujinami, S., Nakajima, K., Nishi, T. and Shimomura, M. Self-assembled porous templates allow pattern transfer to poly(dimethyl siloxane) sheets through surface wrinkling, *Polymer Journal*. **2012**, 44, 573-578
- [403]. Chan, E. P., Lin, Q. and Stafford, C. M. Quantifying the elasticity and viscosity of geometrically confined polymer films via thermal wrinkling, *Journal of Polymer Science Part B-Polymer Physics*. **2012**, 50, 1556-1561
- [404]. Chandra, D. and Crosby, A. J. Self-Wrinkling of UV-Cured Polymer Films, *Advanced Materials*. **2011**, 23, 3441-3445
- [405]. Lin, P.-C. and Yang, S. Mechanically switchable wetting on wrinkled elastomers with dual-scale roughness, *Soft Matter*. **2009**, 5, 1011-1018
- [406]. Huck, W. T. S., Bowden, N., Onck, P., Pardoen, T., Hutchinson, J. W. and Whitesides, G. M. Ordering of spontaneously formed buckles on planar surfaces, *Langmuir*. **2000**, 16, 3497-3501
- [407]. Nair, D. P., Cramer, N. B., Gaipa, J. C., McBride, M. K., Matherly, E. M., McLeod, R. R., Shandas, R. and Bowman, C. N. Two-Stage Reactive Polymer Network Forming Systems, *Advanced Functional Materials*. **2012**, 22, 1502-1510
- [408]. Nair, D. R., Cramer, N. B., McBride, M. K., Gaipa, J. C., Shandas, R. and Bowman, C. N. Enhanced two-stage reactive polymer network forming systems, *Polymer*. **2012**, 53, 2429-2434

- [409]. O'Brien, A. K. and Bowman, C. N. Impact of oxygen on photopolymerization kinetics and polymer structure, *Macromolecules*. **2006**, 39, 2501-2506
- [410]. O'Brien, A. K. and Bowman, C. N. Modeling the effect of oxygen on photopolymerization kinetics, *Macromolecular Theory and Simulations*. **2006**, 15, 176-182
- [411]. Li, Y. Y., Dai, S. X., John, J. and Carter, K. R. Superhydrophobic Surfaces from Hierarchically Structured Wrinkled Polymers, *Acs Applied Materials & Interfaces*. **2013**, 5, 11066-11073
- [412]. Zhang, Z., Zhang, T., Zhang, Y. W., Kim, K.-S. and Gao, H. Strain-Controlled Switching of Hierarchically Wrinkled Surfaces between Superhydrophobicity and Superhydrophilicity, **2012**, 28, 2753-2760
- [413]. Harrison, C., Stafford, C. M., Zhang, W. H. and Karim, A. Sinusoidal phase grating created by a tunably buckled surface, *Applied Physics Letters*. **2004**, 85, 4016-4018
- [414]. Khang, D. Y., Rogers, J. A. and Lee, H. H. Mechanical Buckling: Mechanics, Metrology, and Stretchable Electronics, *Advanced Functional Materials*. **2009**, 19, 1526-1536
- [415]. Ma, Y. J., Jang, K. I., Wang, L., Jung, H. N., Kwak, J. W., Xue, Y. G., Chen, H., Yang, Y. Y., Shi, D. W., Feng, X., Rogers, J. A. and Huang, Y. G. Design of Strain-Limiting Substrate Materials for Stretchable and Flexible Electronics, *Advanced Functional Materials*. **2016**, 26, 5345-5351
- [416]. Kim, B., Peterson, E. T. K. and Papautsky, I. Long-term stability of plasma oxidized PDMS surfaces, *Proceedings of the 26th Annual International Conference of the Ieee Engineering in Medicine and Biology Society, Vols 1-7*. **2004**, 26, 5013-5016
- [417]. Kim, J., Chaudhury, M. K. and Owen, M. J. Hydrophobicity loss and recovery of silicone HV insulation, *Ieee Transactions on Dielectrics and Electrical Insulation*. **1999**, 6, 695-702
- [418]. Morra, M., Occhiello, E., Marola, R., Garbassi, F., Humphrey, P. and Johnson, D. On the Aging of Oxygen Plasma-Treated Polydimethylsiloxane Surfaces, *Journal of Colloid and Interface Science*. **1990**, 137, 11-24
- [419]. Cordeiro, A. L., Nitschke, M., Janke, A., Helbig, R., D'Souza, F., Donnelly, G. T., Willemsen, P. R. and Werner, C. Fluorination of poly(dimethylsiloxane) surfaces by low pressure CF(4) plasma - physicochemical and antifouling properties, *Express Polymer Letters*. **2009**, 3, 70-83

- [420]. Maheshwari, N., Kottantharayil, A., Kumar, M. and Mukherji, S. Long term hydrophilic coating on poly(dimethylsiloxane) substrates for microfluidic applications, *Applied Surface Science*. **2010**, 257, 451-457
- [421]. Mosadegh, B., Tavana, H., Lesher-Perez, S. C. and Takayama, S. High-density fabrication of normally closed microfluidic valves by patterned deactivation of oxidized polydimethylsiloxane, *Lab on a Chip*. **2011**, 11, 738-742
- [422]. Sharma, V., Dhayal, M., Govind, Shivaprasad, S. M. and Jain, S. C. Surface characterization of plasma-treated and PEG-grafted PDMS for micro fluidic applications, *Vacuum*. **2007**, 81, 1094-1100
- [423]. Yao, M. J. and Fang, J. Hydrophilic PEO-PDMS for microfluidic applications, *Journal of Micromechanics and Microengineering*. **2012**, 22,
- [424]. Tan, S. H., Nguyen, N. T., Chua, Y. C. and Kang, T. G. Oxygen plasma treatment for reducing hydrophobicity of a sealed polydimethylsiloxane microchannel, *Biomicrofluidics*. **2010**, 4,
- [425]. Zhang, Z. L., Crozatier, C., Le Berre, M. and Chen, Y. In situ bio-functionalization and cell adhesion in microfluidic devices, *Microelectronic Engineering*. **2005**, 78-79, 556-562
- [426]. Roth, J., Albrecht, V., Nitschke, M., Bellmann, C., Simon, F., Zschoche, S., Michel, S., Luhmann, C., Grundke, K. and Voit, B. Surface Functionalization of Silicone Rubber for Permanent Adhesion Improvement, *Langmuir*. **2008**, 24, 12603-12611
- [427]. Frimat, J. P., Menne, H., Michels, A., Kittel, S., Kettler, R., Borgmann, S., Franzke, J. and West, J. Plasma stencilling methods for cell patterning, *Analytical and Bioanalytical Chemistry*. **2009**, 395, 601-609
- [428]. Hillborg, H., Ankner, J. F., Gedde, U. W., Smith, G. D., Yasuda, H. K. and Wikstrom, K. Crosslinked polydimethylsiloxane exposed to oxygen plasma studied by neutron reflectometry and other surface specific techniques, *Polymer*. **2000**, 41, 6851-6863
- [429]. Wang, P. Y., Yu, H. T. and Tsai, W. B. Modulation of Alignment and Differentiation of Skeletal Myoblasts by Submicron Ridges/Grooves Surface Structure, *Biotechnology and Bioengineering*. **2010**, 106, 285-294
- [430]. Kilian, K. A., Bugarija, B., Lahn, B. T. and Mrksich, M. Geometric cues for directing the differentiation of mesenchymal stem cells, *Proceedings of the National Academy of Sciences of the United States of America*. **2010**, 107, 4872-4877

- [431]. Collins, J. M., Porter, K. A., Singh, S. K. and Vanier, G. S. High-Efficiency Solid Phase Peptide Synthesis (HE-SPPS), *Organic Letters*. **2014**, 16, 940-943
- [432]. Merrifield, R. B. Solid Phase Peptide Synthesis .1. Synthesis of a Tetrapeptide, *Journal of the American Chemical Society*. **1963**, 85, 2149-&
- [433]. Sawicki, L. A. and Kloxin, A. M. Design of thiol-ene photoclick hydrogels using facile techniques for cell culture applications, *Biomaterials Science*. **2014**, 2, 1612-1626
- [434]. Fairbanks, B. D., Schwartz, M. P., Bowman, C. N. and Anseth, K. S. Photoinitiated polymerization of PEG-diacrylate with lithium phenyl-2,4,6-trimethylbenzoylphosphinate: polymerization rate and cytocompatibility, *Biomaterials*. **2009**, 30, 6702-6707
- [435]. Rana, D. and Matsuura, T. Surface modifications for antifouling membranes, *Chem Rev*. **2010**, 110, 2448-71
- [436]. Rufin, M. A., Barry, M. E., Adair, P. A., Hawkins, M. L., Raymond, J. E. and Grunlan, M. A. Protein resistance efficacy of PEO-silane amphiphiles: Dependence on PEO-segment length and concentration, *Acta Biomaterialia*. **2016**, 41, 247-252
- [437]. Sebra, R. P., Reddy, S. K., Masters, K. S., Bowman, C. N. and Anseth, K. S. Controlled polymerization chemistry to graft architectures that influence cell-material interactions, *Acta Biomaterialia*. **2007**, 3, 151-161
- [438]. Frith, J. E., Mills, R. J., Hudson, J. E. and Cooper-White, J. J. Tailored Integrin-Extracellular Matrix Interactions to Direct Human Mesenchymal Stem Cell Differentiation, *Stem Cells and Development*. **2012**, 21, 2442-2456
- [439]. Wong, S. T., Teo, S. K., Park, S., Chiam, K. H. and Yim, E. K. F. Anisotropic rigidity sensing on grating topography directs human mesenchymal stem cell elongation, *Biomechanics and Modeling in Mechanobiology*. **2014**, 13, 27-39
- [440]. Subramony, S. D., Dargis, B. R., Castillo, M., Azeloglu, E. U., Tracey, M. S., Su, A. and Lu, H. H. The guidance of stem cell differentiation by substrate alignment and mechanical stimulation, *Biomaterials*. **2013**, 34, 1942-1953
- [441]. Suzuki, K., Hirai, Y. and Ohzono, T. Oscillating Friction on Shape-Tunable Wrinkles, *Acs Applied Materials & Interfaces*. **2014**, 6, 10121-10131
- [442]. Lowe, A. B. Thiol-ene "click" reactions and recent applications in polymer and materials synthesis: a first update, *Polymer Chemistry*. **2014**, 5, 4820-4870

- [443]. Brei, M. R., Donovan, B. R., Patton, D. L. and Storey, R. F. Synthesis and thiol-ene photopolymerization of (meth)allyl-terminated polysulfides, *Journal of Applied Polymer Science*. **2017**, 134,
- [444]. Gould, S. T., Darling, N. J. and Anseth, K. S. Small peptide functionalized thiol-ene hydrogels as culture substrates for understanding valvular interstitial cell activation and de novo tissue deposition, *Acta Biomaterialia*. **2012**, 8, 3201-3209
- [445]. Chen, T. F., Siow, K. S., Ng, P. Y., Nai, M. H., Lim, C. T. and Majlis, B. Y. Ageing properties of polyurethane methacrylate and off-stoichiometry thiol-ene polymers after nitrogen and argon plasma treatment, *Journal of Applied Polymer Science*. **2016**, 133,
- [446]. Lu, H., Carioscia, J. A., Stansbury, J. W. and Bowman, C. N. Investigations of step-growth thiol-ene polymerizations for novel dental restoratives, *Dental Materials*. **2005**, 21, 1129-1136
- [447]. Zuo, Y. J., Gou, Z. M., Zhang, C. Q. and Feng, S. Y. Polysiloxane-Based Autonomic Self-Healing Elastomers Obtained through Dynamic Boronic Ester Bonds Prepared by Thiol-Ene "Click" Chemistry, *Macromolecular Rapid Communications*. **2016**, 37, 1052-1059
- [448]. Cheng, C. J., Zhang, X., Chen, X. H., Li, J., Huang, Q. H., Hu, Z. Y. and Tu, Y. M. Self-healing polymers based on eugenol via combination of thiol-ene and thiol oxidation reactions, *Journal of Polymer Research*. **2016**, 23,
- [449]. He, L. R., Szopinski, D., Wu, Y., Luinstra, G. A. and Theato, P. Toward Self-Healing Hydrogels Using One-Pot Thiol-Ene Click and Borax-Diol Chemistry, *Acs Macro Letters*. **2015**, 4, 673-678
- [450]. Ware, T. H., Perry, Z. P., Middleton, C. M., Iacono, S. T. and White, T. J. Programmable Liquid Crystal Elastomers Prepared by Thiol-Ene Photopolymerization, *Acs Macro Letters*. **2015**, 4, 942-946
- [451]. Davis, R. L., Jayaraman, S., Chaikin, P. M. and Register, R. A. Creating Controlled Thickness Gradients in Polymer Thin Films via Flowcoating, *Langmuir*. **2014**, 30, 5637-5644
- [452]. Stafford, C. M., Roskov, K. E., Epps, T. H. and Fasolka, M. J. Generating thickness gradients of thin polymer films via flow coating, *Review of Scientific Instruments*. **2006**, 77,

- [453]. Park, H. Y., Kloxin, C. J., Scott, T. F. and Bowman, C. N. Covalent Adaptable Networks as Dental Restorative Resins: Stress relaxation by addition-fragmentation chain transfer in allyl sulfide-containing resins, *Dental Materials*. **2010**, 26, 1010-1016
- [454]. Michal, B. T., Spencer, E. J. and Rowan, S. J. Stimuli-Responsive Reversible Two-Level Adhesion from a Structurally Dynamic Shape-Memory Polymer, *Acs Applied Materials & Interfaces*. **2016**, 8, 11041-11049
- [455]. Amamoto, Y., Kamada, J., Otsuka, H., Takahara, A. and Matyjaszewski, K. Polymers through Reshuffling of Trithiocarbonate Units, *Angewandte Chemie-International Edition*. **2011**, 50, 1660-1663
- [456]. Nicolay, R., Kamada, J., Van Wassen, A. and Matyjaszewski, K. Responsive Gels Based on a Dynamic Covalent Trithiocarbonate Cross-Linker, *Macromolecules*. **2010**, 43, 4355-4361
- [457]. Tokudome, Y., Suzuki, K., Kitanaga, T. and Takahashi, M. Hierarchical Nested Wrinkles on Silica-Polymer Hybrid Films: Stimuli-Responsive Micro Periodic Surface Architectures, *Scientific Reports*. **2012**, 2,
- [458]. Leocmach, M., Nespoulous, M., Manneville, S. and Gibaud, T. Hierarchical wrinkling in a confined permeable biogel, *Science Advances*. **2015**, 1,
- [459]. Li, F. D., Hou, H. H., Yin, J. and Jiang, X. S. Multi-Responsive Wrinkling Patterns by the Photoswitchable Supramolecular Network, *Acs Macro Letters*. **2017**, 6, 848-853
- [460]. Tokudome, Y., Kuniwaki, H., Suzuki, K., Carboni, D., Poologasundarampillai, G. and Takahashi, M. Thermoresponsive Wrinkles on Hydrogels for Soft Actuators, *Advanced Materials Interfaces*. **2016**, 3,
- [461]. Bandara, H. M. D. and Burdette, S. C. Photoisomerization in different classes of azobenzene, *Chemical Society Reviews*. **2012**, 41, 1809-1825
- [462]. Ichimura, K., Oh, S. K. and Nakagawa, M. Light-driven motion of liquids on a photoresponsive surface, *Science*. **2000**, 288, 1624-1626
- [463]. Klajn, R. Immobilized azobenzenes for the construction of photoresponsive materials, *Pure and Applied Chemistry*. **2010**, 82, 2247-2279
- [464]. Kumar, G. S. and Neckers, D. C. PHOTOCHEMISTRY OF AZOBENZENE-CONTAINING POLYMERS, *Chemical Reviews*. **1989**, 89, 1915-1925

- [465]. Li, C. S., Lo, C. W., Zhu, D. F., Li, C. H., Liu, Y. and Jiang, H. R. Synthesis of a Photoresponsive Liquid-Crystalline Polymer Containing Azobenzene, *Macromolecular Rapid Communications*. **2009**, 30, 1928-1935
- [466]. Natansohn, A. and Rochon, P. Photoinduced motions in azo-containing polymers, *Chemical Reviews*. **2002**, 102, 4139-4175
- [467]. Pace, G., Ferri, V., Grave, C., Elbing, M., von Haenisch, C., Zharnikov, M., Mayor, M., Rampi, M. A. and Samori, P. Cooperative light-induced molecular movements of highly ordered azobenzene self-assembled monolayers, *Proceedings of the National Academy of Sciences of the United States of America*. **2007**, 104, 9937-9942
- [468]. Chen, Y. and Chen, K. H. Synthesis and reversible photocleavage of novel polyurethanes containing coumarin dimer components, *Journal of Polymer Science Part a-Polymer Chemistry*. **1997**, 35, 613-624
- [469]. He, J., Tremblay, L., Lacelle, S. and Zhao, Y. Preparation of polymer single chain nanoparticles using intramolecular photodimerization of coumarin, *Soft Matter*. **2011**, 7, 2380-2386
- [470]. Iliopoulos, K., Krupka, O., Gindre, D. and Salle, M. Reversible Two-Photon Optical Data Storage in Coumarin-Based Copolymers, *Journal of the American Chemical Society*. **2010**, 132, 14343-14345
- [471]. Kaur, G., Johnston, P. and Saito, K. Photo-reversible dimerisation reactions and their applications in polymeric systems, *Polymer Chemistry*. **2014**, 5, 2171-2186
- [472]. Kim, C., Trajkovska, A., Wallace, J. U. and Chen, S. H. New insight into photoalignment of liquid crystals on coumarin-containing polymer films, *Macromolecules*. **2006**, 39, 3817-3823
- [473]. Kiskan, B. and Yagci, Y. Self-Healing of Poly(propylene oxide)-Polybenzoxazine Thermosets by Photoinduced Coumarine Dimerization, *Journal of Polymer Science Part a-Polymer Chemistry*. **2014**, 52, 2911-2918
- [474]. Mal, N. K., Fujiwara, M. and Tanaka, Y. Photocontrolled reversible release of guest molecules from coumarin-modified mesoporous silica, *Nature*. **2003**, 421, 350-353
- [475]. Hou, H. H., Li, F. D., Su, Z. L., Yin, J. and Jiang, X. S. Light-reversible hierarchical patterns by dynamic photo-dimerization induced wrinkles, *Journal of Materials Chemistry C*. **2017**, 5, 8765-8773

- [476]. Lai, J. T., Filla, D. and Shea, R. Functional polymers from novel carboxyl-terminated trithiocarbonates as highly efficient RAFT agents, *Macromolecules*. **2002**, 35, 6754-6756
- [477]. Ware, T. H. and White, T. J. Programmed liquid crystal elastomers with tunable actuation strain, *Polymer Chemistry*. **2015**, 6, 4835-4844
- [478]. McBride, M., Baranek, A. and Bowman, C. Shape memory properties of polymer networks formed using photomediated copper(I)-catalyzed azide alkyne cycloaddition (photo-CuAAC), *Abstracts of Papers of the American Chemical Society*. **2015**, 249,
- [479]. McBride, M. K., Gong, T., Nair, D. P. and Bowman, C. N. Photo-mediated copper(I)-catalyzed azide-alkyne cycloaddition (CuAAC) "click" reactions for forming polymer networks as shape memory materials, *Polymer*. **2014**, 55, 5880-5884
- [480]. Ramdas, M. R., Kumar, K. S. S. and Nair, C. P. R. Click polymerizations: Encouraging route for shape memory polymers, *Materials Letters*. **2016**, 172, 216-221
- [481]. Zhang, H. Y., Zhu, Y., Chen, J. D. and Zhang, S. M. Preparation of polyHIPE via CuAAC "click" chemistry and its application as a highly efficient adsorbent of Cu(II) ions, *Journal of Polymer Science Part a-Polymer Chemistry*. **2017**, 55, 2129-2135
- [482]. Doran, S., Murtezi, E., Barlas, F. B., Timur, S. and Yagci, Y. One-Pot Photo-Induced Sequential CuAAC and Thiol-Ene Click Strategy for Bioactive Macromolecular Synthesis, *Macromolecules*. **2014**, 47, 3608-3613
- [483]. Lallana, E., Sousa-Herves, A., Fernandez-Trillo, F., Riguera, R. and Fernandez-Megia, E. Click Chemistry for Drug Delivery Nanosystems, *Pharmaceutical Research*. **2012**, 29, 1-34
- [484]. Lutz, J. F. and Zarafshani, Z. Efficient construction of therapeutics, bioconjugates, biomaterials and bioactive surfaces using azide-alkyne "click" chemistry, *Advanced Drug Delivery Reviews*. **2008**, 60, 958-970
- [485]. Oyman Eyrilmez, G., Doran, S., Murtezi, E., Demir, B., Demirkol, D. O., Coskunol, H., Timur, S. and Yagci, Y. Selective Cell Adhesion and Biosensing Applications of Bio-Active Block Copolymers Prepared by CuAAC/Thiol-ene Double Click Reactions, *Macromolecular Bioscience*. **2015**, 15, 1233-1241

- [486]. Song, H. B., Baranek, A., McBride, M., Gong, T., Flores, A., Stansbury, J., Kloxin, C. and Bowman, C. Optimizing photo-CuAAC polymerization kinetic for dental restorative materials, *Abstracts of Papers of the American Chemical Society*. **2015**, 249,
- [487]. Song, H. B., Sowan, N., Shah, P. K., Baranek, A., Flores, A., Stansbury, J. W. and Bowman, C. N. Reduced shrinkage stress via photo-initiated copper(I)-catalyzed cycloaddition polymerizations of azide-alkyne resins, *Dental Materials*. **2016**, 32, 1332-1342
- [488]. Song, H. B., Wang, X., Patton, J. R., Stansbury, J. W. and Bowman, C. N. Kinetics and mechanics of photo-polymerized triazole-containing thermosetting composites via the copper(I)-catalyzed azide-alkyne cycloaddition, *Dental Materials*. **2017**, 33, 621-629
- [489]. Adzima, B. J., Tao, Y. H., Kloxin, C. J., DeForest, C. A., Anseth, K. S. and Bowman, C. N. Spatial and temporal control of the alkyne-azide cycloaddition by photoinitiated Cu(II) reduction, *Nature Chemistry*. **2011**, 3, 256-259
- [490]. Bowman, C. N., Gong, T. and Alzahrani, A. Photopolymerizations and polymers based on the CuAAC reaction, *Abstracts of Papers of the American Chemical Society*. **2014**, 248,
- [491]. Gong, T., Adzima, B. J., Baker, N. H. and Bowman, C. N. Photopolymerization Reactions Using the Photoinitiated Copper (I)-Catalyzed Azide-Alkyne Cycloaddition (CuAAC) Reaction, *Advanced Materials*. **2013**, 25, 2024-2028
- [492]. Alzahrani, A. A., Nair, D. P., Smits, D. J., Saed, M., Yakacki, C. M. and Bowman, C. N. Photo-CuAAC Induced Wrinkle Formation in a Thiol-Acrylate Elastomer via Sequential Click Reactions, *Chemistry of Materials*. **2014**, 26, 5303-5309
- [493]. Shete, A. U. and Kloxin, C. J. One-pot blue-light triggered tough interpenetrating polymeric network (IPN) using CuAAC and methacrylate reactions, *Polymer Chemistry*. **2017**, 8, 3668-3673
- [494]. Cao, G. X., Chen, X., Li, C. R., Ji, A. and Cao, Z. X. Self-assembled triangular and labyrinth buckling patterns of thin films on spherical substrates, *Physical Review Letters*. **2008**, 100,
- [495]. Chan, H. K. and Chew, N. Y. K. Novel alternative methods for the delivery of drugs for the treatment of asthma, *Advanced Drug Delivery Reviews*. **2003**, 55, 793-805
- [496]. Chew, N. Y. K. and Chan, H. K. Use of solid corrugated particles to enhance powder aerosol performance, *Pharmaceutical Research*. **2001**, 18, 1570-1577

- [497]. Fogle, C., Rowat, A. C., Levine, A. J. and Rudnick, J. Shape transitions in soft spheres regulated by elasticity, *Physical Review E*. **2013**, 88,
- [498]. Hano, N., Takafuji, M. and Ihara, H. One-pot preparation of polymer microspheres having wrinkled hard surfaces through self-assembly of silica nanoparticles, *Chemical Communications*. **2017**, 53, 9147-9150
- [499]. Ina, M., Zhushma, A. P., Lebedeva, N. V., Vatankhah-Varnoosfaderani, M., Olson, S. D. and Sheiko, S. S. The design of wrinkled microcapsules for enhancement of release rate, *Journal of Colloid and Interface Science*. **2016**, 478, 296-302
- [500]. Kang, J. S., Lim, J., Rho, W. Y., Kim, J., Moon, D. S., Jeong, J., Jung, D., Choi, J. W., Lee, J. K. and Sung, Y. E. Wrinkled silica/titania nanoparticles with tunable interwrinkle distances for efficient utilization of photons in dye-sensitized solar cells, *Scientific Reports*. **2016**, 6,
- [501]. Li, B., Jia, F., Cao, Y. P., Feng, X. Q. and Gao, H. J. Surface Wrinkling Patterns on a Core-Shell Soft Sphere, *Physical Review Letters*. **2011**, 106,
- [502]. Li, M., Joung, D., Hughes, B., Waldman, S. D., Kozinski, J. A. and Hwang, D. K. Wrinkling Non-Spherical Particles and Its Application in Cell Attachment Promotion, *Scientific Reports*. **2016**, 6, 30463
- [503]. Li, M. G., Joung, D. H., Hughes, B., Waldman, S. D., Kozinski, J. A. and Hwang, D. K. Wrinkling Non-Spherical Particles and Its Application in Cell Attachment Promotion, *Scientific Reports*. **2016**, 6,
- [504]. Terwagne, D., Brojan, M. and Reis, P. M. Smart Morphable Surfaces for Aerodynamic Drag Control, *Advanced Materials*. **2014**, 26, 6608-6611
- [505]. Trindade, A. C., Canejo, J. P., Patricio, P., Brogueira, P., Teixeira, P. I. and Godinho, M. H. Hierarchical wrinkling on elastomeric Janus spheres, *Journal of Materials Chemistry*. **2012**, 22, 22044-22049
- [506]. Trindade, A. C., Canejo, J. P., Pinto, L. F. V., Patricio, P., Brogueira, P., Teixeira, P. I. C. and Godinho, M. H. Wrinkling Labyrinth Patterns on Elastomeric Janus Particles, *Macromolecules*. **2011**, 44, 2220-2228
- [507]. Wang, Z. M., Gupta, S. K. and Meenach, S. A. Development and physicochemical characterization of acetalated dextran aerosol particle systems for deep lung delivery, *International Journal of Pharmaceutics*. **2017**, 525, 264-274

- [508]. Zhou, Q. Z., Xiang, H. F., Fan, H. S., Yang, X. L., Zhao, N. and Xu, J. Facile fabrication of golf ball-like hollow microspheres of organic-inorganic silica, *Journal of Materials Chemistry*. **2011**, 21, 13056-13061
- [509]. Hano, N., Takafuji, M. and Ihara, H. One-pot preparation of polymer microspheres having wrinkled hard surfaces through self-assembly of silica nanoparticles, *Chemical Communications*. **2017**, 53,
- [510]. Lee, J., Ku, K. H., Kim, M., Shin, J. M., Han, J., Park, C. H., Yi, G. R., Jang, S. G. and Kim, B. J. Stimuli-Responsive, Shape-Transforming Nanostructured Particles, *Advanced Materials*. **2017**, 29,
- [511]. Cox, L. M., Sun, X. H., Wang, C., Sowan, N., Killgore, J. P., Long, R., Wu, H. A., Bowman, C. N. and Ding, Y. F. Light-Stimulated Permanent Shape Reconfiguration in Cross-Linked Polymer Microparticles, *Acs Applied Materials & Interfaces*. **2017**, 9, 14422-14428
- [512]. Durham, O. Z. and Shipp, D. A. Suspension thiol-ene photopolymerization: Effect of stabilizing agents on particle size and stability, *Polymer*. **2014**, 55, 1674-1680
- [513]. Hessberger, T., Braun, L. and Zentel, R. Microfluidic Synthesis of Actuating Microparticles from a Thiol-Ene Based Main-Chain Liquid Crystalline Elastomer, *Polymers*. **2016**, 8,
- [514]. Jivan, F., Yegappan, R., Pearce, H., Carrow, J. K., McShane, M., Gaharwar, A. K. and Alge, D. L. Sequential Thiol-Ene and Tetrazine Click Reactions for the Polymerization and Functionalization of Hydrogel Microparticles, *Biomacromolecules*. **2016**, 17, 3516-3523
- [515]. Serra, C. A., Khan, I. U., Chang, Z. Q., Bouquey, M., Muller, R., Kraus, I., Schmutz, M., Vandamme, T., Anton, N., Ohm, C., Zentel, R., Knauer, A. and Kohler, M. Engineering Polymer Microparticles by Droplet Microfluidics, *Journal of Flow Chemistry*. **2013**, 3, 66-75
- [516]. Tan, J. J., Li, C. M., Zhou, J., Yin, C. J., Zhang, B. L., Gu, J. W. and Zhang, Q. Y. Fast and facile fabrication of porous polymer particles via thiol-ene suspension photopolymerization, *Rsc Advances*. **2014**, 4, 13334-13339
- [517]. Wang, C., Zhang, X. P., Podgorski, M., Xi, W. X., Stansbury, J. and Bowman, C. N. Monodispersity/Narrow Polydispersity Cross-Linked Microparticles Prepared by Step-Growth Thiol-Michael Addition Dispersion Polymerizations, *Macromolecules*. **2015**, 48, 8461-8470

- [518]. Wang, C., Zieger, M. M., Schenzel, A., Wegener, M., Willenbacher, J., Barner-Kowollik, C. and Bowman, C. N. Photoinduced Tetrazole-Based Functionalization of Off-Stoichiometric Clickable Microparticles, *Advanced Functional Materials*. **2017**, 27,
- [519]. Amato, D., Amato, D., Flynt, A. and Patton, D. Functional polymer nanoparticles via thiol-ene nanoemulsion photopolymerization, *Abstracts of Papers of the American Chemical Society*. **2015**, 249,
- [520]. Amato, D., Amato, D., Brei, M., Storey, R. and Patton, D. Thiol-alkyne photopolymerization in miniemulsion: A facile route to functional polymer nanoparticles, *Abstracts of Papers of the American Chemical Society*. **2015**, 249,
- [521]. Amato, D. V., Amato, D. N., Flynt, A. S. and Patton, D. L. Functional, sub-100 nm polymer nanoparticles via thiol-ene miniemulsion photopolymerization, *Polymer Chemistry*. **2015**, 6, 5625-5632

## Appendix A

### PERMISSION LETTERS



**Title:** Photodirected Formation and Control of Wrinkles on a Thiol-ene Elastomer

**Author:** Stephen J. Ma, Samantha J. Mannino, Norman J. Wagner, et al

**Publication:** ACS Macro Letters

**Publisher:** American Chemical Society

**Date:** Jun 1, 2013

Copyright © 2013, American Chemical Society

#### **PERMISSION/LICENSE IS GRANTED FOR YOUR ORDER AT NO CHARGE**

This type of permission/license, instead of the standard Terms & Conditions, is sent to you because no fee is being charged for your order. Please note the following:

- Permission is granted for your request in both print and electronic formats, and translations.
- If figures and/or tables were requested, they may be adapted or used in part.
- Please print this page for your records and send a copy of it to your publisher/graduate school.
- Appropriate credit for the requested material should be given as follows: "Reprinted (adapted) with permission from (COMPLETE REFERENCE CITATION). Copyright (YEAR) American Chemical Society." Insert appropriate information in place of the capitalized words.
- One-time permission is granted only for the use specified in your request. No additional uses are granted (such as derivative works or other editions). For any other uses, please submit a new request.

#### **AIP PUBLISHING LLC LICENSE TERMS AND CONDITIONS**

Jun 22, 2017

---

---

This Agreement between University of Delaware -- Stephen Ma ("You") and AIP Publishing LLC ("AIP Publishing LLC") consists of your license details and the terms and conditions provided by AIP Publishing LLC and Copyright Clearance Center.

License Number	4134270872876
License date	Jun 22, 2017
Licensed Content Publisher	AIP Publishing LLC
Licensed Content Publication	Applied Physics Letters
Licensed Content Title	Local versus global buckling of thin films on elastomeric substrates
Licensed Content Author	Shuodao Wang, Jizhou Song, Dae-Hyeong Kim, et al
Licensed Content Date	Jul 14, 2008
Licensed Content Volume	93
Licensed Content Issue	2
Type of Use	Thesis/Dissertation
Requestor type	Student
Format	Print and electronic
Portion	Figure/Table
Number of figures/tables	1
Title of your thesis / dissertation	Photodirected Topography through 'Click!' Chemistry
Expected completion date	Jul 2017
Estimated size (number of pages)	150
Requestor Location	University of Delaware 150 Academy Street  NEWARK, DE 19716 United States Attn: University of Delaware
Billing Type	Invoice
Billing Address	University of Delaware 150 Academy Street

NEWARK, DE 19716  
United States  
Attn: University of Delaware

Total 0.00 USD

#### Terms and Conditions

##### AIP Publishing LLC -- Terms and Conditions: Permissions Uses

AIP Publishing hereby grants to you the non-exclusive right and license to use and/or distribute the Material according to the use specified in your order, on a one-time basis, for the specified term, with a maximum distribution equal to the number that you have ordered. Any links or other content accompanying the Material are not the subject of this license.

1. You agree to include the following copyright and permission notice with the reproduction of the Material: "Reprinted from [FULL CITATION], with the permission of AIP Publishing." For an article, the credit line and permission notice must be printed on the first page of the article or book chapter. For photographs, covers, or tables, the notice may appear with the Material, in a footnote, or in the reference list.
2. If you have licensed reuse of a figure, photograph, cover, or table, it is your responsibility to ensure that the material is original to AIP Publishing and does not contain the copyright of another entity, and that the copyright notice of the figure, photograph, cover, or table does not indicate that it was reprinted by AIP Publishing, with permission, from another source. Under no circumstances does AIP Publishing purport or intend to grant permission to reuse material to which it does not hold appropriate rights. You may not alter or modify the Material in any manner. You may translate the Material into another language only if you have licensed translation rights. You may not use the Material for promotional purposes.
3. The foregoing license shall not take effect unless and until AIP Publishing or its agent, Copyright Clearance Center, receives the Payment in accordance with Copyright Clearance Center Billing and Payment Terms and Conditions, which are incorporated herein by reference.
4. AIP Publishing or Copyright Clearance Center may, within two business days of granting this license, revoke the license for any reason whatsoever, with a full refund payable to you. Should you violate the terms of this license at any time, AIP Publishing, or Copyright Clearance Center may revoke the license with no refund to you. Notice of such revocation will be made using the contact information provided by you. Failure to receive such notice will not nullify the revocation.
5. AIP Publishing makes no representations or warranties with respect to the Material. You agree to indemnify and hold harmless AIP Publishing, and their officers, directors, employees or agents from and against any and all claims arising out of your use of the Material other than as specifically authorized herein.
6. The permission granted herein is personal to you and is not transferable or assignable without the prior written permission of AIP Publishing. This license may not be amended except in a writing signed by the party to be charged.
7. If purchase orders, acknowledgments or check endorsements are issued on any forms containing terms and conditions which are inconsistent with these

provisions, such inconsistent terms and conditions shall be of no force and effect. This document, including the CCC Billing and Payment Terms and Conditions, shall be the entire agreement between the parties relating to the subject matter hereof.

This Agreement shall be governed by and construed in accordance with the laws of the State of New York. Both parties hereby submit to the jurisdiction of the courts of New York County for purposes of resolving any disputes that may arise hereunder.



**Title:** A three-dimensional phase diagram of growth-induced surface instabilities  
**Author:** Qiming Wang, Xuanhe Zhao  
**Publication:** Scientific Reports  
**Publisher:** Nature Publishing Group  
**Date:** Mar 9, 2015

Copyright © 2015, Rights Managed by Nature Publishing Group

Logged in as:  
Stephen Ma  
University of  
Delaware  
Account #:  
3001165601

LOGOUT

### Creative Commons

**The article for which you have requested permission has been distributed under a Creative Commons CC-BY license (please see the article itself for the license version number). You may reuse this material without obtaining permission from Nature Publishing Group, providing that the author and the original source of publication are fully acknowledged, as per the terms of the license. For license terms, please see <http://creativecommons.org/>**

CLOSE WINDOW